

TECPR2 cooperates with LC3C to regulate COPII dependent ER export

Dissertation
zur Erlangung des Doktorgrades
der Naturwissenschaften

vorgelegt beim Fachbereich 15
Biowissenschaften
der Johann Wolfgang Goethe – Universität
in Frankfurt am Main

von
Daniela Stadel
aus Karlsruhe

Frankfurt 2015

D30

vom Fachbereich 15 der
Johann Wolfgang Goethe – Universität als Dissertation angenommen.

Dekanin: Prof. Dr. Meike Piepenbrink

Gutachter: Prof. Dr. Heinz D. Osiewacz
Dr. Christian Behrends

Datum der Disputation:

Content

1.	Introduction.....	9
1.1	Hereditary spastic paraparesis (HSP).....	9
1.1.1	Types and clinical aspects of HSP.....	9
1.1.2	Tectonin β -propeller containing protein 2 (TECPR2).....	11
1.2	The secretory pathway.....	12
1.2.1	COPII coat formation.....	13
1.2.2	ERES.....	14
1.2.3	Role of SEC24D.....	15
1.2.4	Regulation and assisting factors of the secretory pathway.....	15
1.2.5	Role of ER architecture in HSP disease.....	16
1.3	The endocytic pathway.....	17
1.3.1	HOPS complex.....	18
1.3.2	BLOC-1 complex.....	20
1.4	Autophagy.....	21
1.4.1	The ubiquitin like conjugation system.....	23
1.4.2	HOPS and BLOC-1 in autophagy.....	26
1.5	Aim of the present work.....	27
2.	Material and Methods.....	28
2.1	Materials.....	28
2.1.1	Chemicals.....	28
2.1.2	Buffers and media.....	30
2.1.3	Kits.....	33
2.1.4	Vectors, oligonucleotides and siRNAs.....	34
2.1.5	Antibodies.....	38
2.2	Methods.....	39
2.2.1	Molecular biological methods.....	39
2.2.2	Cell biological methods.....	43
2.2.3	Protein biochemical methods.....	45
2.2.4	Biophysical and structural methods.....	49

2.2.5	Phenotypical assays	51
3.	Results.....	53
3.1	TECPR2 associates and colocalizes with SEC24D, BLOC-1 and HOPS	53
3.2	TECPR2 binds LC3 and GABARAP proteins in a LIR-dependent manner	57
3.3	Association with SEC24D, BLOC-1 and HOPS requires LC3 binding of TECPR2 .	66
3.4	TECPR2 depletion destabilizes SEC24D, HOPS and BLOC-1.....	69
3.5	Loss of TECPR2 compromises ERES	73
3.6	TECPR2 is required for ER export	77
3.7	TECPR2 depletion affects ER morphology	81
3.8	TECPR2 contributes to autophagosome formation.....	83
4.	Discussion	90
4.1	Model: TECPR2 as scaffold for endomembrane signaling.....	90
4.2	Assembly of the inner COPII coat	92
4.3	HOPS	95
4.4	BLOC-1	96
4.5	LIR motif of TECPR2 and binding preference	97
4.6	ER export and autophagy.....	98
4.7	ER maintenance and neurodegeneration.....	101
4.8	Concluding remarks and future perspectives	103
5.	References	106
	Zusammenfassung	118
	Danksagung.....	123
	Curriculum vitae.....	125
	Publications	126
	Presentations at conferences	127
	Eidesstattliche Erklärung	128

Abbreviations

μ	micro
A	Ampere
Å	Ångström
aa	aminoacid
ABC	ammonium bicarbonate
ACN	acetonitril
ACTBL2	Beta-actine-like protein 2
AIM	ATG interacting motif
ALFY	autophagy-linked FYVE protein
α	alpha, anti
ANP32A	Acidic leucine-rich nuclear phosphoprotein 32 family member A
APS	ammonium persulfate
APSM	average peptide spectral matches
Asp	aspartic acid
ATG	autophagy-related protein
ATL1, SPG3A	atlastin 1
BafA1	Bafilomycin A1
BCA	bicinchoninic acid
β	beta
BLOC-1	biogenesis of lysosome-related organelles complex 1
BLOS-1/2/3	biogenesis of lysosome-related organelle complex subunit-1/2/3
Btz	Bortezomib
°C	degree celsius
<i>C.elegans</i>	<i>Caenorabditis elegans</i>
CALR	calreticulin
CKAP4, CLIMP63	cytoskeleton-associated protein 4
CMA	chaperone-mediated autophagy
CMV	cytomegalo virus
CNO	cappuccino
COL10A1,COL1A1	collagen alpha-1 chain
COPI/II	coat protein complex I/II
CORVET	class c core vacuole/endosome tethering

CPNC	condensed perinuclear cluster
CSP	chemical shift perturbation
C-terminal	carboxy terminal
D	Aspartic acid
DAPI	4,6-diamidin-2-phenylindol
DAVID	Database for Annotation, Visualization, and Integrated Discovery
del	deletion
DFCP1	double FYVE-containing protein 2
DIC	dynein intermediate chain
DKFZ	Deutsches Krebsforschungszentrum
DMEM	Dulbeccos modified eagle medium
DMSO	dimethylsulfoxide
DNA	deoxyribonucleic acid
DTBP	dimethyl-3,3-dithiobispropionimidate
DTNBP1	dysbindin 1
DTT	dithiotreitol
DUB	deubiquitinase
<i>E.coli</i>	<i>Escherichia coli</i>
e.g.	latin: exemplar gratia, english: for example
E1/2/3	enzyme
ECL	Enhanced chemiluminescence
EDTA	ethylenediaminetetraacetic acid
EGFR	epidermal growth factor receptor
EM	Electron microscopy
ER	endoplasmic reticulum
ERES	ER exit sites
ERGIC	ER-to-Golgi intermediate compartment
ESCRT	escort complex
FRAP	fluorescence recovery after photobleaching
FBS	fetal bovine serum
fig.	figure
FIP200, RB1CC1	RB1-inducible coiled-coil protein 1
FYCO1	FYVE and coiled-coil domain-containing protein 1
g	gravity

GABA	gamma aminobutyric acid
GABARAP	gamma-aminobutyric acid receptor-associated protein
GABARAPL1/2	gamma-aminobutyric acid receptor-associated protein-like1/2
GATE-16	gamma-aminobutyric acid receptor-associated protein-like 2
GAP	guanosine triphosphatase activating protein
GAT1	sodium-and-chloride-dependent GABA transporter 1
GDP	guanosin diphosphate
GEF	guanine exchange factor
GFP	green fluorescent protein
GOLGA2, GM130	golgin subfamily A member 2
GOLGB1	golgin subfamily B member 1
GPI	glycosylphosphatidylinositol
GST	glutathione sepharose
GTP	guanosin triphosphate
HA	haemagglutinin
HCIP	high confident interacting protein
HEK	human embryonic kidney
HeLa	Henriette Lacks
HERP1	homocysteine-responsive endoplasmic reticulum-resident protein
HOPS	homotypic fusion of vacuole and sorting
HP1/2	hydrophobic pocket 1/2
HPS	Hermansky-Pudlak Syndrome
hr/hrs	hour/hours
HRP	horseradish peroxidase
HSAN	hereditary sensory-autonomic neuropathy
HSP	Hereditary spastic paraparesis
i.e.	latin: id est, english: that is to say
IAA	iodoacetamide
IF	immunofluorescence
IP	immunoprecipitation
IPTG	isopropyl-beta-D-1-thiogalactopyranoside
ITC	isothermal titration calorimetry
K _D	dissociation constant
kd	knockdown

kDa	kilodalton
KIF5A	kinesin heavy chain isoform 5A
l	liter
L	lysate
L1-CAM	neural cell adhesion molecule L1
LAMP	lysosome-associated membrane glycoprotein
LB	lysogeny broth
LC	liquid chromatography
LIR	LC3 interacting region
LMAN1, ERGIC53	lectin mannose-binding 1
log	logarithm
M	Molar, medium
MAN2A1	mannosidase II
MAP1LC3A/B/C	microtubuli-associated protein light chain 3 A/B/C
MCLB	mammalian cell lysis buffer
MFI	mean fluorescence intensity
min	minute/minutes
MRI	magnetic resonance interference
mRNA	messenger RNA
MS	mass spectrometry
MSCV	murine stem cell virus
mTORC1	mammalian target of rapamycin complex 1
MUTED	biogenesis of lysosome-related organelle complex 1 subunit 5
MVB	Multivesicular bodies
n	nano
NAD	neuroaxonal dystrophy
NEM	N-ethylmaleimide
Ni-NTA	nickel nitrilotriacetic acid
NIX, BNIP3L	BCL2 protein-interacting protein 3-like
NMR	nuclear magnetic resonance spectroscopy
NRF2	nuclear factor erythroid 2-related factor 2
NSF	N-ethylmaleimide-sensitive factor
N-terminal	amino terminal
OD	optical density

OptiMEM	optimal modified eagle medium
OPTN	optineurin
ORF	open reading frame
p	pellet
p125A, SEC23IP	SEC23 interacting protein
PAGE	polyacrylamide gel electrophoresis
PARK2	E3 ubiquitin-protein ligase parkin
PAS	preautophagosomal structures
PBS	phosphate buffered saline
PCNA	proliferating cell nuclear antigen
PCR	polymerase chain reaction
PE	phosphatidylethanolamine
PFA	paraformaldehyde
pH	latin: potentia hydrogenii
PI3KIII	class III phosphatidylinositol-3-kinase
PI3P	phosphatidylinositol-3-phosphate
PLEKHM1	pleckstrin homology domain-containing family M member 1
PLP-1	proteolipid protein 1
PROPPINS	beta-propeller containing proteins that bind phosphoinositides
PURO	puromycin
PVDF	polyvinylidenfluorid
qPCR	quantitative polymerase chain reaction
Rab	ras-related protein
REEP1	receptor expression-enhancing protein 1
RNA	ribonuclic acid
RSK2	ribosomal protein S6 kinase alpha-3
RUSH	retention using selective hook
s	soluble
SBP	streptavidin binding protein
SD	standard deviation
SDS	sodium dodecyl sulfat
sec	second/seconds
siRNA	small interfering RNA
SM	SNARE master

SNAPIN	biogenesis of lysosome-related organelle complex 1 subunit 7
SNARE	soluble NSF attachment protein receptor
SPAST,SPG4	spastin
SQSTM1, p62	sequestosome 1
STX17	syntaxin 17
SUPT5H	transcription elongation factor SPT5
T	Tween
TAE	TRIS-Acetate-EDTA
TANGO1	transport and Golgi organization protein 1
TBP	TATA-binding protein
TECPR2	tectonin beta-propeller containing protein 2
TEMED	tetramethylethylenediamin
TFG	trk-fused gene
TGN	trans-Golgi network
TGOLN2, TGN46	trans-Golgi network integral membrane protein 2
TIAM1	T-lymphoma invasion and metastasis-inducing protein 1
TRAPA	translocon-associated protein subunit alpha
TRAPP	transport protein particle
TRIS	tris(hydroxymethyl)-aminomethan
Trp	tryptophan
Tyrp1	5,6-dihydroxyindole-2-carboxylic acid oxidase
Ub	ubiquitin
ULK1/2	serine/threonine-protein kinase
UV	ultra violet
UVRAG	UV radiation resistance-associated protein
VPS	vacuolar protein sorting
W	tryptophan
WD ⁿ	weighted D-Score
WIPI	WD repeat domain phosphoinositide-interacting protein
YFP	yellow fluorescent protien
ZFYVE	Zink finger FYVE-domain containing protein

Summary

Tectonin β -propeller containing protein 2 (TECPR2) was first identified in a mass-spectrometric approach as an interactor of GABARAP, an ATG8-family protein playing a role in autophagy. The mammalian ATG8 protein family consists of seven members, namely MAP1LC3A (LC3A), MAP1LC3B (LC3B), MAP1LC3C (LC3C), GABARAP, GABARAPL1 and GABARAPL2. All share an ubiquitin-like core and possess two additional N-terminal α -helices, which are important for the distinct functions of the proteins. First determined in various organelles the ATG8 proteins are shown to be involved in autophagy, supporting the formation and cargo recruitment of autophagosomes, the vesicles transporting cargo for autophagic degradation.

Autophagy is the process of recycling cytoplasmic contents by degradation of misfolded proteins or damaged organelles in order to supply nutrients. Also clearance of pathogens can be achieved via autophagy. Importantly, LC3B is incorporated into the autophagosomal membrane and is therefore used as the main marker for autophagosomes. Previous studies exhibited that depletion of TECPR2 leads to a loss of LC3B-positive structures in cells, which suggests TECPR2 to positively regulate autophagic processes.

A frame shift deletion in the gene encoding for TECPR2 causes the generation of a premature stop codon and subsequent an unstable version of the protein, which is then degraded. Mutation in the *TECPR2* gene triggers a neurodegenerative disorder termed hereditary spastic paraparesis (HSP). HSPs are a diverse group of neurodegenerative diseases that are characterized by spasticity in prevalent lower extremities and were mediated by a loss of axonal integrity of the corticospinal motor neurons. In the context of HSP more than 50 gene loci were identified by now. While TECPR2 is a human ATG8 binding protein and positive regulator of autophagy causing a form of HSP, the exact function of TECPR2 is unknown.

This study primarily focused on the determination of TECPR2's binding mode to ATG8 proteins *in vitro* and in cells. The association of TECPR2 to all ATG8-family proteins was confirmed in *in vitro* pulldown experiments. Following fragment-based binding and peptide array experiments, the LC3-interacting region (LIR) of TECPR2 could be verified with mutants of TECPR2 lacking the LIR motif. Nuclear magnetic resonance (NMR) and isothermal titration calorimetry (ITC) were conducted to gain deeper insights into the binding preference to the different ATG8-family members. Moreover, the crystal structure of TECPR2-LIR was solved. In cells colocalization studies with overexpressed ATG8 proteins unraveled a preferential binding to the LC3-subfamily.

Further, mass spectrometric analysis revealed novel association partners of TECPR2: SEC24D, HOPS and BLOC-1, all of those participating in different endomembrane trafficking pathways. Interaction and colocalization of TECPR2 with these components was validated with several immunoprecipitation experiments and the N-terminal part of the protein comprising the

WD40-domain could be defined as the binding site for all three of the association partners. In further approaches, the requirement of the LIR-motif and the necessity of the availability of LC3 protein for the particular interactions were determined. Interestingly, in the absence of LC3C the binding of TECPR2 to SEC24D was completely disrupted whereas a loss of LC3B only resulted in a decreased association. Notably, the binding proteins were not subjected to autophagosomal degradation, indicating that TECPR2 may operate as a multifunctional scaffold protein. While depletion of TECPR2 destabilized HOPS and BLOC-1, the autophagy defect observed in TECPR2-deficient cells could not be attributed to functional impairment of these two complexes.

Moreover, loss of TECPR2 led to a decline in protein levels of SEC24D and of its heterodimer partner SEC23A. Thus, TECPR2 is required to regulate the protein levels of SEC23A and SEC24D and subsequently the formation of the heterodimers. Together, SEC24D and SEC23A form the inner coat of COPII vesicles. These vesicles are responsible for the anterograde transport of cargo from the ER toward the Golgi compartment. COPII-coated vesicles are secreted from ER at distinct sites, termed ER exit sites (ERES). The small GTPase SAR1A maintains the vesicle budding, coating and secretion at the ERES. Together with SEC13, SEC31 forms the outer coat of the COPII vesicles and therefore serves as a general ERES marker.

Consistent with a defect in COPII coat assembly, the number of ERES diminished in the absence of TECPR2. These phenotypes could be rescued by the wildtype TECPR2 protein but not by the LIR-mutant. Intriguingly, these results were mimicked by depletion of LC3C, which localized to ERES. By monitoring the release of various cargos from ER in dependency of TECPR2 or LC3C, a role of both proteins in ER export was determined. These facts indicated that TECPR2 cooperates with LC3C to facilitate COPII assembly, ERES maintenance and ER export. Notably, fibroblast derived from a HSP patient carrying mutated *TECPR2* showed diminished SEC24D protein levels and delayed ER export.

Concurrent with emerging evidence for a role of ERES in autophagosome formation, depletion of TECPR2 or LC3C or overexpression of a constitutive inactive SAR1 mutant reduced puncta formation of the early autophagosomal protein WIPI2.

In summary, this study uncovered a role for TECPR2 in ER export at ERES through interaction and stabilization of SEC24D, a COPII coat protein. This process also depended on ATG8-family protein LC3C, which is localized at ERES. Both proteins are required for correct COPII-mediated secretion. Moreover, the presence of TECPR2 and LC3C on ER allows development of omegasomes, membranous structures budding ER to form autophagosomes, by stabilization of WIPI2 and therefore contribute to autophagosome formation.

1. Introduction

1.1 Hereditary spastic paraparesis (HSP)

Hereditary spastic parapareses (HSPs) comprise a heterogeneous group of neurodegenerative disorders encoded by more than 50 gene loci and 20 gene products. HSP is characterized by spasticity prevalently in lower extremities mediated by a loss of axonal integrity in the corticospinal motor tract (Blackstone, 2012). Patients mainly suffer from progressive spasticity, paralysis of the lower limbs, and general immune deficiencies. With a prevalence of three to nine cases out of 100,000 in most populations this disease affects several hundred thousand individuals worldwide (Blackstone, 2012). Patients afflicted with HSP mostly have a normal lifespan, but partly with early-onset of symptoms like limited mobility.

1.1.1 Types and clinical aspects of HSP

Depending on the accompaniment of other neurological symptoms, HSPs are grouped into uncomplicated and complicated forms. Uncomplicated HSP is limited to spastic weakness of the lower extremities, balancing problems and stiffness in muscles. Moreover, oculocutaneous albinism occurs and bleeding tendency is increased. The complicated variants show expanded symptoms such as systemic or neurological abnormalities e.g. ataxia, dementia, peripheral neuropathy, or general cognitive impairments (Fink, 1993).

For primary diagnosis the absence of platelet dense granules is tested in electron microscopy (EM). Further, in magnetic resonance imaging (MRI) patients display abnormalities of the brain structure and in the spinal cord. To identify some of the HSP genes molecular analyses are available. The prognosis for HSP patients depends on the different forms of the disease. Individuals with uncomplicated HSP might have a normal or slightly reduced life span, whereas patients suffering from complicated forms of HSP maybe develop prolonged bleeding and lung fibrosis, leading to death in the midlife age.

So far, there are no therapies available to cure or prevent the disease. However, some of the symptoms can be attenuated. For example, patients can be injected with platelet transfusions or drugs against bleeding can be dispensed. Physical therapy and exercise for the spastic limbs to maintain flexibility is also employed to diminish the stiffness of muscles (Fink, 2006). HSPs can be inherited in autosomal dominant, autosomal recessive or X-linked manner. To date, more than 56 HSP loci have been identified. Among others genes involved in myelination (PLP-1), mitochondrial function (paraplegin), cell recognition (L1-CAM) and intracellular trafficking (KIF5A, spastizin, atlastin) are mutated (Fink, 2014). Most common causes of HSP are mutations in the spastin gene (SPAST, SPG4), followed by the atlastin-1 gene (ALT1,

SPG3A) (Kim et al., 2014). Spastin serves as a microtubule disassembling protein, acting on endoplasmic reticulum (ER) to Golgi trafficking (Hazan et al., 1999). Atlastin-1, a GTPase involved in the biogenesis of tubular ER elements, mediates tethering and homotypic fusion of ER membranes (Zhao et al., 2001). Mutation of the *ATL1* gene leads to prevention of vesicle budding from ER, indicating a role in the early secretory pathway (Namekawa et al., 2007). Atlastin-1 directly interacts with spastin, indicating the existence of a common pathway for axonal maintenance (Evans et al., 2006; Sanderson et al., 2006) (fig. 1-1).

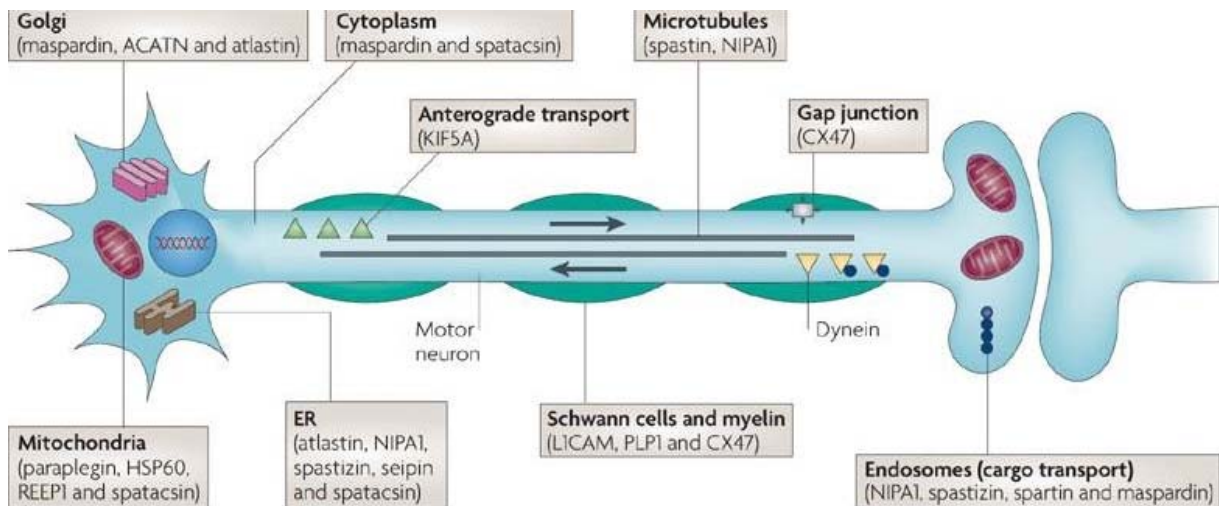


Figure 1-1: HSP causing proteins.

Representative scheme of proteins operating in different organelles of motor neurons. Corresponding genes of these proteins show predisposition for HSP diseases. From (Dion et al., 2009).

Seemingly, a common disturbed compartment in HSP is the ER. Besides spastin and atlastin-1, another interesting candidate gene related to the ER is the *Trk*-fused gene (*TFG*). The *TFG* locus is mutated in patients suffering from an early-onset spastic paraplegia, leading to reduced ability of *TFG* to oligomerize. Inhibition of *TFG* causes reduced secretion from ER and an altered ER architecture (Beetz et al., 2013). *TFG* is known to play a role in the secretory pathway, directly interacting with *SEC16* at ER exit sites (ERES), leading to a reduction of *SEC16* protein levels (Witte et al., 2011).

Spastizin (*ZFYVE26*, *SPG15*) represents another protein involved in an autosomal recessive form of HSP and partially colocalizes with early endosomes and the endoplasmic reticulum (ER). The protein was linked to the process of autophagy, a cellular degradation and recycling pathway, via interaction with *Beclin-1*, a subunit of class III phosphatidylinositol 3-kinase complex (*PI3KIII/VPS34*). *Beclin-1* is a key regulator of autophagy by regulating the process of autophagosome formation. Mutations in spastizin result in immature autophagosomes in

patient fibroblasts and further in an accumulation of autophagosomes in neuronal cells (Vantaggiato et al., 2014; Vantaggiato et al., 2013).

1.1.2 Tectonin β -propeller containing protein 2 (TECPR2)

Recently, autophagy is an emerging and highly debated theme in HSPs. In an immunoprecipitation followed by mass spectrometric (IP-MS) analysis of the human ATG8-proteins the tectonin β -propeller containing protein 2 (TECPR2, SPG49) was initially identified as an high confident interaction candidate (HCIP) for GABA(A) receptor-associated protein (GABARAP) (Behrends et al., 2010). A frameshift deletion in the gene encoding TECPR2 has recently been mapped in patients suffering from an autosomal-recessive complicated HSP (OMIM 615031). The mutation leads to a premature stop codon and the subsequent translation of a C-terminally truncated, unstable version of TECPR2 which is rapidly degraded (Oz-Levi et al., 2012). Further, it was shown that the protein levels of the autophagosome marker LC3B decrease upon depletion of TECPR2. Moreover, the protein amount of LC3B could not be recovered by applying Bafilomycin A1, an inhibitor of H-ATPase blocking lysosomal degradation (Oz-Levi et al., 2012). Therefore, autophagic process is obstructed upon TECPR2 depletion and TECPR2 is characterized as positive autophagy regulator.

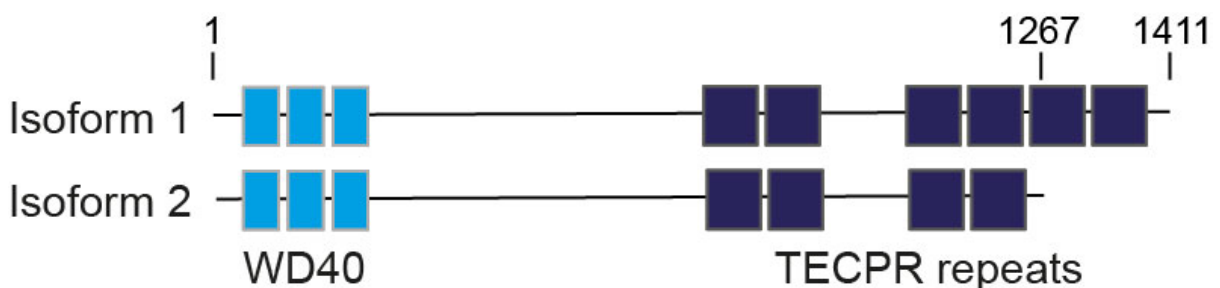


Figure 1-2: Domain structure of the two TECPR2 isoforms.

Numbers on top describe the amino acid length of the TECPR2 variants. Light blue: WD40 domains, dark blue: TECPR domain.

TECPR2 contains three N-terminal WD40 domains and several TECPR domains, dependent on its isoform. The isoform 2 is shorter and comprises four TECPR domains, whereas isoform 1 contains two additional TECPR domains at its C-terminus. Both, WD40 and TECPR domains form β -propeller structures, which are known to supply rigid interaction scaffolds in other proteins (fig. 1-2).

Initially, TECPR proteins were discovered together as β -propeller repeat proteins in the Plasmodium of the slime mould *Physarum polycephalum* and termed tectonin 1 and 2. The tectonins share six tandem repeats which are homologs to the Lectin-6 of the crab *Limulus*

(Huh et al., 1998). Lectins are known to be lipopolysaccharide-binding proteins functioning in several processes such as cell adhesion, targeting hydrolyzing enzymes to lysosome or transmembrane signaling. Remarkably, only the two proteins TECPR1 and TECPR2 are known to encompass TECPR domains.

The WD40 domains are the second domain type in TECPR2. WD40 comprise a large domain family which is conserved in all eukaryotes and involved in signal transduction, transcriptional regulation, cell cycle or apoptosis (Xu and Min, 2011). These domains are about 40 amino acids long, terminate with Trp-Asp (W-D) dipeptides and form β -propeller structures. Therefore, they establish platforms for assembly of protein complexes, such as of E3 ubiquitin ligases (Juris et al., 2015). In this context, a large subset of WD40 β -propellers were defined as ubiquitin-binding domains, being responsible for auto-ubiquitylation and turnover of F box proteins (Pashkova et al., 2010). Encompassing several of these two forms of β -propellers; TECPR2 is predestined for the interaction with various proteins, presumably contributing to different processes in the cell and therefore playing a role in HSP disease.

In contrast to TECPR2, TECPR1 has an established role in selective autophagy. Through binding to ATG5 and colocalization with LC3B in *Shigella*-containing vacuoles TECPR1 targets bacteria or protein aggregates towards degradation via the autophagic pathway, acting as a cargo receptor for autophagy (Ogawa and Sasakawa, 2011; Ogawa et al., 2011). TECPR1 exhibits only 22 percent homology to TECPR2 and comprises several different domains, as for example a pleckstrin homology (PH) domain, which represents an interaction site for inositol phosphates.

1.2 The secretory pathway

Central to the eukaryotic secretory pathway is the shuttling of proteins between the ER and the Golgi apparatus through the *trans*-Golgi network to their destination, for instance the plasma membrane, the extracellular space or lysosomes (Bonifacino and Glick, 2004). The crucial step is the formation of cargo-loaded vesicles and the coordinated traffic of secretory cargo to specific target locations.

Proteins, synthesized and folded in the lumen of the endoplasmic reticulum, are loaded into COPII-coated vesicles, which form and bud at ER exit sites (ERES). The anterograde transport of secretory cargo begins at the ER, passing the ER-Golgi intermediate compartment (ERGIC), entering the *cis*-Golgi and navigate through the Golgi staples. Subsequently, proteins leave at the *trans*-Golgi network (TGN), where they are sorted for their specific destination (Bonifacino and Glick, 2004). Here, either cargo is retrogradely transported back along the pathway in COPI-vesicles or the vesicles fuse with endosomes and lysosomes or are guided to the plasma membrane (fig. 1-3). Finally, cargo for the plasma membrane is integrated into the membrane

for instance as receptors, or released in the extracellular space such as neurotransmitter in neuronal synapses. Further, parts of the cargo operate as adhesive factors to maintain cell-cell contacts at the cell surface, like tight junction proteins. Some proteins also remain to membrane-bound organelles along the secretory pathway (D'Arcangelo et al., 2013; Spang, 2015).

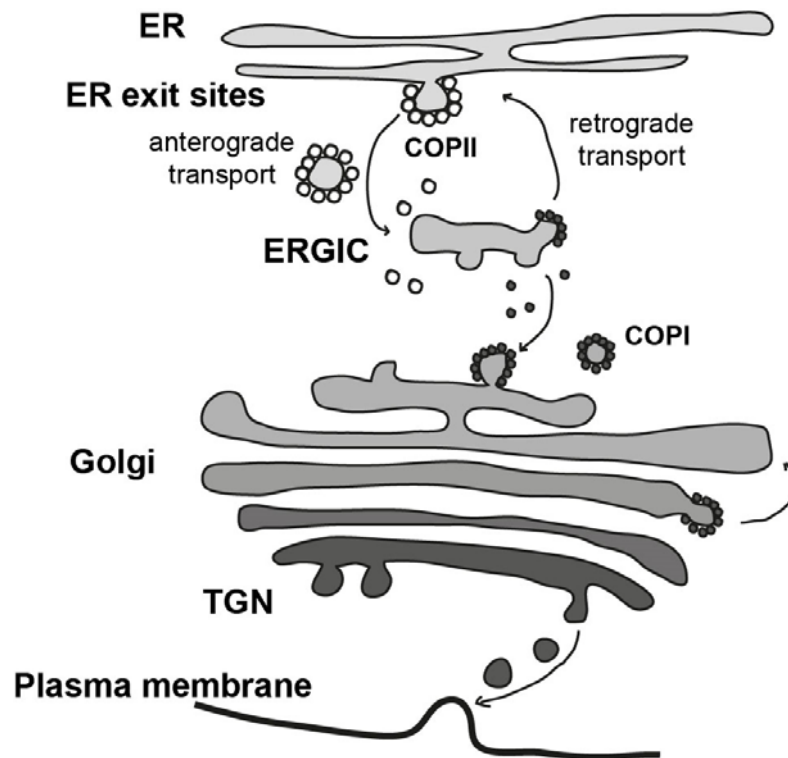


Figure 1-3: Schematic representation of the secretory pathway.

The secretory cargo transport begins at the ER where COPII-coated vesicles bud from ERES and are anterogradely guided to ER-to-Golgi intermediate compartment (ERGIC). Further, the cargo travels via COPI-coated vesicles from ERGIC toward the Golgi compartment. After passing the Golgi-cisterna the cargo enters the *trans*-Golgi network (TGN), from where it is recycled back via COPI vesicles or shuttled toward the plasma membrane.

1.2.1 COPII coat formation

The protein secretion pathway starts with the export of proteins from the ER. Essential initiation step in this process is the formation of cargo-loaded vesicles termed COPII-coated vesicles which are budding from ER exit sites (ERES) (Lee et al., 2004). Assembly of the COPII coat is triggered by recruitment of the small GTPase SAR1A which is activated by the exchange of GDP to GTP and subsequently inserted into ER membrane (Bielli et al., 2005). SEC12, the guanidine exchange factor (GEF) for SAR1A, mediates the GDP-to-GTP switch, which accordingly leads to the deformation and bending of the membrane and to recruitment of SAR1A and its interaction with the inner COPII coat heterodimer SEC23-SEC24 (Bi et al.,

2002). Active SAR1A also regulates vesicle morphology, scission, and uncoating and thereby maintains several functions at different steps of the secretory pathway (Zanetti et al., 2012). SEC23 directly binds to SAR1A whereas SEC24 operates as adaptor for cargo recruitment. In the next step of the process, the so called “pre-budding complex”, consisting of SAR1, SEC23A and SEC24D, binds to the hetero-tetrameric SEC13-SEC31 complex, forming the outer cage of the COPII coat (Jensen and Schekman, 2011). In addition, this drives stabilization and polymerization of the coat sub-complexes and further curvature of the membrane, ending up in the budding of the COPII vesicles from ER (see figure 1-4).

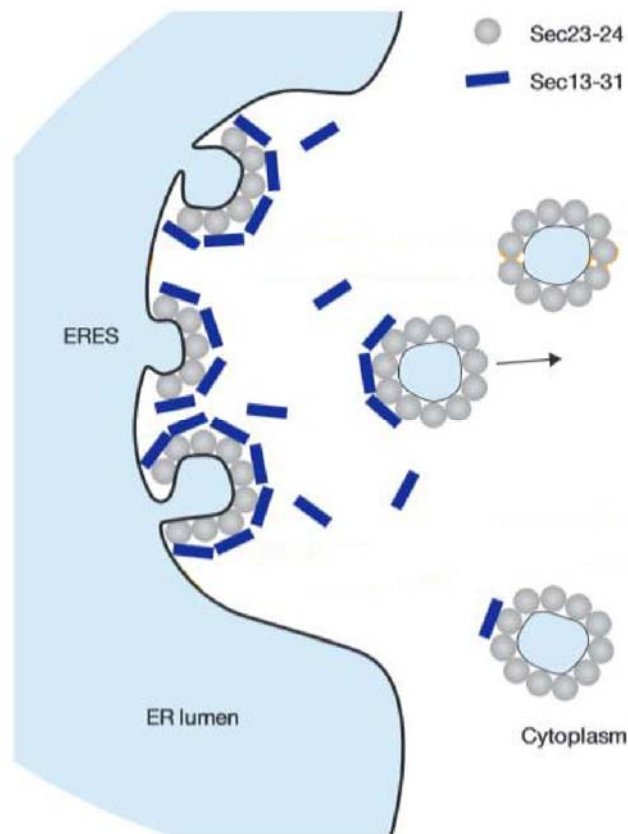


Figure 1-4: Schematic representation of ERES and involved proteins.

COPII-coated vesicles form at cup-like shapes on the ER. The inner COPII-coat consists of SEC23-SEC24 heterodimer and the outer coat is formed by SEC13-SEC31. COPII vesicles traffic towards destined structures (arrow). Adapted from (Zanetti et al., 2012).

1.2.2 ERES

The ER exit sites are the most important loci for proteins to initiate trafficking from the ER through the secretory pathway of the cell and therefore provide a platform for regulation of the cargo recruitment and sorting (fig. 1-3 and 1-4). The size and position of ERES is highly variable and depends on the amount of cargo. With an increase of ER cargo proteins, the

number of exit sites is elevated and the vesicles are enlarged (Farhan et al., 2008). Besides this assembly machinery (described in chapter 1.2.1) two kinds of cargo receptors exist. On the one hand there are membrane receptors that recruit cargo to the inner layer of the vesicle, travel with it along the pathway and are transported back to ER via the retrograde pathway. For instance, such shuttling cargo adaptors are the SEC24 proteins, further described in the next chapter (chapter 1.2.3).

The other class of receptors comprises ER-resident proteins, which assist in the incorporation of cargo into the vesicles. An example for this type of receptors is TANGO1 that was identified in mammals to couple secretory cargo, like collagens, to the COPII machinery. In this process, TANGO1 binds to SEC23 and collagen preventing the recruitment of SEC31 and thereby allowing SAR1 to extend the coat polymerization adapting the vesicle size for bulky collagen fibers (Saito et al., 2009). After the incorporation of collagen TANGO1 dissociates from the site of action, facilitating vesicle scission.

1.2.3 Role of SEC24D

In mammals there are four isoforms of SEC24 (SEC24A-D) that confer selectivity toward cargo export (Lord et al., 2013). The binding specificity of the different isoforms is mediated by their preference to different motifs in the interacting proteins. For example, cargo recruitment specific for SEC24A is di-leucine dependent but the preferences partially overlap, so that SEC24 protein operate in redundant manner (Wendeler et al., 2007). In this context, two distinct subgroups are identified, SEC24A/B and SEC24C/D, which preferentially capture the same cargo proteins (Pagano et al., 1999).

SEC24A/B is required for packaging planar cell polarity receptors (Merte et al., 2010), whereas the SEC24C/D pair mediates export of the neurotransmitter receptors for serotonin and γ -aminobutyric acid (GABA) transporter 1 (GAT1) (Farhan et al., 2007). Further the SEC24C/D couple shows preference for adapting GPI-anchored proteins to COPII vesicles. For instance, the human GPI-anchored protein CD59 exits the ER in an SEC24-dependent manner, with preference for SEC24C/D (Bonnon et al., 2010). The recycling transmembrane protein complex p24-p23 also requires preferentially SEC24C/D for its ER export (Bonnon et al., 2010). Consequently, SEC24 proteins share the cargo recruiting function, but favor different cargo types and therefore provide specificity to COPII vesicles.

1.2.4 Regulation and assisting factors of the secretory pathway

Besides the minimal machinery of the secretory pathway (described in chapter 1.2.1) various additional components and accessory factors participate in the process. Among several cargo receptors is ERGIC53 (LMAN1), a mannose-binding lectin, which is associated to COPII

machinery and is required for transport of glycoproteins and several coagulation factors (Townley et al., 2008).

The transport protein SEC16 plays an essential role in the organization and stabilization of ERES (Sprangers and Rabouille, 2015). SEC16 directly binds to SEC23/24/31, stabilizing the SAR1-SEC23-SEC24 complex and therefore serves as a scaffold for COPII coat assembly. Moreover, SEC16 localizes to cup-like shape membrane structures and regulates the COPII coat formation through controlling the SAR1 activity. Hence, SEC16 functions as a regulatory factor of COPII coat formation and is employed as molecular marker for ERES (Hughes et al., 2009).

Another assisting factor exhibits p125A. Initially identified as SEC23 interacting protein (SEC23IP), p125A is required for COPII-vesicle biogenesis. The protein is enriched in ERES in a SAR1A-dependent manner and directly associates with SEC13/31A. Overexpression of p125A causes clustering of ER proteins at perinuclear spaces whereas depletion of p125A delays ER export and results in fragmentation and dispersion of the Golgi apparatus (Ong et al., 2010). Moreover, p125A facilitates ER export in mammalian cells by stabilization of ERES. The protein encompasses a lipid binding motif, employing lipid signals to control ERES assembly by stabilization of the membrane association and regulation of the COPII segregation from SEC16A (Klinkenberg et al., 2014).

1.2.5 Role of ER architecture in HSP disease

Among the numerous genetic loci linked to HSP, many genes encoding proteins involved in ER associated processes such as ER architecture maintenance and ER export are present, consistent with a critical dependency of motor neurons on accurate intracellular proteins sorting and organelle distribution.

The ER consists of tubular and sheet-like structures, with varying sizes from 30 to 100 nm. In the different structural regions, specific sets of proteins are enriched, defining tubular or sheet organization. For instance cytoskeleton-associated protein 4 (CKAP4 alias CLIMP63) is an ER protein mainly expressed in the sheets and mediating the anchoring of microtubules to ER (Nikonov et al., 2007). An established marker for tubular ER structures is ZFYVE27 (protrudin). Protrudin is described as an interactor of the GDP-bound form of Rab11 and operates as a positive regulator of neurite formation (Shirane and Nakayama, 2006). Interestingly, cells with a mutation in the gene of ZFYVE27 are characterized by aberrant patterns of the tubular ER structures and could be connected to hereditary spastic paraparesis (Mannan et al., 2006).

The GTPase atlastin-1, as one of the most frequent proteins in HSP diseases (see chapter 1.1.1), plays a role in homotypic fusion of tubular ER elements and in maintaining the shape of the ER membranes (Goyal and Blackstone, 2013).

As mentioned in chapter 1.1.1, the HSP linked protein TFG assists in ER export through the interaction of SEC16 to ERES. HSP patients also suffering from atrophy and hereditary motor and sensory neuropathy, show a lack of self-assembly of TFG oligomeric complexes. In fact, driving toxic gain of function of TFG and thereby deceleration of protein secretion from ER as well as alteration of the ER morphology, results in a collapse of the ER network. Moreover, upon malfunction of TFG, cytoplasmic neuronal inclusions carrying ubiquitin arise (Beetz et al., 2013). Notably, TFG is an inhibitory regulator of ubiquitin-proteasome system (UPS) (Yagi et al., 2014). Obviously, the ER architecture and function displays a critical role in HSP pathology and thereby may be important for maintenance of neuronal cells.

1.3 The endocytic pathway

The central transport process of proteins entering the cell is the endocytic pathway, whose main function is the shuttling of internalized cargo such as peptides, fluids, membrane parts or extracellular receptors. An essential aspect of endocytosis is the decision for cargo recycling or degradation. Cargo of early endosomes is transported from the *trans*-Golgi network or plasma membrane towards lysosomal degradation or shuttled back to the TGN for recycling. Both, the early-to-late endosome transition and the fusion to lysosomes comprise critical steps in the endocytic pathway and are described in the following section.

In the endosome maturation process two small GTPases RAB5A (yeast: Vps21) and RAB7A (yeast: Ypt7) play a key role. Rab proteins are GTPases, which exist in either inactive GDP- or active GTP-bound forms. In their active state their conformation allows binding to effector proteins. RAB5A-GTP, located on early endosomes, is involved in the recruitment of RAB7A. Subsequently, RAB5A is replaced by RAB7A, which displays a marker for late endosomes. The conversion is regulated by the SAND1/MON1-CCZ1 complex (Poteryaev et al., 2010). During the maturation intraluminal vesicles (ILVs) are formed by budding the endosomal membrane inwards and cargo is sorted into smaller sub-compartments inside the vesicle (Nickerson et al., 2007). This process is facilitated by the endosome sorting complex required for transport (ESCRT) machinery, which guides ubiquitylated cargo like membrane receptors, e.g. EGFR, into vesicles. Early endosomes pass through various cycles of fusion and fission. In this process RAB5A-GTP interacts with class c core vacuole/endosome tethering (CORVET) complex, which assists and facilitates further merging events of early endosomes (Perini et al., 2014).

Early endosomes result from invagination of the plasma membrane and during the maturation from early to late stage, the size and morphology of endosomes change and they move towards the perinuclear regions. Endosomes increase in size and cargo is sorted into smaller vesicles budding inside the fused endosomes. These emerging structures are termed multi-

vesicular bodies (MVBs). The further maturation process depends on the presence of active RAB7A. Therefore, RAB5A is inactivated and in parallel RAB7A is recruited to the endosomes and gets activated (Poteryaev et al., 2010). Subsequently, RAB7A-GTP interacts with homotypic fusion and vacuole protein sorting (HOPS) complex to mediate the fusion to lysosomes. This process is assisted by soluble NSF (N-ethylmaleimide-sensitive factor) attachment protein receptors (SNAREs) (Bonifacino and Glick, 2004). SNAREs are tail-anchored proteins with a C-terminal transmembrane domain that mix membrane bilayers and fuse the lumina of vesicles (Borgese and Fasana, 2011; Hegde and Keenan, 2011). Eventually, when late endosomes fuse with lysosomes, the cargo is degraded by proteases and endosomal components are recycled.

1.3.1 HOPS complex

To understand the mechanisms of the membrane fusion at endosomes, vacuoles and lysosomes it is necessary to focus on the role of the two tethering complexes mentioned before, CORVET and HOPS. The early-to-late endosome maturation is mediated by RAB5A-RAB7A conversion and the concomitant switch from CORVET to HOPS. Both complexes interact with Rab GTPases, tether membranes and mediate and proof-read SNARE assembly, thereby driving membrane fusion events (Zick and Wickner, 2013). CORVET associates with RAB5A at early endosomes and HOPS with RAB7A on late endosomes (Balderhaar and Ungermann, 2013; Solinger and Spang, 2013). In mammals the two hetero-hexameric complexes share a core complex comprising the four subunits VPS11, VPS16, VPS18 and VPS33. Whereas CORVET consists of additional Rab GTPases binding subunits VPS3 and VPS8, HOPS includes the additive complex members VPS39 and VPS41, which are also able to interact with Rab GTPases (fig. 1-5).

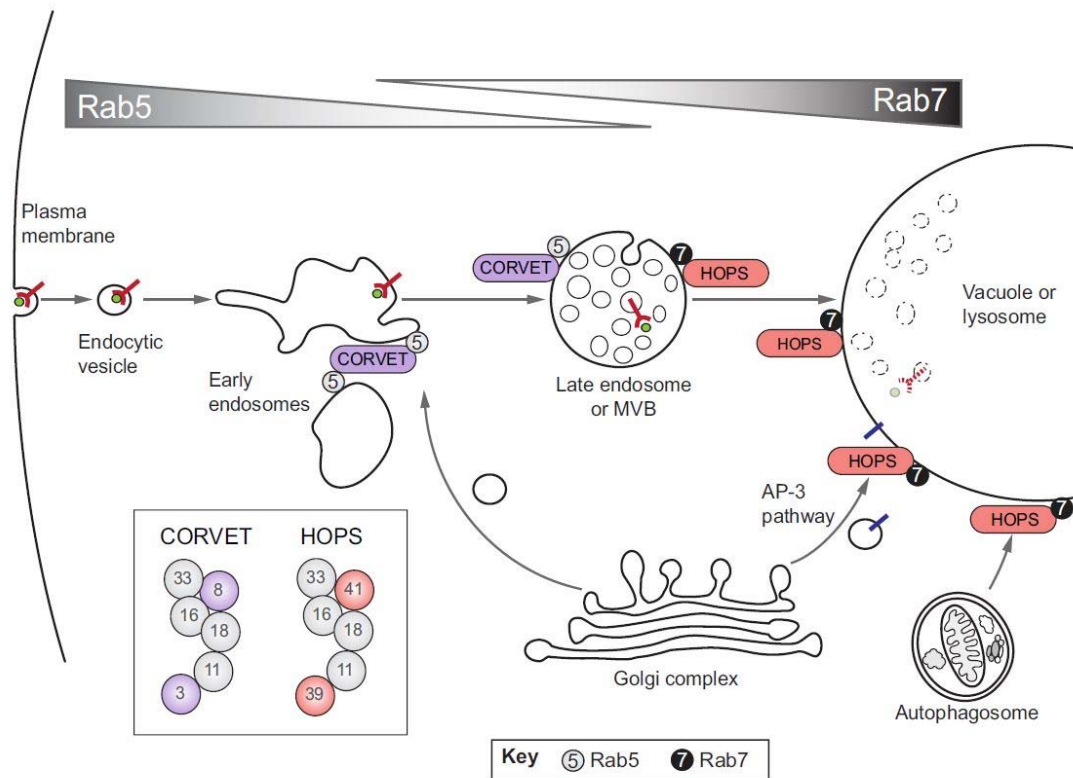


Figure 1-5: Schematic representation of the CORVET and HOPS complexes and their role in endocytosis.

The cargo, here a receptor-bound ligand, is internalized and transported within early endosomes. CORVET interacts with RAB5 and consequently facilitates the endosome-endosome fusion events. During maturation multi-vesicular bodies (MVBs) are formed and RAB5 is replaced by RAB7. Late endosomes bind to the HOPS complex, which leads to fusion to vacuole or lysosomes. Moreover, AP-3 vesicles (further described in chapter 1.3.2) fuse with lysosomes in a HOPS-dependent manner. Structured subunits of both complexes are depicted to visualize core and specific proteins. From (Balderhaar and Ungermann, 2013).

The two HOPS-specific RAB-interacting subunits VPS39 and VPS41 are located at opposing ends of the protein complex. This structural morphology allows the complex to bind to two different organelles at the same time and therefore possibly bridges those organelles, so that SNARE assembly is facilitated via the binding of Rab GTPases to each end of the HOPS complex (Brockner et al., 2012). Depletion of human VPS39 and VPS41 leads to accumulation of late endosomes and a decreased number of lysosomes. Thus, the two HOPS-specific subunits are required for homotypic fusion of endosomes and heterotypic fusion of late endosome to lysosomes (Pols et al., 2013).

Ypt7, the yeast homolog of RAB7A, recruits the HOPS complex to the endosome, while MON1-CCZ1 serves as guanidine exchange factor (GEF) for Ypt7, promoting the exchange of GTP to GDP and therefore leading to an inactivation of the protein. Since RAB7A is active and colocalized with HOPS, vacuolar SNAREs are recruited and assembled. Typically, one R-SNARE pairs with three Q-SNAREs; the SNARE types are defined by a highly conserved arginine (R) and glutamine (Q), respectively. By the correct organization of the SNARE pairs

inactive *cis*-SNARE changes to active *trans*-SNARE form. Appropriate paired SNAREs are prerequisite to drive fusion specificity, which is referred to as the proof-read of SNAREs (Collins and Wickner, 2007). The subunit VPS33, a SNARE master (SM) protein, binds to the *trans*-SNARE to direct the fusogenic activity (Pieren et al., 2010).

Therefore, HOPS is a tethering complex coordinating initial recognition of Rab GTPases and subsequently enabling recruitment of vesicles to facilitate lysosome fusion events.

1.3.2 BLOC-1 complex

The biogenesis of lysosome related organelles-1 complex (BLOC-1) is another complex playing an immense role in endosome trafficking. BLOC-1 contains at least eight subunits, BLOS1, BLOS2, BLOS3, cappuccino (CNO), dysbindin (DTNBP1), MUTED, pallidin (PLDN) and SNAPIN (Lee et al., 2012) (fig. 1-6).

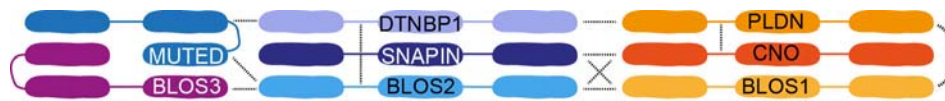


Figure 1-6: Model for organization of the BLOC-1 complex.

Arrangement and distinct position of subunits within the complex. Intra-complex associations are depicted with dashed-lines. Adapted from (Lee et al., 2012).

BLOC-1 interacts with SNARE proteins and may regulate fusion of endosomal membranes. In studies of the Hermansky-Pudlak syndrome (HPS) various mutations in *BLOC-1* genes were identified (Setty et al., 2007).

Hermansky Pudlak syndrome (HPS) defines a group of human autosomal disorders characterized by skin depigmentation, lung fibrosis, immunodeficiency and pigmentary or non-pigmentary albinism (Huizing et al., 2002; Li et al., 2004; Wei, 2006). The worldwide incidence rate adds up to 1:18,000 and the onset varies from early childhood up to seniority cases. First described as pigmentary and non-pigmentary abnormalities by Hermansky and Pudlak (Hermansky and Pudlak, 1959), the disease affects mainly the biogenesis of lysosome-related organelles such as melanosomes and platelet dense granules (Wei and Li, 2013). Nine gene loci causing HPS have been identified, all encoding proteins of five complexes: AP-3, HOPS, BLOC-1, BLOC-2, and BLOC-3 (Di Pietro and Dell'Angelica, 2005; Li et al., 2004).

AP-3 is a coat protein complex involved in vesicle formation and cargo selection in the endo-lysosomal system. Among the genes coding for HOPS subunits mutation of *VPS33* leads to a form of HPS (Suzuki et al., 2003). Besides BLOC-1, two other BLOC-complexes exist. BLOC-2 consists of the subunits HPS3, HPS5, and HPS6 while BLOC-3 comprise HPS1 and HPS4,

which all have been found mutated in patients suffering from HPS. However, most types of HPS are caused by mutations in the genes of BLOC-1 complex subunits.

BLOC-1 is important for the biogenesis of melanosomes and platelet-dense granules since BLOC-1-deficient mice suffer from a dramatically reduced number of melanosomes and a depigmentation of the skin (Morgan et al., 2006). Moreover, loss of BLOC-1 results in missorting of selective cargo proteins from early endosomes destined for melanosomes, e.g. tyrosinase-related protein-1 (Typr1) (Di Pietro et al., 2006).

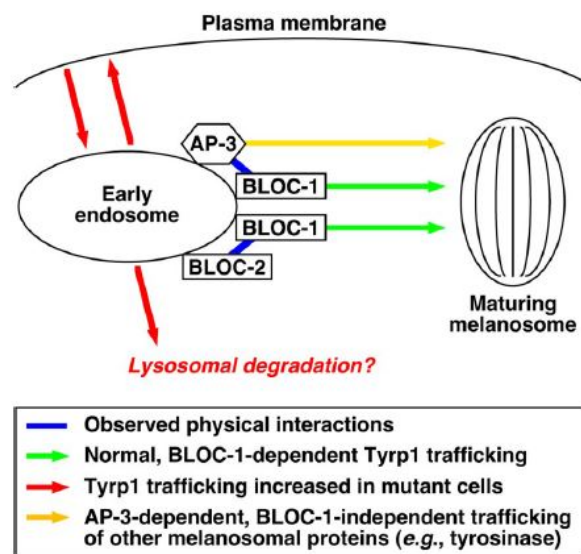


Figure 1-7: Model of interplay between the complexes BLOC-1, BLOC-2 and AP-3.

Trafficking of the specific cargo Typr1 from early endosome to melanosome. From (Di Pietro et al., 2006).

BLOC-1 associates with AP-3 to facilitate trafficking and sorting of AP-3 cargo towards melanosomes (Huizing et al., 2001; Peden et al., 2004) (fig. 1-7). Together, both complexes affect targeting of SNARE and non-SNARE cargos of the AP-3 complex. Thus, BLOC-1 functions as sorting complex for membrane proteins (Salazar et al., 2006). The complex also operates as an adaptor of different parts of the endo-lysosomal pathway. In this regard, BLOC-1 recruits the GTPase activating protein (GAP) for the yeast homolog of RAB5A, Vps21 (John Peter et al., 2013) (compare with chapter 1.3.1). Similar to HOPS, BLOC-1 is responsible for cargo trafficking within the endosomal pathway, but both protein complexes act on different steps and maintain discriminative processes.

1.4 Autophagy

Besides other degradation processes like the endocytic pathway, autophagy is the only lysosome-based degradation pathway for cytosolic cargo. During macroautophagy (referred

to hereafter as autophagy) misfolded proteins, damaged organelles or pathogens are sequestered into double membrane vesicles, termed autophagosome, and subsequently delivered to lysosomes for degradation (fig. 1-8). To date, two other general types of autophagy are known. Firstly, during microautophagy substrates are directly invaginated by endosomal and lysosomal membranes. Secondly, in chaperone-mediated autophagy (CMA) the Hsp70 chaperone captures soluble proteins with KFERQ-like penta-peptides and translocates those to lysosomes in a LAMP2A-dependent manner (Rogov et al., 2014).

The autophagic pathway is an essential cellular process associated with cancer, neurodegenerative diseases, clearance of microbial infections and ageing. This pathway developed as an adaption to deprivation of nutrients and their mobilization within the cell. Further, autophagy is critical for degradation of potential toxic structures such as misfolded proteins, defect organelles or intracellular pathogens. Besides bulk autophagy, in which portion of the cytosol are randomly sequestered into autophagosomes in response to nutrient limitations, selective autophagy allows degradation of specific cargo. Different types of selective autophagy in distinct organelles are determined by discriminating selective cargo receptors. For instance, sequestosome-1 (SQSTM1, p62) was the first described mammalian autophagy receptor, recruiting protein aggregates to growing autophagosomes (Bjorkoy et al., 2005; Pankiv et al., 2007). Another autophagy receptor displays NIX (alias BCL-2), which mediates autophagic engulfment of mitochondria, coined mitophagy (Novak et al., 2010), or optineurin (OPTN) important for xenophagy, which represents autophagosomal clearance of intracellular pathogens (Wild et al., 2011).

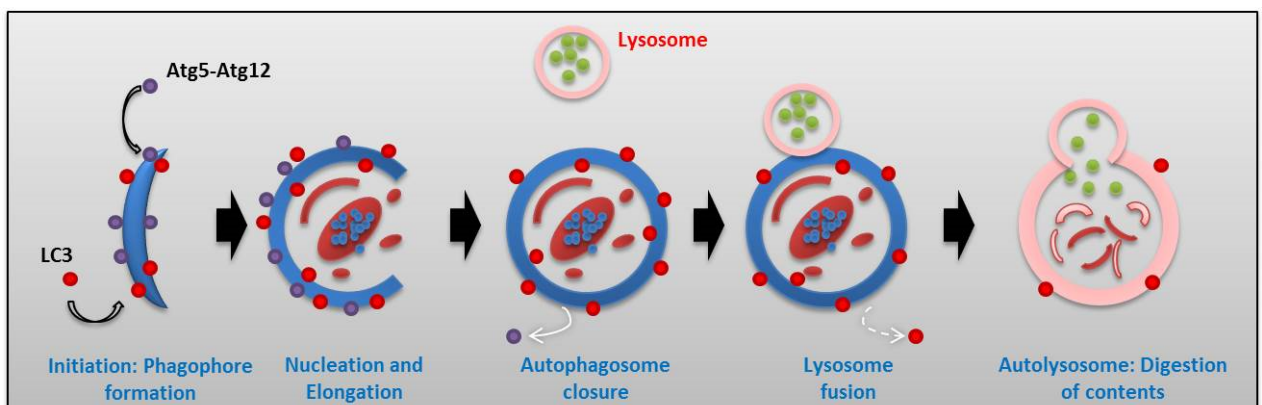


Figure 1-8: Representative overview of the autophagic pathway.

Initiated by the generation of a phagophore, membranes are nucleated and elongated and cytoplasmic contents are engulfed. After their closure autophagosomes fuse with lysosomes. Finally, the contents are degraded in the autolysosomes upon acidification.

Autophagy is a tightly regulated process, which is initiated by a signaling cascade involving the serine-threonine kinase Unc-51-like kinase (ULK1/2) (Carlsson and Simonsen, 2015). ULK1/2

is activated by the release of the inhibitory kinase mammalian TOR complex (mTORC1), which leads to phosphorylation of ATG13 and FIP200, the regulatory subunits of ULK1/2 (Ganley et al., 2009). ATG9, a transmembrane protein derived from recycling endosomes, delivers membranes to nucleate the lipid-bilayers termed phagophore, which engulfs cytoplasmic cargo (Webber and Tooze, 2010; Yamamoto et al., 2012). The nucleation process of pre-autophagosomal structures (PAS) is mediated by the phosphoinositide-3-kinase (PI3K) complex comprising VPS34 (PIK3C3), VPS15, Beclin-1 and ATG14L (Itakura et al., 2008). This lipid kinase complex generates phosphatidylinositol 3-phosphate (PI(3)P), a key lipid of autophagy, which recruits PI(3)P effector proteins promoting phagophore nucleation (Lamb et al., 2013).

One of those effectors, contributing to autophagy initiation phase, is PI(3)P-binding double FYVE-containing protein-1 (DFCP1), located at omegasomes, which are the autophagosome formation sites on ER membrane (Axe et al., 2008). The second group of PI(3)P effectors are the WD-repeat protein interacting with phosphoinositides (WIPI) proteins. This is a family of human β -propeller containing proteins that bind phosphoinositides (PROPPINS) (Michell et al., 2006), comprising four members: WIPI1-4. WIPI1 was the first WIPI family member shown to be involved in the autophagic pathway (Proikas-Cezanne et al., 2004). Similar to WIPI1, WIPI2 bridges PI(3)P production and LC3-lipidation (further described in chapter 1.4.1) (Lamb et al., 2013). This bridging is mediated by WIPI2 specifically binding to ATG16L1 and thereby recruiting the ATG12~5-16L1 complex which is required for the LC3 lipidation (Dooley et al., 2014). Both proteins bind PI(3)P at early autophagosomes and are located at the outer and inner autophagosomal membrane upon autophagy induction, but only during initiation process (Polson et al., 2010). Under basal conditions WIPI1/2 is located at the plasma membrane and the ER, providing membrane sources for autophagy. On ER, WIPI2 positions the LC3 UBL conjugation machinery (further described in the next chapter) by recruitment of ATG16L1 at the phagophore formation site (Dooley et al., 2014).

1.4.1 The ubiquitin like conjugation system

During autophagy ATG8 proteins are lipidated by an UBL machinery. The underlying process of the ubiquitin-like conjugation system is the catalysis of the covalent attachment of the UBL protein to another protein or a lipid. After synthesis as precursor, the UBL protein exposes the C-terminal glycine during the maturation process and is conjugated to the lysine of another protein. The cascade involves activating (E1), conjugating (E2) and ligating (E3) enzymes (Rogov et al., 2014). As mentioned above, two ubiquitin-like (UBL) proteins display a key role in the elongation and closure phase of autophagy.

The first is ATG12 which is part of the ATG12~5-16L1 complex (in which ~ refers to a covalent bond) that functions as the E3 ligase for the second UBL ATG8. During the conjugation

process, the E1 ATG7 initiates the transfer of ATG12 to its E2 ATG10, which mediates covalent attachment of ATG12 to ATG5. ATG16L1 joins the ATG12~5 conjugate and mediates localization of this complex to the PAS. The ATG12~5-16L1 complex is responsible for the recruitment of the soluble ATG8-family proteins (ATG8-I) and their conjugation to phosphatidylethanolamine (PE) (lipidated ATG8 or ATG8-II) (Slobodkin and Elazar, 2013). The ATG8 precursor is processed by the cysteine protease ATG4 to expose the C-terminal glycine. Activated by ATG7 (E1), ATG8 is subsequently transferred to ATG3 (E2) and finally linked to PE via ATG12~5-16L1 complex (E3). Lipidated ATG8 is embedded into both layers of the autophagosomal membrane, where it operates as a receptor for autophagic cargo. In the following step, ATG8-PE tethers lipid bilayers and provide a docking site for additional factors assisting in autophagosome closure. Finally, after closure the autophagosome fuses with a lysosome to form an autolysosome, followed by its acidification and subsequent degradation of enclosed cytosolic cargo.

In mammals the family of ATG8 proteins encompasses seven members (MAP1LC3A (LC3A), MAP1LC3B (LC3B), MAP1LC3B2 (LC3B2), MAP1LC3C (LC3C), GABARAP, GABARAPL1, GABARAPL2 (GATE-16)), which all share high sequence homologies and a structural similarity to ubiquitin (fig. 1-9) (Shpilka et al., 2011).

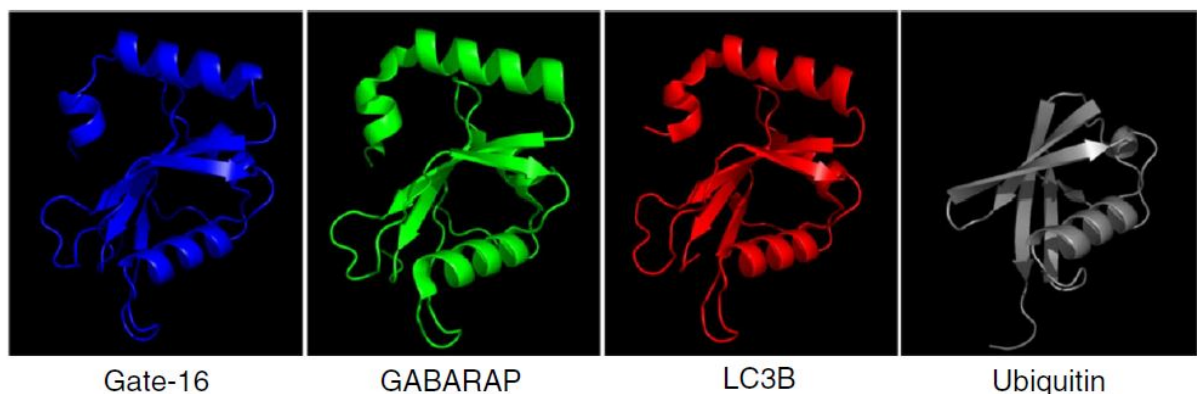


Figure 1-9: Crystal structure of the ATG8 subfamily representatives and ubiquitin.

ATG8 proteins share an ubiquitin-like fold with two additional N-terminal α -helices. Helices represent α -helices and arrows represent β -sheets. From (Shpilka et al., 2011).

Besides the UBL core, mammalian ATG8 proteins comprise two additional N-terminal α -helices. ATG8 proteins apply a highly conserved docking site for specific non-covalent binding partners. These sites are termed hydrophobic pockets, of which exist two in ATG8 proteins. The first hydrophobic pocket (HP1) is formed by the additional N-terminal α -helices and another (HP2) between the central α -helix and the second β -sheet of the UBL core (Shpilka et al., 2011).

Proteins associating with the ATG8 ubiquitin-like proteins for instance include autophagic cargo receptors (e.g. SQSTM1) and effector proteins (e.g. FYCO1), respectively. These proteins employ a canonical motif termed ATG8-family interacting motif (AIM) or LC3 interacting region (LIR) which incorporate the four amino acid consensus motif W/F/Y-X-X-L/I/V (x stands for any amino acids) (Johansen and Lamark, 2011). The side chain of the aromatic residue fits into HP1 and the hydrophobic side chain into HP2. Acidic or phosphorylated groups directly upstream of the LIR sequence contribute to the negative charge and therefore strengthen the association (Ichimura et al., 2008; Rogov et al., 2014).

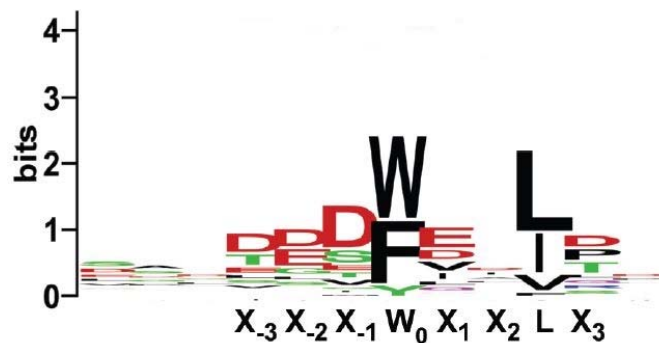


Figure 1-10: Consensus sequence of the LIR motif.

Logo is based on 25 different LIR sequences of 21 proteins directly interacting with ATG8 family members. From (Johansen and Lamark, 2011).

Furthermore, the ATG8 proteins are classified in three subfamilies. The LC3 family with its members LC3A-C was discovered as microtubule-associated proteins (MAP1LC3) predominantly expressed in the cytoplasm and endomembrane system (Kuznetsov and Gelfand, 1987; Mann and Hammarback, 1994). The GABARAP proteins subgroup consists of GABARAP and GABARAPL1, which are also localized in the cytoplasm and endomembrane system (Wang et al., 1999) but in addition also at autophagosomes and Golgi membranes (Kabeya et al., 2004; Kittler et al., 2001). They are known to play a role in the transport of GABA(A) receptors (Chen et al., 2000). Third subfamily includes Golgi-associated ATPase enhancer of 16kDa (GATE-16, GABARAPL2), which is mainly expressed in the Golgi apparatus and in cytoplasmic vesicles like autophagosomes (Kabeya et al., 2004). GABARAPL2 modulates the intra-Golgi transport via coupling the NSF and SNARE activation. The best understood family member is MAP1LC3B (LC3B), whose PE conjugates are incorporated into both layers of incipient autophagosomes, thereby providing a docking site for cargo receptors and regulatory adaptor proteins (Stolz et al., 2014).

While the MAP1LC3 subfamily is involved in the elongation of the phagophore membrane, GABARAP/GATE-16 members act in later stages of autophagosome maturation (Weidberg et al., 2010).

1.4.2 HOPS and BLOC-1 in autophagy

Recently, the HOPS complex was linked to the autophagic pathway. Whereas the interaction of UV radiation resistance-associated protein (UVRAG) to Beclin-1 controls the fusion of endosomes, UVRAG cooperates with HOPS to promote the fusion of autophagosomes to lysosomes (Liang et al., 2008). Depletion of the subunit VPS16 disrupts the HOPS complex and reduces the number of LC3 localized with lysosomes. This fact reveals a role for HOPS in the delivery of LAMP1 to the lysosomal membrane.

HOPS subunits VPS33A and VPS16 also interact with Syntaxin 17 (STX17), which was identified as the autophagic SNARE required for autophagosome-lysosome fusion (Itakura et al., 2012). Depletion of HOPS complex results in accumulation of STX17 and LC3-positive autophagosomes, giving rise to the following model: Upon induction of autophagy STX17, residing on ER, mitochondria, and in the cytosol, translocates to the autophagosomes and then recruits the HOPS complex from the endo-lysosomal system (Jiang et al., 2014). Moreover RAB7A regulates maturation of late autophagic vacuoles dependent on its GTPase activity (Gutierrez et al., 2004; Jager et al., 2004). As HOPS complex serves as the GEF for RAB7A, it seems very likely that HOPS is involved in regulating autophagosome maturation as well (Wang et al., 2011).

Another linking element between endo-lysosomal pathway and autophagy is PLEKHM1. This adaptor protein promotes fusion of endosomes and lysosomes dependent on HOPS and Rab7. Moreover PLEKHM1 interacts with ATG8-family proteins and mediate auto-lysosomal fusion. This protein is a functional link between autophagic and endocytic parts of the endo-lysosomal system and acts as an endocytic adaptor generally involved in lysosome fusion events (McEwan et al., 2015).

Also, the BLOC-1 subunit SNAPIN is connected to autophagic processes. SNAPIN interacts with the dynein intermediate chain (DIC) of the dynein complex and regulates the recruitment of late endosomes toward lysosomes. Upon depletion of SNAPIN in neurons immature lysosomes accumulate and retrograde transport of RAB7A-positive late endosomes is impaired. Moreover, loss of SNAPIN causes an increase of lipidated LC3, pointing to a blockage of autophagy. On the other hand, overexpression of SNAPIN leads to elevated formation of lysosomes and facilitates fusion between late endosomes and lysosomes. Notably, SNAPIN improves fusion frequency of endosomes as well as autophagosomes to lysosomes by concentration of lysosomes in the perinuclear region (Cai et al., 2010; Yuzaki, 2010).

1.5 Aim of the present work

TECPR2 was initially discovered as a positive regulator of autophagy interacting with GABARAP, a member of the mammalian ATG8 protein family (Behrends et al., 2010). TECPR2 was linked to autophagic dysfunction in an autosomal-recessive form of hereditary spastic paraparesis (HSP) (Oz-Levi et al., 2012). An exome sequencing of four unrelated patients revealed a single-base deletion resulting in a premature stop codon in the *TECPR2* gene, which drives rapid degradation of the encoded protein in these patients. Using HSP patient derived fibroblasts it was shown that the *TECPR2* mutation driving decreased accumulation of lipidated LC3B upon blockage of autophagy with the inhibitor Bafilomycin A1 preventing of lysosomal degradation.

The key question of this study dealt with the identification of an explanation for the autophagic phenotype of TECPR2. In order to achieve the aim several intermediate steps needed to be performed. First of all potential interacting candidates of TECPR2 were sought to be identified in proteomic studies, the cellular localization of the protein was intended to be determined and a detailed analysis of the phenotype upon knockdown should be performed. After choosing several of the validated candidates the focus would move on the exploration of phenotypes on these candidates upon TECPR2 depletion and the definition of the most upstream event causing those. To strengthen the published data about TECPR2 this work also should provide evidence for the binding of TECPR2 to ATG8 proteins by identification of the ATG8 interacting motif (AIM).

Eventually, the first link between autophagy, TECPR2 and its mechanistic contribution to HSP was aimed to decipher.

2. Material and Methods

2.1 Materials

2.1.1 Chemicals

Acetic acid (Sigma, St. Louis, USA)

Acetone (Sigma, St. Louis, USA)

Acetonitrile (Sigma, St. Louis, USA)

Acrylamide (AppliChem)

Agarose (Lonza)

Ammonium bicarbonate (Fluka)

Ammonium persulfate (APS) (Sigma, St. Louis, USA)

AppliChem 1kb DNA ladder (NEB)

Bacto tryptone (Becton Dickinson)

Bafilomycin A1 (Sigma, St. Louis, USA)

Benzonase (Millipore)

Biotin (Sigma)

Blasticidine (Sigma, St. Louis, USA)

Bortezomib/Velcade® (Millennium Pharmaceuticals Inc., Cambridge, USA)

Bovine serum albumin (Sigma, St. Louis, USA)

Brefeldin A (Tocris)

Bromophenol Blue sodium salt (Sigma, St. Louis, USA)

Carbenicillin (Sigma, St. Louis, USA)

Chloramphenicol (Sigma, St. Louis, USA)

Complete EDTA-free protease inhibitor tablets (Roche)

Coomassie Brilliant Blue R-250 (Fisher Scientific)

Disodium phosphate (Sigma, St. Louis, USA)

Dithiothreitol (DTT) (Roth)

DMEM (Life technologies)

DMSO (Sigma, St. Louis, USA)

Doxycycline (Sigma, St. Louis, USA)

EDTA (AppliChem)

EGTA (AppliChem)

Ethanol (Roth)

FBS (Life technologies)

Gateway® BP Clonase Enzyme mix (self-made; gift from W. Harper)

Gateway® LR Clonase Enzyme mix (Life technologies)

Material and Methods

Glutathione sepharose 4B (GE Healthcare)
Glycine (Sigma, St. Louis, USA)
Glycerol (VWR)
Hygromycin (Invitrogen)
IGEPAL® CA-630 (Sigma, St. Louis, USA)
Influenza Hemagglutinin (HA) peptide (Sigma, St. Louis, USA)
Isopropyl β -D-1-thiogalactopyranoside (IPTG) (Sigma, St. Louis, USA)
Kanamycin sulfate (Roth)
KOD Hot Start Polymerase (Novagen)
LB (Roth)
LB-Agar (Roth)
L-Glutamine 200 mM (Life technologies)
Lipofectamine 2000 (Life technologies)
Lipofectamine RNAiMax (Life technologies)
Low fat milk (Roth)
Lysozyme (Sigma, St. Louis, USA)
Magnesium sulfate (Sigma, St. Louis, USA)
Manganese chloride (Sigma, St. Louis, USA)
Methanol (Sigma, St. Louis, USA)
 β -Mercaptoethanol (Sigma, St. Louis, USA)
Midori Green (Biozym)
Monoclonal Anti-HA-Agarose antibody (HA beads) (Sigma, St. Louis, USA)
MOPS buffer (Sigma, St. Louis, USA)
NativePAGE™ Novex® 4-16% Bis-Tris Gels (Life technologies)
Neon transfection system (Life technologies)
N-Ethylmaleimide (Sigma, St. Louis, USA)
Nitrocellulose membranes (NitroBind 0.45 μ m, Fisher Scientific)
Nonidet™ P40 substitute (Sigma, St. Louis, USA)
OptiMEM (Life technologies)
Paraformaldehyde; 4% in PBS (Santa Cruz)
PBS (Life technologies)
Penicillin-Streptomycin (10,000U/ml) (Life technologies)
Polybrene (Merck Millipore)
Poly-L-lysine solution (Sigma, St. Louis, USA)
Polyethylenimine (PEI) (Polysciences Europe GmbH)
Ponceau S (AppliChem)
Potassium chloride (Sigma, St. Louis, USA)

Material and Methods

Potassium phosphate (Sigma, St. Louis, USA)
PMSF (Sigma, St. Louis, USA)
Prolong Gold with/without DAPI (Life technologies)
Protein -A/G-sepharose (Santa Cruz)
Protein Marker VI (10-245) prestained (AppliChem)
Puromycin dihydrochloride (Sigma, St. Louis, USA)
Restore PLUS Western Blot Stripping Buffer (Thermo Fisher)
Restriction endonucleases (NEB)
RPMI (Life technologies)
Rubidium chloride (VWR)
Spectinomycin (Sigma, St. Louis, USA)
Sodium chloride (Sigma, St. Louis, USA)
Sodium deoxycholate (Roth)
Sodium dodecyl sulfate (SDS) (Sigma, St. Louis, USA)
T4 DNA ligase (Fermentas)
Tetramethylethylenediamine (Roth)
Torin1 (Tocris)
Trichloroacetic acid (Sigma, St. Louis, USA)
Tris (AppliChem)
Triton-X-100 (VWR)
Trypsin (sequence-grade) (Promega)
Trypsin-EDTA 0.5% / 0.25% (Life technologies)
Tween-20 (Roth)
Western Lightening Plus-ECL (Perkin Elmer)
Westran Clear Signal, 0.45µm PVDF blotting membrane (Whatman)
Yeast extract (Becton Dickinson)
Zeocin™ (Invitrogen)

2.1.2 Buffers and media

PBS-T

137 mM NaCl
2.7 mM KCl
9 mM Na₂HPO₄
3 mM KH₂PO₄
0.1% Tween 20
pH 7.40

Material and Methods

MCLB buffer

50 mM Tris [pH 7.4]

150 mM NaCl

1% NP40

complete EDTA-free protease inhibitor tablets (Roche)

Denaturing buffer for denaturing IP

2% SDS

10 mM Tris [pH 7.4]

150 mM NaCl

10 mM NEM

Dilution buffer for denaturing IP

10 mM Tris [pH 7.4]

150 mM NaCl

0.5% IGEPAL

10 mM NEM

1 mM PMSF

complete EDTA-free protease inhibitor tablets (Roche)

Wash buffer for denaturing IP

10 mM Tris [pH 7.4]

150 mM NaCl

0.5% IGEPAL

10 mM NEM

complete EDTA-free protease inhibitor tablets (Roche)

1x Wet Blot transfer buffer

190 mM glycine

25 mM Tris [pH 8.8]

0.37% SDS

20% Methanol

Laemmli buffer

25 mM Tris

190 mM glycine

1% SDS

Material and Methods

1x TAE buffer

40 mM Tris
20 mM acetic acid
1 mM EDTA
pH 8.3

1x GST-PD wash buffer

50 mM Tris [pH 7.5]
10 mM EDTA
5 mM EGTA
150 mM NaCl
1 mM DTT

5x SDS-PAGE loading buffer

200 mM Tris [pH 6.8]
6% SDS
20% Glycerol
10% β -Mercaptoethanol
Bromophenol Blue

NativePAGE lysis buffer

25% NativePAGE sample buffer (Invitrogen, 4x)
10% G-250 sample additive (Invitrogen)
0.1% Triton-X 100

NativePAGE Running buffers

20x NativePAGE Running buffer
Cathode additive (dark cathode buffer: 5%, light cathode buffer: 0.5%)

TFB1 buffer

100mM rubidium chloride
50 mM manganese chloride
30 mM potassium acetate
10 mM calcium chloride
15% glycerol

Material and Methods

TFB2 buffer

10 mM MOPS [pH 8.0]
10 mM rubidium chloride
30 mM potassium acetate
10 mM calcium chloride
15% glycerol

SOB medium

2% (m/v) bacto tryptone
0.5% (m/v) yeast extract
10 mM NaCl
25 mM KCl
10 mM MgCl₂
10 mM MgSO₄
pH 6.7-7.0

DMEM

Dulbecco's Modified Eagle Medium, high glucose, pyruvate (Life technologies Cat.-No. 41966-029)

OptiMEM

OptiMEM® I Reduced Serum Medium (Life technologies Cat.-No. 31985-062)

RPMI

RPMI 1640 Medium (Life technologies Cat.-No. 21875-034)

Fetal Bovine Serum

Fetal Bovine Serum, qualified, E.U.-approved, South America origin (Life technologies Cat.-No. 10270-106)

2.1.3 Kits

GenElute MiniPrep kit (Sigma)
GenElute HP Plasmid MaxiPrep kit (Sigma)
KOD Hotstart DNA polymerase (Merck Millipore)
LightCycler® 480 SYBR Green I Master (Roche)
Pierce BCA Protein Assay kit (Thermo scientific)
QIAquick Gel Extraction kit (Qiagen)

RNeasy Plus Mini kit (Qiagen)

Transcriptor First Strand cDNA Synthesis kit (Roche)

2.1.4 Vectors, oligonucleotides and siRNAs

Table 1: Vectors used for cloning and expression:

vector	description	resistance	reference
pcDNA™5/FRT	mammalian expression vector	hygromycin	Life technologies
pDONR223	Gateway entry vector	spectinomycin	W. Harper
pHAGE-N-Flag-HA	for mammalian expression (transient and lentiviral), CMV promoter	carbenicillin puromycin	W. Harper
pHAGE-N-GFP	for mammalian expression (transient and lentiviral), CMV promoter	carbenicillin blasticidine	W. Harper
MSCV-I(N-Flag-HA)-IRES-PURO	for mammalian expression (transient and lentiviral), LTR-driven	carbenicillin puromycin	W. Harper
pOG44	Flp-Recombinase Expression vector	none	Life technologies
pRETRO-VSVG	packaging plasmid for retroviral transduction	carbenicillin	W. Harper
pRETRO-GAGPOL	packaging plasmid for retroviral transduction	carbenicillin	W. Harper
HDM-VSV-G	packaging plasmid for retroviral transduction	carbenicillin	W. Harper
HDM-tatlb	packaging plasmid for retroviral transduction	carbenicillin	W. Harper
HDM-Hgpm2	packaging plasmid for retroviral transduction	carbenicillin	W. Harper
RC-CMV-RevIb	packaging plasmid for retroviral transduction	carbenicillin	W. Harper
pET-60-DEST	vector for bacterial expression of a GST-fusion protein, T7 promoter	carbenicillin	Life technologies

Table 2: Open reading frames (ORF) used for cloning and expression vectors:

ORF	origin	accession number
BLOC1S1	OBS	BC130640
BLOC1S2	ORFeome	NM_001001342.1
BLOC1S3	OBS	BC151152
CNO	OBS	BC067815
DTNBP1	ORFeome	BC011912.2
GABARAP	ORFeome	NM_007278.1
GABARAPL1	ORFeome	NM_031412.2
GABARAPL2	ORFeome	NM_007285.6
MAP1LC3A	ORFeome	NM_032514.3
MAP1LC3B	ORFeome	NM_022818.4
MAP1LC3C	ORFeome	NM_001004343.2
MUTED	ORFeome	NM_201280.2
PLDN	ORFeome	BC004819.1
SAR1A	gift from H. Farhan	NM_001142648.1
SAR1A-T39N	gift from H. Farhan	NM_020150.4
SEC23A	gift from H. Farhan	NM_006364.2
SEC24D	Dharmacon	BC035761
SNAPIN	ORFeome	NM_012437.4
TECPR2	Life technologies	NM_014844.3
TIAM1	OBS	BC117196.1
VPS16	ORFeome	NM_022575.2
VPS18	ORFeome	NM_020857.2
VPS33A	ORFeome	NM_022916.4
VPS39	OBS	BC068559
VPS41	ORFeome	NM_014396.3

Table 3: Oligonucleotides used for cloning into pDONR223 (BP primers):

name	nucleotide sequence 5'-> 3'
BLOS1_for	GGGGACAACCTTTGTACAAAAAAGTTGGCATGGCCCCGGGGA
BLOS1_rev	GGGGACAACCTTTGTACAAGAAAGTTGGGTACTAGGAAGGGGCAGACTGC
BLOS3_for	GGGGACAACCTTTGTACAAAAAAGTTGGC ATGGCGTCCCAGGGTC
BLOS3_rev	GGGGACAACCTTTGTACAA GAAAGTTGGGTACTAGGCCCGCGGCC
CNO_for	GGGGACAACCTTTGTACAAAAAAGTTGGCATGGGAGGGTAGCTTTTCGGA
CNO_rev	GGGGACAACCTTTGTACA GAAAGTTGGGTATCAGAGCTGAGGCCTTTCAC
DTNBP1_for	GGGGACAACCTTTGTACAAAAAAGTTGGCATGCTGGAGACCCTTCGC
DTNBP1_rev	GGGGACAACCTTTGTACAAGAAAGTTGGGTATTAAGAGTCGCTGTCCTCACC
SEC23A_for	GGGGACAACCTTTGTACAAAAAAGTTGGCATGACAACCTATTTGGAATTCATT
SEC23A_rev	GGGGACAACCTTTGTACAAGAAAGTTGGCAAGCAGCCTGGACACGCA

name	nucleotide sequence 5'-> 3'
SEC24D_for	GGGGACAACCTTTGTACAAAAAAGTTGGCATGAGTCAACAAGTTACGTGG
SEC24D_rev	GGGGACAACCTTTGTACAAGAAAGTTGGGCACTAATTAAGCAGCTGACAGATCTCC
SNAPIN_for	GGGGACAACCTTTGTACAAAAAAGTTGGCATGGCGGGGGCTG
SNAPIN_rev	GGGGACAACCTTTGTACAAGAA AGTTGGGTATTATTTGCTGGGGAGCC
TECPR2_1-155aa_rev	GGGGACAACCTTTGTACAAGAAAGTTGGGTAAGAAGAATAAACAATTTTGCCTTTG
TECPR2_1260-1411_for	GGGGACAACCTTTGTACAAAAAAGTTGGCATGCCTGTCCAGCCCCG
TECPR2_1260-1411_rev	GGGGACAACCTTTGTACAAGAAAGTTGGGTGCTGGCCATGGAAGAGC
TECPR2_156-750aa_for	GGGGACAACCTTTGTACAAAAAAGTTGGCATGCTGGATCTAGACCAGGG
TECPR2_156-750aa_rev	GGGGACAACCTTTGTACAAGAAAGTTGG GTATTACTCATCGCTGGACGTTCA
TECPR2_270-1267aa_for	GGGGACAACCTTTGTACAAAAAAGTTGGCATGTTTGAAGTGCACCCGC
TECPR2_270-1267aa_rev	GGGGACAACCTTTGTACAAGAAAGTTGGGTACTACTAACTTCTGCTTACCTGGACAGG
TECPR2_for	GGGGACAACCTTTGTACAAAAAAGTTGGCATGGCATCGATATCAGAGCC
TECPR2_rev	GGGGACAACCTTTGTACAAGAAAGTTGGTCAGATGACCTCCCACTCGT
TECPR2-C-term_for	GGGGACAACCTTTGTACAAAAAAGTTGGCATGGAGGGACATCTATGCCCA
TECPR2-C-term_rev	GGGGACAACCTTTGTACAAGAAAGTTGG GCATCAGATGACCTCCCACTCGT
TECPR2-N-term_for	GGGGACAACCTTTGTACAAAAAAGTTGGCATGGCATGGATATCAGAGCC
TECPR2-N-term_rev	GGGGACAACCTTTGTACAAGAAAGTTGG GCAttACTCATCGCTGGACGTCA
VPS11_for	GGGGACAACCTTTGTACAAAAAAGTTGGCATGGTTCATCAAGAAAAAGAGTGAGAGTG
VPS11_rev	GGGGACAACCTTTGTACAAGAAAGTTGGTTAAGTGCCCTCCTGGAGT
VPS16_for	GGGGACAACCTTTGTACAAAAAAGTTGGCATG GACTGCTACACGGCG
VPS16_rev	GGGGACAACCTTTGTACAAGAAAGTTGGGCATCACTTCTTCTGGGCTTGTG
VPS18_for	GGGGACAACCTTTGTACAAAAAAGTTGGCATG GCGTCCATCCTGGAT
VPS18_rev	GGGGACAACCTTTGTACAAGAAAGTTGGGTA CTACAGCCAAGTCTGAGCTGCTC
VPS33A_for	GGGGACAACCTTTGTACAAAAAAGTTGGCATGGCGGCZCAZCTGTCC
VPS33A_rev	GGGGACAACCTTTGTACAAGAAAGTTGGGTACTAGAAAGTTTTTCCATCAGAGC
VPS39_for	GGGGACAACCTTTGTACAAAAAAGTTGGCATGCACGACGCTTTCGA
VPS39_rev	GGGGACAACCTTTGTACAAGAAAGTTGGTCAAGTGTGAGCTGGGTTTAC
VPS41_for	GGGGACAACCTTTGTACAAAAAAGTTGGCATGGCGGAAGCAGAGGA
VPS41_rev	GGGGACAACCTTTGTACAAGAAAGTTGGGTACTATTTTTTTCATCTCCAAATTGCA

Table 4: Oligonucleotides used for mutagenesis:

name	nucleotide sequence 5'-> 3'
LC3C-si1res-for	CCGGATTCCAGCAACTTCCTCCTGCCTTATGGCCAAGCTTTTCCTCTGCTTG
LC3C-si1res-rev	CAAGCAGAGGAAAAGCTTGGCCATAAGGCAGGAGGAAGTTGCTGGAATCCGG
TECPR2_deltaLIR_for	GGACCTTGGAGGACGAGTGATACCCAACCTTC
TECPR2_deltaLIR_rev	AGAAAGTTGGGTATCACTCGTCCTCCAGGTCC
TECPR2_F1138A_for	CCACGAAGGAAGGAAGCGCTCTGTGGCTGTGCCAGAG
name	nucleotide sequence 5'-> 3'
TECPR2_F1138A_rev	CTCTGGCACAGCCACAGAGCGCTTCCTTCCTTCGTGG

TECPR2_sires_for	CGGGCTGCTCAAGCCAGACCAATTCGCGGAAAGCTGGATGGGCTAC
TECPR2_sires_rev	GTAGCCCATCCAGCTTTCCGCGAATTGGTCTGGCTTGAGCAGCCCG
TECPR2_W1408A_for	GGACCTGGAGGACGAGGCTGAGGTCATCTGATACCC
TECPR2_W1408A_rev	GGGTATCAGATGACCTCAGCCTCGTCCTCCAGGTCC
TECPR2-C-term_for	GGGGACAACCTTTGTACAAAAAAGTTGGCATGGAGGACATCTATGCCCA
TECPR2-C-term_rev	GGGGACAACCTTTGTACAAGAAAGTTGGGCATCAGATGACCTCCCCTCGT
TECPR2-N-term_for	GGGGACAACCTTTGTACAAAAAAGTTGGCATGGCATCGATATCAGAGCC
TECPR2-N-term_rev	GGGGACAACCTTTGTACAAGAAAGTTGGGCATTACTCATCGCTGGACGTCA

Table 5: Oligonucleotides used for sequencing:

name	nucleotide sequence 5'-> 3'
CMV_for	CGCAAATGGGCGGTAGGCGTG
eGFP_328_for	ACGACGGCAACTACAAGACC
HA_for	CAAGGATGACGATGACAAGC
LC3C-for	ATGCCGCCTCCACAGA
LC3C-rev	CTAGAGAGGATTGCAGGGTCTG
M13_uni(-21)	TGTAAAACGACGGCCAGT
Myc-for	GCATCAATGCAGAAGCTGAT
T7	TAATACGACTCACTATAG GG
TECPR2_1370_for	GGACTTTGACCAGGAGCTTG
TECPR2_2281_for	GGGCTTCCTTCTTCATCCT
TECPR2_2836_for	AGATCACAGCCCGGAACAAT
TECPR2_3601_for	ACGGGCATGCACTGGAC
TECPR2_4081_for	GTGACTGCGTCAGATGAGCT
TECPR2-for	ATGGCATCGATATCAGAGCC
TECPR2-rev	CTAACTTCTGCTTACCTGGACAGG

Table 6: siRNAs (siGENOME) from GE Healthcare (Dharmacon) or Invitrogen (stealth):

siRNA	order number	sequence
si-custom control	custom made	GAUCCGCAGCGACAUCAACCUGA
si-ATG12	LU-010212-00-0002	GCAGUAGAGCGAACACGAA
si-DTNBP1	MQ-017455-01-0002	GAGCACACCCAGCAAUUGA
si-LC3B	MQ-012846-01-0002	CAAAGUUCUUGUACCUGA
si-LC3C	5260180 (Invitrogen-stealth)	GCUUGGCAAUCAGACAAGAGGAAGU
si-PIK3C3	LU-005250-00-0002	GAGAUGUACUUGAACGUAA
si-TECPR2	MU-014181-01-0002	CCAGAUCAGUUUGCAGAAA
si-VPS41	MU-006972-01-0002	GAGAAUGAAUGUAGAGAAU

2.1.5 Antibodies

Table 7: Listed are all antibodies used in immunoblot or immunostaining:

antigen	company	order number
ANP32A	Thermo	PA-30552
ATG12	Cell signaling	2010
ATG13	MBL	M183-3
BIP	Enzo	
BLOC1S3	Novus biologicals	NBP1-98303
CALR	Santa Cruz	sc-6467
CKAP4	gift from H. Farhan	
c-Myc	Santa Cruz	sc-40
DTNBP1	Bethyl	A303-360A
GABARAP	Abcam	ab109364
GOLGA2	Abcam	ab169276
GOLGB1	gift from H. Farhan	
GST-HRP	GE / Amersham	RPN1236
HA	Covance	MMS-101P
HERP	Enzo	
KPNA6	Abcam	ab105350
LC3B	Cell signaling	2775S
LC3B	MBL	PM036
LC3C	Immunoglobe	self-production
LF-68 (COL10A1)	gift from L. Fisher	
LMAN1	Sigma	E1031
NRF2	Abcam	ab62352
NUP98	Cell signaling	2598
PCNA	Santa Cruz	sc-7907
PIK3C3	Cell signaling	3358
RSK2	Abcam	ab32062
SAR1A	Novus biologicals	NBP2-20261
SEC16	Bethyl	A300-648A
SEC23A	Abcam	ab50672
SEC24D	Abcam	ab1222732
SEC31	BD	612350
SNAPIN	Sigma	SAB1407227
SQSTM1	MBL	PM045
TECPR2	Immunoglobe	self-production
TFG	Abnova	H00010342-B01P
TGOLN2	Sigma	T7576
TIAM1	Abcam	ab54458
USO1	gift from Z. Elazar	
VPS11	Abcam	ab125083
VPS39	Abcam	ab107570
VPS41	Santa Cruz	SC377118
VPS8	Acris	15079-1-AP
WIPI2	Abcam	ab105459

2.2 Methods

2.2.1 Molecular biological methods

2.2.1.1 Polymerase chain reaction (PCR)

PCR for amplification of DNA fragments was performed as followed:

5µl	10x KOD PCR buffer
1.5 mM	MgSO ₄
0.2mM each	dNTPs
32 µl	ddH ₂ O
0.3 µM	forward primer
0.3 µM	reverse primer
100-300 ng	template DNA
1 µl	KOD Hot Start Polymerase (1U/µl)
1 µl	DMSO

Reaction was performed in a S1000™ thermocycler (BioRad) with usually 35 cycles of denaturing annealing and elongation. Annealing phase temperature was set 5-10 °C below primer melting temperature and the length of elongation phase was adjusted to the size of amplified DNA fragment.

denaturing	94 °C	2 min	} 39 cycles
denaturing	94 °C	20 sec	
annealing	65-85 °C	10 sec	
elongation	72 °C	30 sec/kb	
	4 °C	~	

2.2.1.2 Cloning with Gateway system

Cloning of ORFs was performed with Gateway® technology. ORFs (listed in table 2) were cloned into pDONR223 and further recombined into Gateway destination vectors (listed in table 1) for mammalian and bacterial expression. First, the entire ORF was amplified using primers adding specific attachment sites on both sites of the ORF (primers are listed in table 3). Second, the purified ORF was recombined into the entry vector pDONR223 by performing a BP clonase reaction.

BP clonase reaction

- 5 µl purified PCR product
- 1 µl pDONR223 (~ 150 ng/µl)
- 2 µl 5x BP Buffer
- 2 µl BP clonase enzyme mix

BP reactions were incubated overnight at room temperature and subsequently transformed into competent TOP10 *E.coli* cells. After successful sequencing of the pDONR vector a LR reaction was performed to recombine the ORF into Gateway® destination vectors for mammalian or bacterial expression.

LR clonase reaction

- 1 µl pDONR-ORF (~ 150 ng/µl)
- 1 µl destination vector (~ 150 ng/µl)
- 1 µl 5x LR Buffer
- 1 µl LR clonase enzyme mix
- 1 µl water

The LR reaction was incubated for 4 hrs at room temperature and subsequently transformed into competent TOP10 *E.coli* cells. Finally, the purified plasmid DNA was sequenced and subjected for transfection experiments.

2.2.1.3 Agarose gel electrophoresis

For analysis of the PCR products reaction was loaded on a Midori Green containing agarose gel (1-2% agarose in 1x TAE buffer). Electrophoresis was conducted at 100 V in TAE buffer until bands were separated. Bands were visualized with a GelDoc™XR+ with UV light and excised for further cloning.

2.2.1.4 DNA purification, measurement of DNA concentration and Sequencing

DNA was purified directly from the PCR reaction or extracted from excised bands of an agarose gel with the Qiagen Gel Extraction kit (Qiagen). DNA concentration was determined with a NanoDrop (ND-1000).

Plasmid DNA was transformed into TOP10 or DB3.1 *E.coli* bacteria and grown for 16 hrs at 37 °C. DNA was extracted from harvested bacteria cultures (centrifugation 3,500xg, 5 min) with GenElute MiniPrep kit according to manufacturer's instructions. DNA was sequenced by Eurofins Genomics, Ebersberg. Sequencing primers are listed in table 5.

2.2.1.5 Site-directed mutagenesis

Fragments, point mutations or deletions were generated via site-directed mutagenesis of plasmid DNA using KOD Hot Start DNA Polymerase (Merck Millipore) with primers including specific mutations or fragments. These primers were designed with the QuickChange Primer Design program (Agilent) and are listed in table 4. A modified mutagenesis PCR protocol was employed:

2,5 µl	Buffer
1,5 µl	MgSO ₄
2,5 µl	dNTPs
17,25 µl	H ₂ O
0,75 µl	Primer (10 µM)
0,5 µl	Template DNA
0,5 µl	KOD polymerase

94 °C	2 min	
94 °C	20 sec	} 19 cycles
65-85 °C	10 sec	
72 °C	30 sec/kb	
4 °C	~	

To digest the template DNA 1 µl DpnI enzyme was added to completed PCR reaction and incubated for 2 hrs at 37 °C. Purification of DNA was accomplished using the QIAquick Gel Extraction kit before transformation into *E.coli*. Subsequently, plasmid DNA was purified from single bacteria colonies and subjected to sequencing.

2.2.1.6 RNA isolation, preparation of cDNA and quantitative PCR

RNA was isolated with RNeasy Plus Mini Kit (Qiagen) transcribed with Transcriptor First Strand cDNA Synthesis Kit, processed with LightCycler 480 SYBR Green I Master (Roche) according to user's manual and analyzed with a LightCycler 480. Relative gene expression was analyzed by employing PBDG, ACTB and TBP as reference genes.

Table 8: qPCR primers used in this study:

SEC23-for	GATGTGCTTAGGTGGCTGGA
SEC23-rev	TGAAACATAAACTGTGGATAAAGGG
SEC24D-for	CCTGGACCCCATCAGTTTGG
SEC24D-rev	TGTGCAGAGGGTTGGTATGG
DTNBP1-for	ACCTCCGGGCTGAAGACTTT
DTNBP1-rev	AGTGCAGCCCATGTATCCTC
VPS39-for	AGCCAGTGCCGATCCTAGA
VPS39-rev	TGTTGCAACTGCCGCTTTC
PBDG-for	CCCTGGAGAAGAATGAAGTGG
PBDG-rev	TTCTCTGGCAGGGTTTCTAGG
ACTB-for	CGGGAAATCGTGCGTGACATTAAG
ACTB-rev	TGATCTCCTTCTGCATCCTGTCCG
TBP-for	CACCTTACGCTCAGGGCTT
TBP-rev	TATTGGTGTTCTGAATAGGCTGTG

2.2.1.7 Preparation of competent *E.coli*

E.coli bacteria strains (TOP10, DB3.1 or Rosetta) were streaked on a LB agar plate without antibiotics and incubated overnight at 37 °C. A single colony was picked and an overnight culture of 50 ml was inoculated. Next day, 15 ml of the overnight culture were inoculated into 300 ml of SOB medium rotating at 30 °C till OD_{600nm} of 0.5 to 0.8 was reached. After centrifugation (3,000xg, 4 °C, 20 min) the bacterial pellet was resuspended in 50 ml TFB1 buffer and incubated for 60 to 90 min on ice. After next centrifugation (3,000xg, 4 °C, 20 min) the pellet was resuspended in 15 ml TFB2 buffer and aliquoted into Eppendorf tubes, which were finally quick-frozen in liquid nitrogen and stored at -80 °C.

2.2.1.8 Transformation of *E.coli*

To transform plasmid DNA into *E.coli* the method applied was the heat shock. Therefore, the DNA was added to competent bacteria and incubated for 30 min on ice. The heat shock was performed at 42 °C for 1 min and subsequent chill phase of 2 min on ice. Bacteria were recovered in LB medium at 37 °C for 1 hr before plating them on LB agar plates containing specific antibiotics.

2.2.2 Cell biological methods

2.2.2.1 Mammalian cell culture

HeLa, U2OS, 293T or 293T-Rex cells and human skin fibroblasts (CCD-1117sk) were grown in Dulbecco's modified Eagle's medium (DMEM) supplemented with 10% fetal bovine serum, 2 mM glutamine and Pen/Strep. Cells were grown in 10 cm tissue culture dishes at 37 °C and 5% CO₂ until 70-80% confluency. Skin fibroblast derived from healthy and HSP-affected individuals were isolated and grown as previously described (Oz-Levi et al., 2012). To passage the cells, they were washed with PBS and detached with 0.25% trypsin/EDTA (HeLa, U2OS, and CCD-1117sk) or 0.05% trypsin/EDTA (293T, 293T-Rex) and appropriate amounts were transferred into new dishes. For storage, cells were harvested and frozen in FBS containing 10% DMSO and stored at -80 °C. For long term storage the cells were transferred to -150 °C after a few days at -80 °C. For thawing, the cells were added to a dish containing fresh pre-warmed medium and let settle overnight. Next day, the medium was exchanged and cells were grown the usual way. For treatments, the following reagent concentrations were used: Bortezomib (Btz) (Millennium Pharmaceuticals Inc., 1 µM), Torin1 (Tocris, 250 nM), BafA1 (Sigma, 100 nM), Brefeldin A (Tocris, 1 µg/ml) and biotin (Sigma, 40 µM).

2.2.2.2 Preparation of stable cell lines

To generate 293T or 293T-Rex cells stable expressing different proteins lentiviral or retroviral transduction was used. For virus production seeded cells were transfected with packaging and expression vectors as following:

Retroviral transduction

1 µg pRETRO-VSVG

1 µg pRETRO-GAGPOL

2 µg pMSCV-I(N-Flag-HA)-GW-IRES-PURO including entire ORF

Lentiviral transduction

0.5 µg HDM-VSV-G

0.5 µg HDM-tatlb

0.5 µg HDM-Hgpm2

0.5 µg RC-CMV-Revllb

3 µg pHAGE-N-Flag-HA

First, 10 µl Lipofectamine 2000 were incubated with 250 µl OptiMEM for 5 min. In the meantime, the vector DNA was mixed with 250 µl OptiMEM. Second, the two mixtures were

merged and incubated for further 20 min. Meanwhile, the medium of the cells was change to 1.5 ml DMEM (10% FBS, glutamine, no antibiotics) and subsequently the transduction mix was drop-wise added to the cells. Medium was changed the next day and the supernatant harvested at day four. Supernatant was sterile filtered through a 0.45 μ m filter and polybrene (retroviral: 4 μ g/ml; lentiviral: 8 μ g/ml) and FBS were added. Recipient cells (retroviral: 293T-Rex; lentiviral: 293T) were infected with the supernatant. Selection with antibiotics started on day six and continued through medium changes every day. Lentiviral transfected cells carrying the pHAGE-N-Flag-HA plasmid required selection in puromycin while retroviral transfected cells with the pMSCV-i(N-Flag-HA)-GW-IRES-PURO were selected with puromycin and blasticidine to maintain their inducibility. Expression of the HA-tagged proteins was induced with 4 μ g/ml doxycycline (Sigma) for 24 hrs.

The HeLa Flp-IN cell line was used to generate stable cell lines using the Flp-IN T-Rex system (Invitrogen). Therefore, cells were seeded in DMEM (with supplements) plus blasticidine (4 μ g/ml) and zeocin (330 μ g/ml). Next day, transfection was performed with 3 μ l Lipofectamine 2000 in 97 μ l OptiMEM including 80 ng pcDNATM5/FRT vector-construct plus 720 ng pOG44 helper vector. Two days later, the selection with 4 μ g/ml blasticidine and 100 μ g/ml hygromycin (Invitrogen) started. Induction of cells was performed with 4 μ g/ml doxycycline (Sigma) for 2 to 4 hrs depending on the expression rate of the distinct proteins in the cells.

2.2.2.3 *Transient transfection of cells*

For transient expression DNA plasmids were forward transfected with different transfection reagents. Transfection of HA-, GFP- or YFP-constructs into cells was performed with Lipofectamine 2000. Polyethylenimine (PEI) (Polysciences Europe GmbH) was employed for large scale experiments e.g. IP-MS. For all rescue experiments Turbofect Transfection Reagent (Thermo Scientific) and for all RUSH assays the Neon transfection system (Invitrogen) was applied. The transfection procedure for all reagents proceeded as following. Cells were seeded into a 6-well dish at least 6 hrs before transfection. Then, 250 μ l OptiMEM was mixed with 2-10 μ l of the transfection reagent and incubated for 5 min. Meanwhile, 100-500 ng plasmid DNA was added to 250 μ l OptiMEM. Next, both mixtures were merged and incubated for another 20 min. Medium of the cells was replaced by 1.5 ml DMEM (without antibiotics). Transfection mixture was added drop-wise to the cells. After 48 hrs cells were harvested after one medium change 24 hrs post-transfection. For the transfection using PEI, PBS instead of OptiMEM was employed.

2.2.2.4 RNAi experiments

Cells were seeded one day before transfection and harvested 72 hrs post-transfection. For a 6-well dish 2 μ l Lipofectamine RNAiMax (Life technologies) was added to 250 μ l OptiMEM and 1 μ l RNA (20 μ M stock solution) to another 250 μ l OptiMEM and incubated for 5 min. The two mixtures were merged and after incubation of another 20 min it was dropwise added to the cells in 2.5 ml DMEM (without antibiotics), resulting in 10 nM final concentration of RNA. After one day medium without antibiotics was exchanged. For reconstitution experiments siRNA-resistant variants of TECPR2 and LC3C were transiently transfected 24 hrs after siRNA transfection using Turbofect Transfection reagent as described above (chapter 2.2.2.3). For other culture formats the amounts were adapted accordingly. The siRNAs were purchased from Dharmacon/GE Healthcare or Invitrogen (stealth). Sequences are listed in table 6.

2.2.2.5 Immunofluorescence staining

Cells were grown on lysine-coated coverslips (\varnothing 15mm) in 12well dishes, fixed and permeabilized with 4% paraformaldehyde and 0.5% Triton-X 100 in phosphate buffered saline [pH 7.4] (PBS) for 10 min each or with methanol for 10 min on ice. Blocked with 1% bovine serum albumin in PBS for 1 hr, coverslips were sequentially incubated with indicated primary and AlexaFluor-coupled secondary antibodies (Life Technologies) for 1 hr each. Coverslips were mounted with Prolong gold containing DAPI (Invitrogen) placed on glass plates and dried for 24 hrs at room temperature in the dark. Images were acquired on a Leica TCS SP8 (63x oil-immersion objective), a LeicaSP5 (636/1.4 NA oil-immersion objective at threefold digital magnification) or a Zeiss LSM780 microscope (63x oil-immersion objective). Software used was Leica application suite advanced fluorescence (LASAF). Images shown are representative for at least two experiments. Mean fluorescence intensity and quantifications were analyzed with ImageJ for at least 30 cells per condition and Pearson's correlation coefficient was determined with the JaCoP plugin (Bolte and Cordelieres, 2006).

2.2.3 Protein biochemical methods

2.2.3.1 Lysis of cells

Cells transfected with siRNAs or expression plasmids were washed with PBS, detached using 0.05% trypsin/EDTA (293T, 293T-Rex) or 0.25% trypsin/EDTA (HeLa, HeLa-Flp-IN, U2OS and CCD-1117sk), centrifuged in a tabletop centrifuge (3,000xg, 4 $^{\circ}$ C, 5 min) and washed twice with PBS. Pellets were resuspended in suitable amounts MCLB (50-100 μ l for a 6well dish) and lysis proceeded for 20-30 min at 4 $^{\circ}$ C rotating. After centrifugation (20,000xg, 4 $^{\circ}$ C, 10 min) the supernatant was transferred to a new Eppendorf tube. Protein amounts were

measured using Pierce BCA Protein Assay kit (Thermo scientific) and equalized with water and Laemmli buffer. Probes were denatured by boiling for 5 min at 95 °C and subjected to SDS-PAGE.

2.2.3.2 SDS-PAGE

For separation of proteins according to their molecular weight SDS-PAGE was conducted. Therefore, samples were loaded on pre-cast (4-20%, BioRad) or self-cast gels (8% or 12%) gels, which run in Laemmli buffer at a voltage of 200 V for pre-cast and 80 V (stacking gel) followed by 130 V (separating gel) for the self-cast ones. Polyacrylamide gels were casted using the BioRad system. First an 8% or 12% separating gel was prepared and after polymerization the 4% stacking gel was poured on top, in which the sample pockets were introduced by combs of varying sizes.

separating gel

8% or 12% Bis-acrylamide solution

375 mM Tris-HCl [pH 8.8]

0.1% SDS (m/v)

0.1% APS (m/v)

0.1% TEMED (m/v)

stacking gel

4% Bis-acrylamide solution

125 mM Tris-HCl [pH 6.8]

0.1% SDS (m/v)

0.1% APS (m/v)

0.1% TEMED (m/v)

2.2.3.3 Immunoblotting

After separation using SDS-PAGE proteins were transferred to nitrocellulose membrane (NitroBind 0.45 µm, Fisher Scientific) by Western Blot technology. Therefore, a Wet Blot chamber (Mini Trans-Blot®, BioRad) was assembled and filled with Wet Blot transfer buffer. Transfer was achieved with 3 mA for 2 hrs and membranes were reversibly stained with Ponceau S for verification of the protein transfer. Subsequently, membranes were blocked with PBS including 0.1 % Tween 20 (Roth) containing 5 % low fat milk (Roth) and incubated over night with primary antibodies at 4 °C in blocking buffer. As secondary antibodies α-mouse-HRP or α-rabbit-HRP (Promega) were used. For visualization Western Lightening Plus ECL (Perkin Elmer) was used. Primary antibodies used for Immunoblotting are listed in table 7. PCNA served as loading control. All blots are representative for at least three experiments.

2.2.3.4 Immunoprecipitations (IPs)

Cells transiently expressing HA-tagged proteins or stable cell lines induced with 4 µg/ml doxycycline were harvested and lysed as described before (see chapter 2.2.3.1). Lysates with

equalized protein amounts were incubated with pre-equilibrated anti-HA-agarose (Sigma) overnight rotating at 4 °C and subsequently the beads were washed five times before elution with 5x SDS-PAGE loading buffer. Bound HA-immune complexes were analyzed by SDS-PAGE and immunoblotting.

For immunoprecipitation of endogenous TECPR2, cells were lysed in MCLB on ice for 30 min. After clarification of the lysate the supernatant was pre-cleared with protein-A/G-sepharose (Santa Cruz) for 4 hrs at 4 °C. Beads were then removed and α -TECPR2 antibody was added to the lysate. α -c-Myc antibody served as IgG control. After incubation overnight at 4 °C with gentle rotation, protein-A/G-sepharose was added for another 2 hrs. Thereafter, beads were washed five times with lysis buffer and 5x SDS-PAGE loading buffer was added to elute the bound proteins, which were subsequently analyzed by SDS-PAGE and immunoblotting.

2.2.3.5 Preparation of cells for Native PAGE and Mass Spectrometry

For Native PAGE the cells expressing HA-tagged proteins were lysed in 1x NativePAGE lysis buffer for 30 min at 4 °C rotating and centrifuged at 20,000xg for 30 min at 4 °C. Supernatant was subjected to immunoprecipitation as described before (see chapter 2.2.3.4) and further processed for mass spectrometric analysis or immediately loaded on NativePAGE Novex 4-16% Bis-Tris Gels (Invitrogen). Separation of native protein complexes was performed at 130 V in NativePAGE Running buffers, first light cathode buffer for 45 min and another 90 min in dark cathode buffer. Proteins were blotted on PVDF membranes (GE Healthcare) and detected with antibodies listed in table 7.

For in-gel digestion, gel bands of a NativePAGE 4-16% Bis-Tris-gel (Novex) were excised and pieces were washed three times with 200 μ l 50% acetonitrile (ACN) in 50 mM ammonium bicarbonate (ABC) [pH 8.0] shaking at 22 °C on a thermomixer. Dehydration was performed with 200 μ l ACN for 10 min shaking on a thermomixer. Gel pieces were reduced with 200 μ l 10 mM Dithiothreitol (DTT) in 20 mM ABC for 45 min at 56 °C. Alkylation was performed in darkness with 200 μ l 55 mM iodoacetamide (IAA) in 20 mM ABC. Gel pieces were washed two times with 200 μ l 50% ACN in 5 mM ABC, dehydrated with 200 μ l ACN and dried in a vacuum centrifuge. Trypsin digest was completed with 12.5 ng/ μ l sequence-grade trypsin in 20 mM ABC shaking overnight. Supernatants of three elutions with increasing ACN concentration were pooled. Volume was decreased with a speed-vacuum centrifuge.

For mass spectrometric analysis (Behrends et al., 2010), HA-tagged proteins were expressed by inducing stable cell lines with 4 μ g/ml doxycycline for 24 hrs grown in four 15 cm culture dishes. After washing steps cells were harvested and lysed in 4 ml MCLB as described before (see chapter 2.2.3.1). For clarification of the lysates they were passed through 0.45 μ m spin filters (Millipore) and subjected to immunoprecipitation with 60 μ l anti-HA-agarose overnight

rotating at 4 °C. Subsequently, beads were washed five times with MCLB and another five times with PBS. Elution was achieved with 250 µg/ml Influenza Hemagglutinin (HA) peptide (Sigma) in three sequential elution steps, applying 50 µl peptide to the dried beads and shaking 30 min at room temperature each time. Elutions were pooled and proteins were precipitated with ice-cold trichloroacetic acid (TCA) at a final concentration of 20%. The sample was centrifuged (20,000xg, 30 min, 4 °C) and the pellet was washed four times with acetone (-20°C) following drying in a speed-vacuum centrifuge. Next, proteins were digested with 750 ng sequence-grade trypsin in 30 µl 100 mM ABC containing 10% ACN for 4 hrs at 37 °C. For desalting the peptides stage tips were assembled with Empore C18 extraction media (3 M) and pretreated as following: Activation with 80 µl methanol (1,000 rpm, 3 min), washing with 80 µl 50% / 5% ACN/formic acid (2,500 rpm, 5 min) and equilibration with 80 µl 5% / 5% ACN/formic acid (2,500 rpm, 5 min). Digested peptides, resuspended in 30 µl 5% / 5% ACN/formic acid, were loaded on the stage tips and washed with 80 µl 5% formic acid (2,500 rpm, 5 min, each). Peptides were eluted with 40 µl 75% / 5% ACN/formic acid (1,500 rpm, 10 min), dried in a speed-vacuum centrifuge and resuspended in 10 µl 5% / 5% ACN/formic acid for loading the liquid chromatography (LC) instrument of the mass spectrometer.

2.2.3.6 Mass Spectrometric analysis

HA-immunoprecipitations of cells expressing designated baits were analyzed by liquid chromatography tandem mass spectrometry (LC-MS/MS) followed by data processing with the CompPASS software. Samples were analyzed in technical duplicates on a LTQ Velos (Thermo Scientific). For CompPASS analysis, we employed 98 unrelated bait proteins that were all previously processed in the same way (Sowa et al., 2009). Normalized and weighted D scores (WD^N -scores) were calculated based on average peptide spectral matches (APSMs). Proteins with $WD^N \geq 1$ and $APSM \geq 3$ were considered as high-confident candidate interacting proteins (HCIPs).

In-gel digested peptides were analyzed using an LTQ Orbitrap Elite (Thermo Scientific).

All Peptides were identified using Maxquant software (Version 1.2.2.5; <http://www.maxquant.org>).

2.2.3.7 Purification of GST-tagged proteins

All ATG8 family members were cloned into pET-60-DEST vector and expressed as an N-terminal GST fusion in *E.coli* Rosetta cells. Cells were grown at 37°C in LB to an OD_{600nm} of 0.6 induced with 400 µM isopropylthiogalactoside (IPTG) and grown for 4 h at 37°C. Harvested cells were resuspended in lysis buffer (20 mM Tris-HCl [pH 7.5]; 10 mM EDTA; 5 mM EGTA;

150 mM NaCl; 10 % NP40; 1 % TRITON-X-100; Benzonase (10 μ l per 50 ml buffer), 1 mM DTT; 2 mg/ml lysozyme; Protease inhibitor cocktail (Roche)) and disrupted by freeze-thawing in liquid nitrogen followed by short sonification. After centrifugation at 10,000xg and 4°C for 20 min the lysate was incubated with Glutathione Sepharose 4B beads (GE Healthcare) overnight. GST-fused proteins were washed five times in lysis buffer and amounts of proteins were equalized by checking the expression on a SDS-PAGE gel followed by Coomassie staining. Beads were stored at 4 °C or directly used for GST pulldown.

2.2.3.8 Pulldown assays with GST-tagged proteins

Cells expressing HA-tagged proteins or untreated cells were lysed in MCLB for 30 min at 4 °C rotating and pre-cleared with 40 μ l Glutathione Sepharose beads for 1 hr at 4 °C rotating. Subsequent, lysate was incubated with GST-beads slurry overnight at 4 °C rotating. Next day, beads were washed 5 times with lysis buffer and proteins were eluted with 5x SDS-PAGE loading buffer, denatured and subjected to SDS-PAGE and immunoblotting.

2.2.3.9 Peptide array

To identify putative LIR-candidates of full-length TECPR2 a peptide array was employed. Therefore, a cellulose membrane spotted with 20mer peptides with an overlap of three peptides (INTAVIS) was incubated with GABARAP-GST beads and binding was detected with GST-HRP antibody as described before (Alemu et al., 2012).

2.2.4 Biophysical and structural methods

2.2.4.1 Preparation of proteins for ITC, NMR and X-ray studies

LC3 and GABARAP proteins were cloned as modified ubiquitin fusion proteins within pET-vectors (Rogov et al., 2012). For the purification of LC3C, GABARAP and GABARAPL2 slight modifications in the purification buffers were made upon the cleavage with self-made TEV protease. The pH was adjusted for LC3C and GABARAP to 7.3 and for GABARAPL2 to 8, according to the isoelectric point of the proteins. 5 mM β -Mercaptoethanol was added to the buffers used. Following two Ni-NTA chromatography purifications a size-exclusion chromatography on a Superdex S75 HR-16-60 column in 50 mM sodium phosphate, 100 mM NaCl [pH 7.0] was performed. TECPR2 (EDLEDEWEVI) LIR peptide ordered from GeneScript was equilibrated with buffer containing 20 mM Tris-HCl, 100 mM NaCl [pH 8.0]. Thermodynamic parameters are provided in table 9.

2.2.4.2 Isothermal titration calorimetry (ITC)

ITC measurements with TECPR2 (EDLEDEWEVI) LIR peptide (GeneScript) were performed at 25 °C with the VP-ITC micro calorimeter (MicroCal Inc., MA, USA) and analyzed with the ITC-Origin 7.0 software (MicroCal Inc.) based on a “one-site binding” reaction. The TECPR2 peptide at a concentration of ~400 µM was titrated to 20-25 µM of human ATG8 proteins (10 µl injection).

2.2.4.3 Nuclear magnetic resonance (NMR) measurements

All NMR experiments were performed at 298 K on Bruker Advance spectrometers at proton frequencies of 500 or 900 MHz Backbone HN resonances for LC3B, LC3C, GABARAP and GABARAPL2 were assigned using a [¹⁵N-¹H] TROSY version of 3D HNCAB and TROSY-H(CCCO)NH-total correlation spectroscopy experiments at protein concentrations of 0.8-1 mM NMR Titrations were performed with 190 µM ¹⁵N-labelled LC3B, 150 µM ¹⁵N-labelled LC3C, 170 µM ¹⁵N-labelled GABARAP or 120 µM ¹⁵N-labelled GABARAPL2 proteins to which the non-labelled peptide was stepwise titrated until saturation was observed. [¹⁵N-¹H] heteronuclear single quantumcoherence (HSQC) spectra were recorded at each step.

2.2.4.4 Crystallization, X-ray data collection and structural determination

TECPR2 LIR (1402-1411)-LC3B (2-119) fusion protein in pETM60 was expressed as N-terminal modified Ubiquitin His tag fusion protein (Rogov et al., 2013) in *E.coli* BL21 DE3. Cells were grown at 37°C to an OD₆₀₀ of 0.5, followed by induction with 0.5 mM isopropyl-β-d-thiogalactoside and further incubation at 20 °C for 20 hrs. Cells were lysed by sonication in lysis buffer (25 mM Tris, 100 mM NaCl, pH 8.5), and the lysate was cleared by centrifugation (15,000xg, 4 °C, 40 min). The expressed protein was purified by *TALON* Metal Affinity Resin (Clontech), cleaved by TEV Protease, and further purified by size exclusion chromatography (HiLoad 16/600 Superdex 75 column, GE Life Sciences) in 20 mM Tris, 100 mM NaCl, pH 8.5. The crystals of TECPR2 LIR in complex with LC3B were obtained using 1.8 M Lithium sulfate, 0.01 M Magnesium chloride, 0.05 M MES monohydrate, pH 5.6 as a reservoir solution by the sitting-drop vapor diffusion method at 293 K. Diffraction data were collected at Swiss Light source SLS, beam line PX1 and processed with XDS (Kabsch, 2010). The crystal structure was determined by molecular replacement using the LC3B structure (PDB: 2ZJD) as a search model. Manual model building and refinement were done with Coot, CCP4 software suite and Phenix (Adams et al., 2010; Emsley et al., 2010; Winn et al., 2011). The final statistics of refined models are shown in table 10 and the atomic coordinates have been deposited in the Protein Data Bank (PDB: 5DCN).

2.2.5 Phenotypical assays

2.2.5.1 Fluorescence recovery after bleaching (FRAP) assay

To determine the recruitment of SEC24D to the ER exit sites FRAP assay was performed. Therefore, cells expressing YPF-tagged SEC24D were bleached at an ERES region and the recovery rate at this region was quantified. Measurements were determined with a Leica SP5 confocal microscope using a 63x / 1.4 NA oil-immersion objective at five-fold digital magnification equipped with a Ludin chamber. After acquisition of a pre-bleach image, the ERES was bleached at 100% laser intensity for 750 ms. Upon bleaching, images were acquired at one image per second and were analyzed using ImageJ. For fitting FRAP curves, the reaction-dominated single-exponential recovery that has been widely used in the literature (Sprague et al., 2006) was used. The mobile fraction was calculated as $q5(F'2F0)/(Fi2F0)$, where F' is fluorescence in the bleached region after recovery, Fi is the fluorescence in the bleached region before bleaching, and $F0$ is the fluorescence in the bleached region directly after bleaching.

2.2.5.2 Retention using selective hook (RUSH) assay

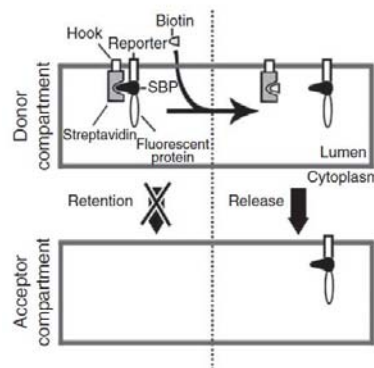


Figure 2-1: RUSH principle.

A reporter protein is fused to a streptavidin-binding protein (SBP) and a fluorescent protein. This reporter binds specifically to the streptavidin-peptide containing hook in the donor compartment. Upon biotin treatment the release of the reporter into its acceptor compartment can be followed by fluorescence microscopy. From (Boncompain et al., 2012).

HeLa cells were transfected with 1 μ g GFP-RUSH-construct per 2 cm well 24 hrs prior to the experiment. After transfection with the RUSH-construct, 40 μ M biotin (Sigma) was added to the cells and they were fixed in 3% PFA at the indicated time points and immunostained for α -GOLGB1, a Golgi apparatus located protein (Sohda et al., 1994). Images were acquired using a Leica SP5 confocal microscope, with a 63x / 1.4NA oil immersion objective at 1.7 fold digital magnification. Arrival at the Golgi was quantified using ImageJ as by measuring mean

fluorescence intensity at the Golgi region and subtracting the mean fluorescence intensity at a non-Golgi region of similar size to correct for background and differences in expression level.

2.2.5.3 Statistical analysis

Data represent mean + SD and statistical analysis was performed using GraphPad Prism. Statistical significance was determined with Student's t-test and one-way ANOVA followed by Bonferroni's multiple comparison test.

3. Results

3.1 TECPR2 associates and colocalizes with SEC24D, BLOC-1 and HOPS

To elucidate the function of TECPR2, 293T cells stably expressing N-terminal hemagglutinin (HA)-tagged TECPR2 were generated with retroviral transfection to perform interaction proteomics. Lysates derived from these cells were subjected to HA immunoprecipitation followed by LC-MS/MS. Mass spectrometric data was processed using CompPASS (Sowa et al., 2009) to identify high-confidence candidate interacting proteins (HCIPs). TECPR2 was found to associate with its known interactor GABARAP (Behrends et al., 2010) and two other members of the human ATG8 family (GABARAPL1 and GABARAPL2) (fig. 3-1A). Included among the HCIPs were also the COPII coat protein SEC24D and several subunits of the HOPS complex and the biogenesis of lysosome related organelles complex (BLOC)-1 (fig. 3-1A). Reciprocal IP-MS experiments revealed association of TECPR2 with the HOPS member VPS41 and the BLOC-1 subunits DTNBP1, BLOC1S1 and BLOC1S3 albeit without passing the strict threshold for HCIP determination (fig. 3-1B).

Besides several proteins associated with TECPR2 suggest a role of TECPR2 in RNA trafficking in and out of the nucleus. Examples are, SUPT5H (transcription elongation factor SPT5), which is a factor involved in mRNA processing (Diamant et al., 2012; Wada et al., 1998), the GINS proteins, which acts in the initiation of DNA replication (Kamada, 2012; Kamada et al., 2007), and members of the ANP32 (Acidic leucine-rich nuclear phosphoprotein 32) family, which are involved in RNA trafficking and transcriptional expression (Seo et al., 2001).

In addition, a set of HCIPs was found as common interactors of TECPR2 and HOPS or BLOC-1 complex as well as of TECPR2 and SEC24D. Shared binding partners were also found between HOPS and BLOC-1 complexes, indicating a potential interplay between the underlying vesicle trafficking pathways.

BCAS4 (Breast carcinoma-amplified sequence 4), a protein overexpressed in many breast carcinoma cell lines (Van Damme et al., 2012) was found in several IP-MS analyses of the BLOC-1 complex subunits indicating to represent a new component of the BLOC-1 complex. C17orf59 is an uncharacterized protein possibly bridging the BLOC-1 and HOPS complexes. ACTBL2 (beta-actin-like protein 2) is a ubiquitously expressed protein and most likely involved in cell motility (Chang et al., 2006).

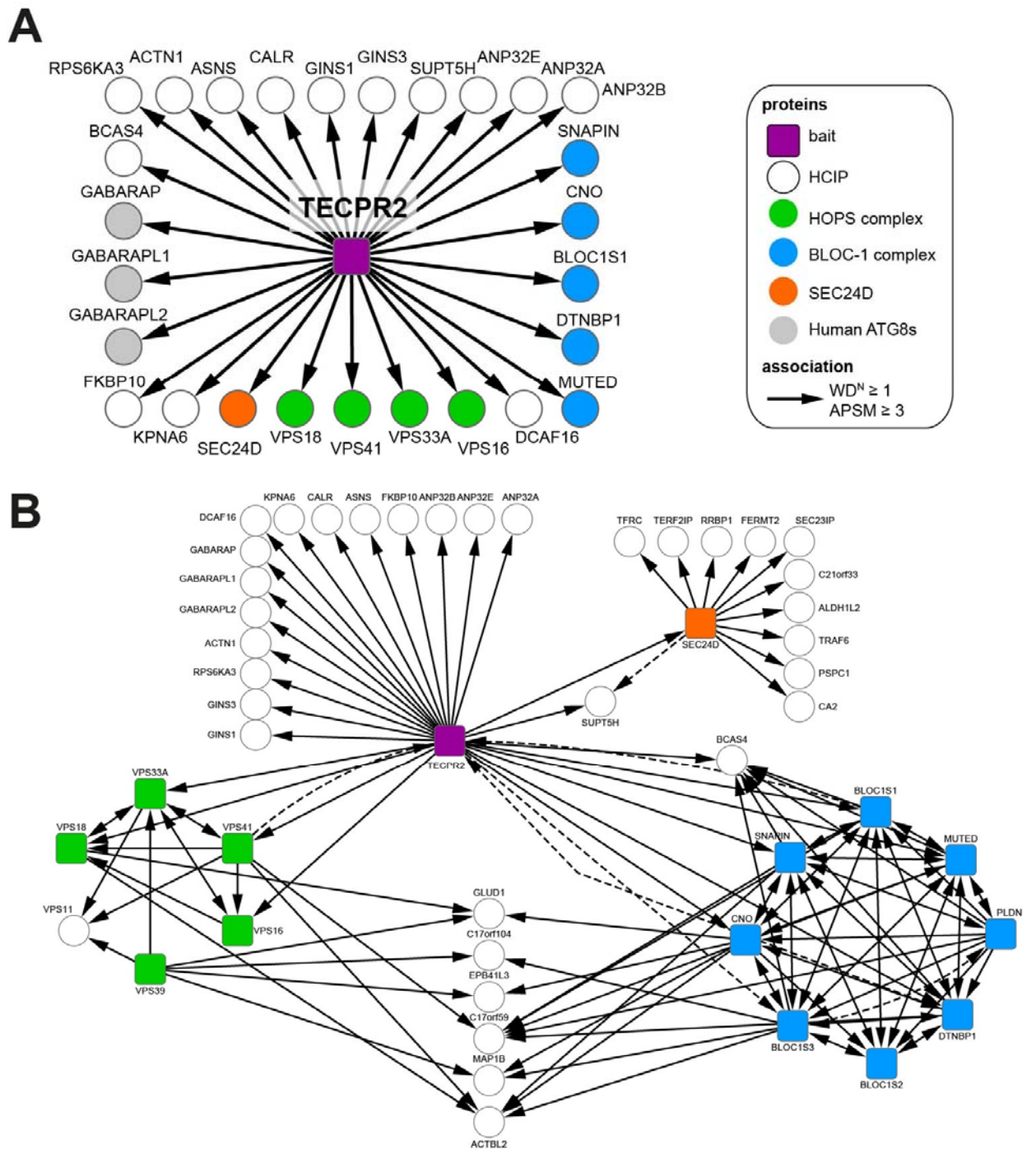


Figure 3-1: Interaction networks of TECPR2.

(A-B) TECPR2 interaction networks obtained from IP-MS analysis of TECPR2, BLOC-1 and HOPS subunits as well as SEC24D (color-coded round squares). Solid lines, association of high-confident candidate interaction proteins (HCIPs). Dashed lines, interactions with subthreshold WD^N -scores and APSM values.

To validate the interaction of TECPR2 to a part of the association candidates, the binding was confirmed with HA-tagged TECPR2 to endogenous HOPS subunits VPS41 and VPS11 (fig. 3-2A) and BLOC-1 components DTNBP1 and BLOC1S3 (fig. 3-2A).

Results

The interaction to COPII coat protein SEC24D was first strengthened by IP-Western analysis with both proteins overexpressed. By immunoprecipitating GFP-TECPR2 HA-SEC24D was detected and vice versa (fig. 3-2B). To further validate this connection the immunoprecipitate (IP) of TECPR2 was repeated under endogenous conditions with anti-TECPR2 antibody and indeed SEC24D was found to interact with TECPR2, while c-Myc antibody and the unrelated protein RSK2 served as negative controls (fig. 3-2D).

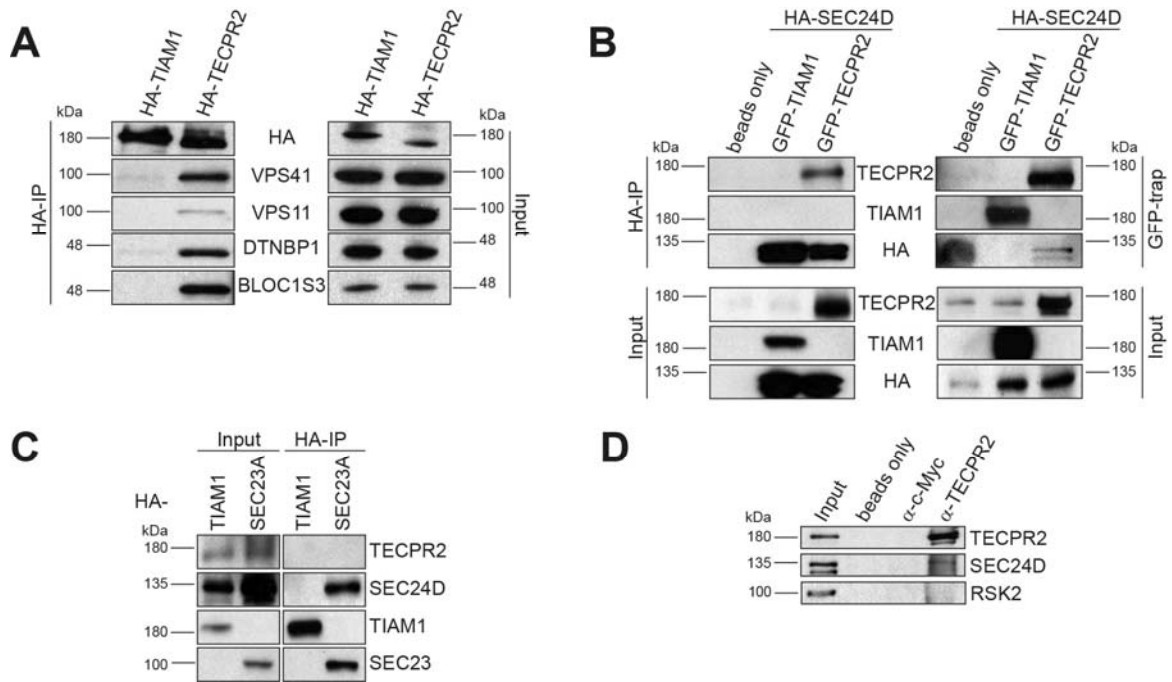


Figure 3-2: TECPR2 interacts with HOPS, BLOC-1 and SEC24D.

(A) Immunoblotting of α -HA immunoprecipitates from HeLa cells expressing HA-TECPR2 or -TIAM1. 5 mM DTBP was used as cross linker. (B) HeLa cells expressing HA-SEC24D and GFP-TECPR2 or -TIAM1 were subjected to IP with α -GFP or -HA beads and analyzed by immunoblotting. (C) Immunoblot analysis of α -HA immunoprecipitates from HeLa cells transiently expressing HA-SEC23A or HA-TIAM1. 5 mM DTBP was used as cross linker. (D) Endogenous IP of TECPR2 was subjected to immunoblotting. α -c-Myc and -RSK2 antibodies served as controls.

While TECPR2 and SEC24D bound each other also at endogenous level (fig. 3-2D), the dimer partner of SEC24D, SEC23A was not found associated with TECPR2 (fig. 3-2C). This suggests that TECPR2 binds SEC24D before heterodimerization of SEC24D with SEC23.

To determine which regions of TECPR2 mediate binding to HOPS, BLOC-1 and SEC24D a panel of TECPR2 fragments was employed (fig. 3-3A). By engaging a panel of HA-tagged TECPR2 variants in IP experiments, the N-terminal region of TECPR2 encompassing the WD40 repeat was found to be both required and sufficient for mediating the interaction with HOPS and BLOC-1 components as well as with SEC24D (fig. 3-3B).

To examine whether TECPR2 binds to HOPS and BLOC-1 or to their unassembled subunits, HA-TECPR2 expressing cells were subjected to anti-HA IP and Native PAGE. MS analysis of

Results

in-gel digested tryptic peptides revealed that six BLOC-1 members: BLOC1S1, BLOC1S3, CNO, DTNBP1, MUTED and SNAPIN and four HOPS components: VPS16, VPS18, VPS33A and VPS41 migrated together with TECPR2 in a high molecular weight complex between 720 and 1048 kDa (fig. 3-3C).

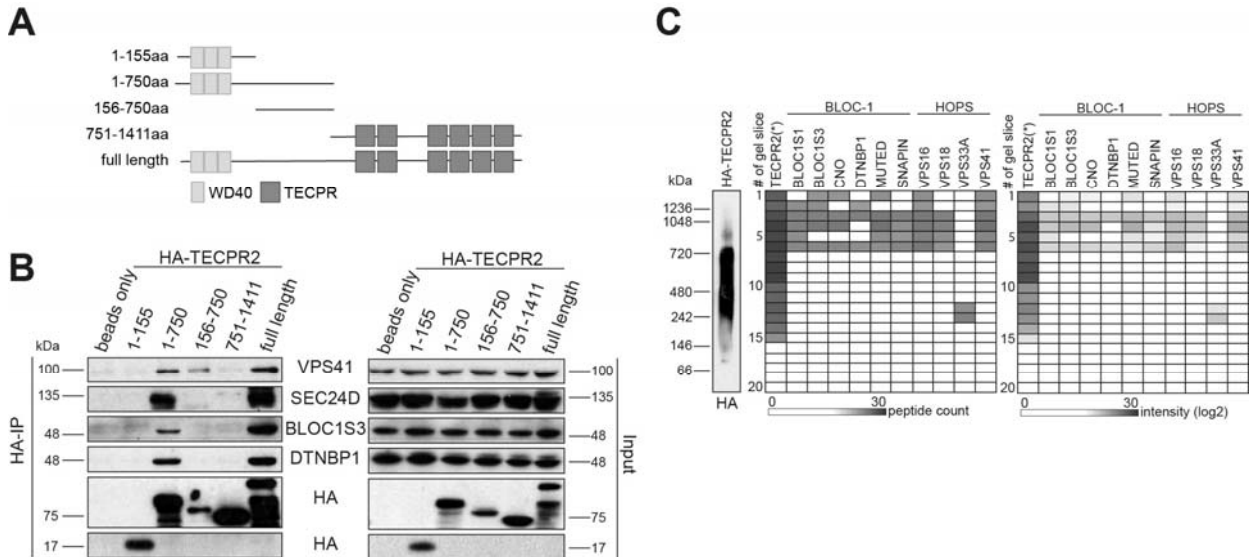


Figure 3-3: The N-terminal part of TECPR2 mediates the interaction with SEC24D, HOPS and BLOC-1.

(A) Schematic representation of TECPR2 constructs. (B) α -HA immunoprecipitates from 293T cells expressing indicated constructs were analyzed by immunoblotting. (C) TECPR2 associates with BLOC-1 and HOPS subunits in a high-molecular weight complex. α -HA immunoprecipitates from cells stably expressing HA-TECPR2 constructs were subjected to Native PAGE followed by immunoblotting (left) or by analysis of in-gel digested tryptic peptides using MS (right). Grey scale on heat map representation indicates numbers of identified peptides or intensities (log2).

Next, the relative cellular distribution of endogenous TECPR2, HOPS and SEC24D was examined by immunofluorescence and confocal microscopy. Endogenous TECPR2 was detected in punctuated cytosolic structures of which a major fraction was also positive for SEC24D and only a minor for the HOPS subunit VPS41 (fig. 3-4A). Furthermore, up to 40% of TECPR2 positive vesicles did not colocalize with either binding partner and less than 5% were positive for all three proteins (fig. 3-4A). TECPR2 also partially colocalized with HA-tagged DTNBP1 (fig. 3-4B). These results display that TECPR2 is engaged in separate associations with distinct functional entities involved in vesicular trafficking, namely SEC24D, BLOC-1 and HOPS.

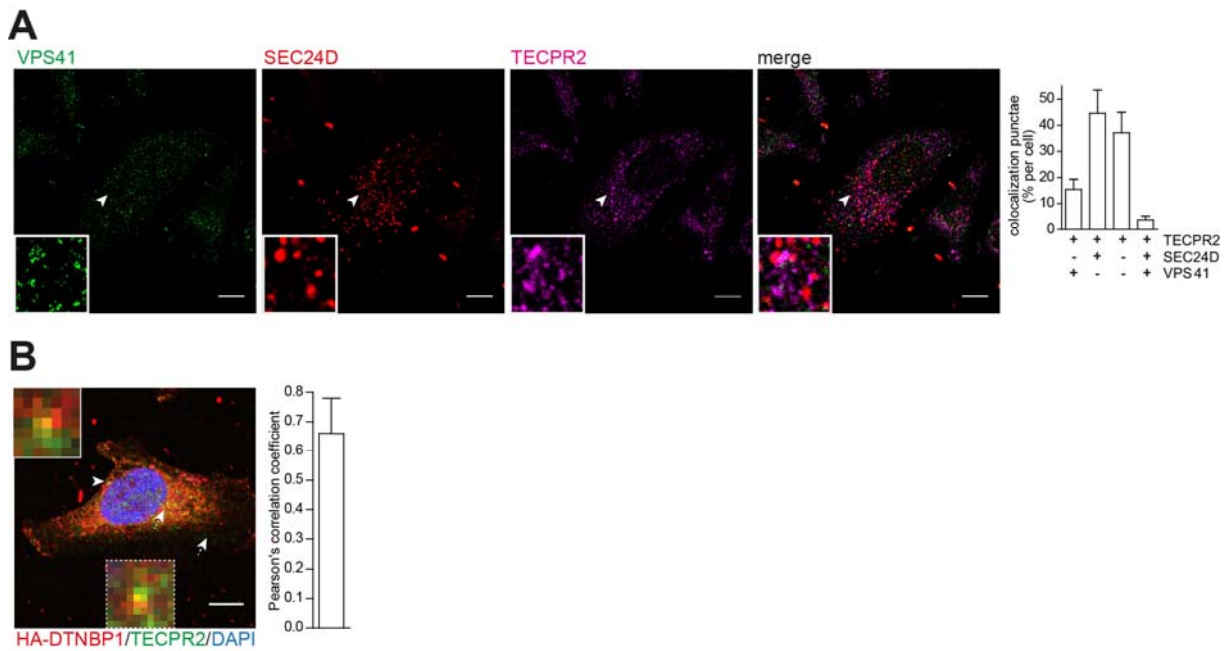


Figure 3-4: Endogenous TECPR2 colocalize with SEC24D, HOPS and BLOC-1.

(A-B) HeLa cells left untransfected (A) or transfected with HA-DTNBP1 (B) were fixed and stained with indicated antibodies. Boxes, inset regions marked with arrowheads. Scale bar, 10 μ m. Quantification was performed with ImageJ. Data represent mean +SD.

3.2 TECPR2 binds LC3 and GABARAP proteins in a LIR-dependent manner

Subsequent, we confirmed the association of TECPR2 with human ATG8 proteins in GST pull-downs (fig. 3-5). Therefore, the ATG8 family proteins were purified as GST fusion proteins from bacteria. Immobilized GST-ATG8 variants were incubated with cell lysate, washed intensively and subjected to SDS-PAGE and Western analysis. First the general binding of ATG8 proteins to TECPR2 was determined (fig. 3-5A). In this assay, interactions of TECPR2 with all ATG8 proteins were observed, although LC3A and GABARAPL2 seemed to be weaker binding partners. The known autophagic cargo receptor sequestosome1 (SQSTM1, p62), which binds to all ATG8 family members, served as positive control. To investigate whether TECPR2 binds to human ATG8 proteins in a LIR-dependent manner, a panel of TECPR2 fragments was employed in binding assays with LC3B and GABARAP (fig. 3-5B, 3-5C). For both ATG8 proteins the binding region was narrowed down to the C-terminal end of TECPR2 (1260-1411aa).

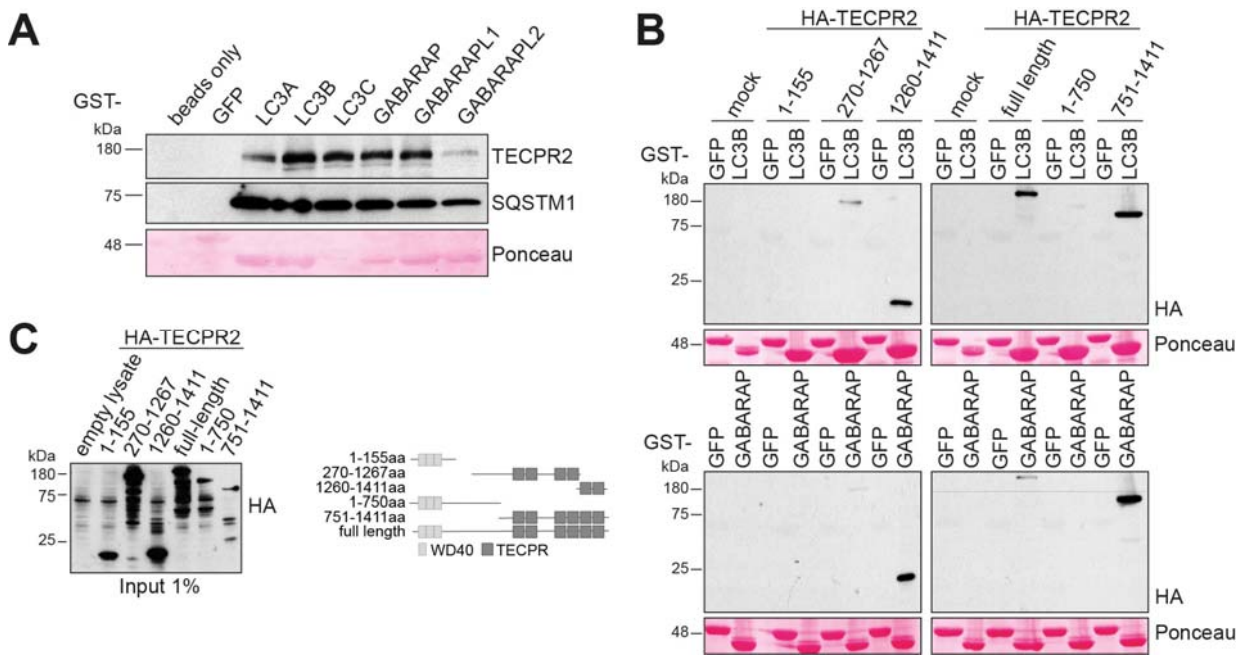


Figure 3-5: TECPR2 binds human ATG8 family members.

(A) Pull-down using purified GST-ATG8 proteins and 293T cell lysate analyzed by immunoblotting and Ponceau staining. (B) 293T cells transfected with fragments or full-length protein were employed in GST pull-down assay. (C) Expression control of TECPR2 variants for GST pull-down assays and depicted TECPR2 fragments.

To complementarily probe for the LIR motif, peptide array technology was used. Therefore, an array with 20mer overlapping peptides of TECPR2 spotted on a cellulose membrane was incubated with purified GST-tagged GABARAP protein. Subsequently, GABARAP binding to TECPR2-derived peptides was detected with GST-antibody. Using this approach three LIR candidate motifs were identified (fig. 3-6A, 3-6B). Subsequently, the potential LIRs were mutated either by point mutation in the first residue (W1408A, F1138A) or by deletion of the entire LIR sequence (Δ LIR) through C-terminal truncation. These LIR candidate deficient TECPR2 variants were subjected to GST pull-down assays. However, only mutation of the aromatic residue in candidate LIR#3 (WEVI) affected the binding to LC3 and GABARAP proteins. Consistently, TECPR2- Δ LIR showed a complete loss of ATG8 binding lead to a total loss of the binding (fig. 3-6C, 3-6D). Thus, a canonical LIR motif was mapped to the very C-terminal part of TECPR2 (fig. 3-6E).

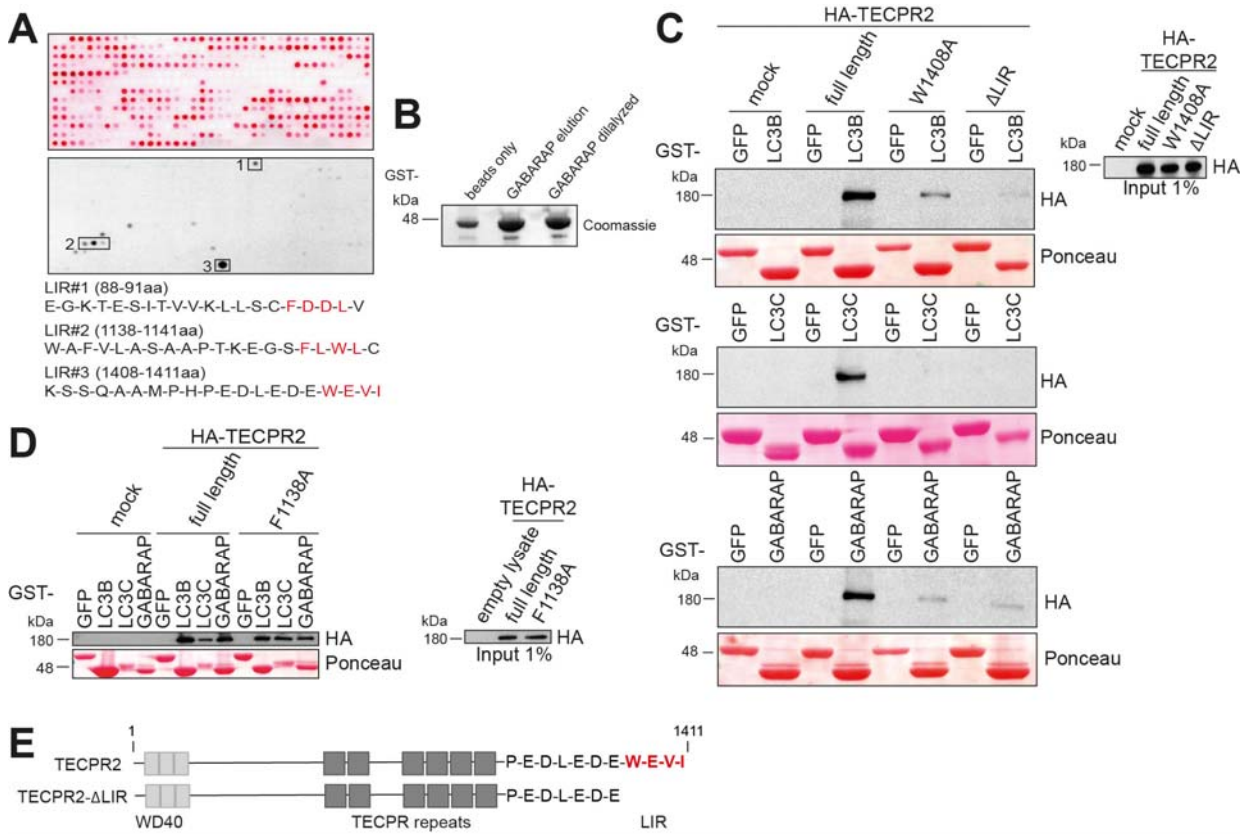


Figure 3-6: LIR mapping in TECPR2.

(A) A peptide array of overlapping 20mer peptides of TECPR2 was incubated with purified GST-GABARAP and probed with anti-GST antibody. Depicted sequences encompass candidate LIR motifs in red (B) Protein expression control for (A) Coomassie stained gel of purified GST-GABARAP. (C-D) 293T cells transfected with indicated TECPR2 variants were employed in GST pull-down assays. Corresponding expression controls are provided on the right, respectively. (E) Domain architecture of TECPR2 with LIR (red).

To assess whether the TECPR2 LIR is evolutionary conserved, TECPR2 protein sequences from different organisms were aligned (fig. 3-7A). Remarkably, even for TECPR2 orthologues found in distant species, there is a strong conservation within the WD40 repeat domain (predicted for residues 23-343), the tectonin β -propeller repeat domain (predicted for residues 945-1353) and the C-terminal LIR (residues 1408-1411) with some preceding negatively charged or polar residues (fig. 3-7A, 3-7B).

Results

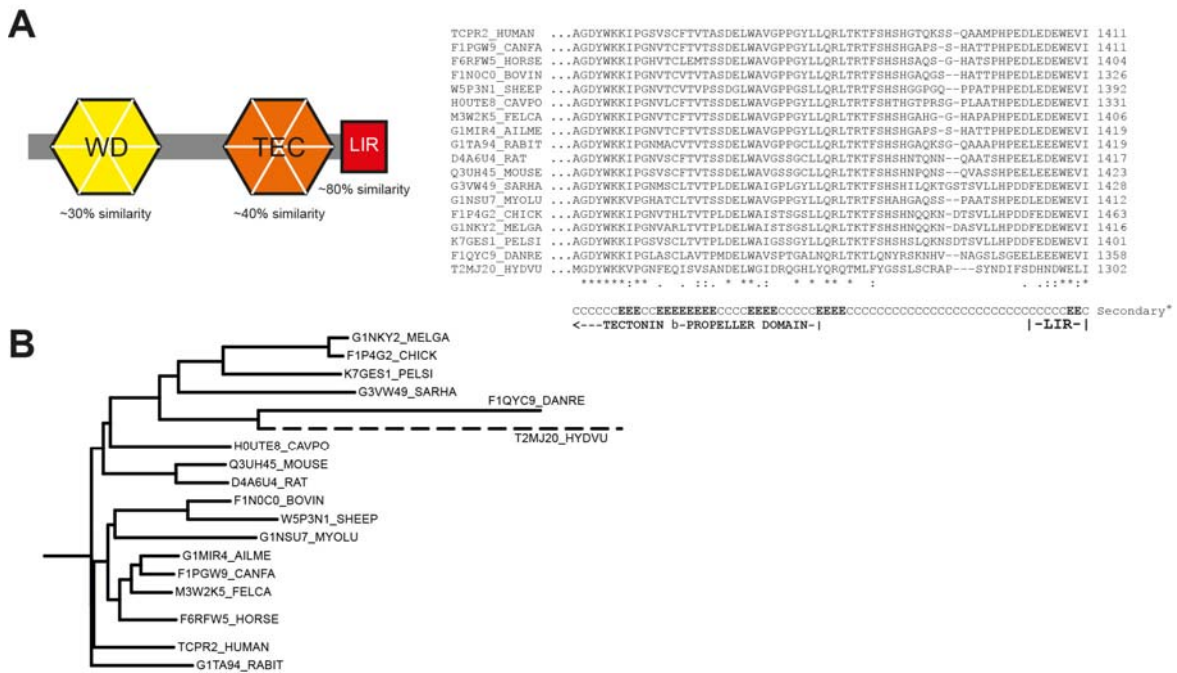


Figure 3-7: Homology among TECPR2 proteins across vertebrates.

(A) The schematic presentation of the TECPR2 protein (plot left) shows conservation within predicted structural elements of the protein - WD40-repeat domain (~30% of similarity), tectonin beta-propeller repeat domain (~40% of similarity) and LIR motif (~80% of similarity for core LIR and E/D/N-reach stretch directly prior to the conserved Trp). Linkers between these elements (gray) possess <10% similarity and seems are disordered. Each row in the sequences alignment displays UniProtKB entry number (left), amino acid sequence of corresponding TECPR2, last residues number, and common name of organism. Similarity is shown in consensus row (* - identical, - very similar, . - similar residues). Predicted (by PsiPred) elements of secondary structure are given in the last row (C - Coil, E - β -strand, H - α -helix). Alignment was done by Clustal Omega program integrated into the UniProt - server (Sievers et al., 2011). (B) Phylogenetic diagram constructed by neighborhood joining method for the proteins used in alignment above

To quantitatively determine the binding affinities of TECPR2, isothermal titration calorimetry (ITC) was performed using peptide spanning the LIR of TECPR2 and purified human ATG8 variants (fig. 3-8, 3-9, table 9). These experiments were performed in close collaboration with Dr. Vladimir Rogov and Jessica Huber from the group of Prof. Dr. Volker Dötsch.

These experiments showed that the TECPR2 LIR binds to all six proteins with similar K_D values in the sub-micromolar range, which are slightly lower than previous reported affinities (in the low micromolar range) for other typical LIR motifs (Rozenknop et al., 2011).

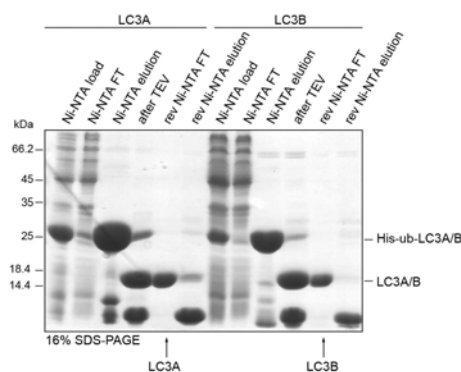


Figure 3-8: Purification of human ATG8 proteins for ITC measurements.

(A) Ni-NTA purification of His-ubiquitin-LC3A and –LC3B following removal of His-ubiquitin tag with TEV cleavage and subsequent reverse (rev) Ni-NTA yielding LC3A and LC3B in the flow-through (FT). Coomassie stained gel.

The lowest affinity was detected for GABARAPL1 (K_D 1.7 μ M), for which the least favorable entropy of interaction (+11 cal/mol/K) and hence the more rigid complex formation resulted in the same ability to bind full-length TECPR2 in pulldown experiments. GABARAPL2 displayed a significantly smaller binding enthalpy (-0.7 Kcal/mol vs -4.7 Kcal/mol for GABARAPL1), which is compensated by the increased favorable entropy (+27 cal/mol/K), indicating the formation of a more flexible complex. In agreement with the ITC data, GABARAPL2 exhibits only little binding in the pulldown experiments, highlighting a lower binding preference compared to the other human ATG8 proteins (fig. 3-5A). Measurement parameters of ITC experiments are listed in table 9.

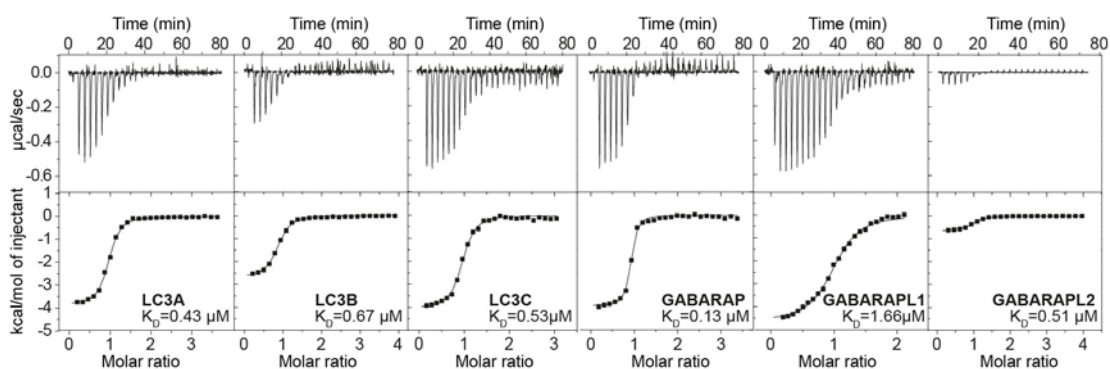


Figure 3-9: Biophysical properties of TECPR2 LIR binding to purified human ATG8 proteins.

(B) ITC profiles of TECPR2 LIR peptide titration to LC3 and GABARAP proteins. Top: Raw measurements; Bottom: integrated heat per titration step. K_D values are included in each plot.

To understand the molecular mechanism of these interactions, NMR titration experiments with different members of the two subfamilies were performed in collaboration with Dr. Vladimir

Results

Rogov and Jessica Huber from the group of Prof. Dr. Volker Dötsch. Series of NMR spectra were recorded for ¹⁵N-labelled LC3B, LC3C, GABARAP (as the strongest binders) and GABARAPL2 (as the weakest binder), to which increasing amounts of non-labelled TECPR2 LIR were titrated until saturation. In all cases, significant chemical shift perturbations (CSP) were observed (fig. 3-10). For LC3B, LC3C and GABARAP, CSP were in the intermediate to slow exchange modes, corresponding to the obtained K_D and entropy values in the ITC experiments. In contrast to that, GABARAPL2 showed CSP mostly in the fast to intermediate exchange modes upon TECPR2 titration, which corresponds to a formation of more flexible complex. CSP mapping on the surface of each protein displayed occupancy of both hydrophobic pockets and the formation of an intermolecular β -sheet, as expected for binding of typical LIR peptide. Thus, LC3- and GABARAP-subfamily proteins efficiently bind to TECPR2 through its C-terminal LIR (fig. 3-10).

Table 9: Thermodynamic parameters obtained by ITC measurements.

Values obtained of TECPR2 LIR peptide to all six human ATG8 proteins. All experiments were performed at 25 °C and the parameters for the interactions (ΔH , ΔS and K_D) were calculated with the assumption of a 'one-site binding' model:

	ΔH [kcal mol ⁻¹]	ΔS [cal mol ⁻¹ K ⁻¹]	$-T\Delta S$ [kcal mol ⁻¹]	ΔG [kcal mol ⁻¹]	K_A [*10 ⁶ M ⁻¹]	K_D [μ M]	N
LC3A	-3.88 ± 0.03	16.1	-4.80	-8.68	2.3	0.43	0.92 ± 0.01
LC3B	-2.72 ± 0.02	19.1	-5.69	-8.68	1.5	0.67	0.83 ± 0.01
LC3C	-4.07 ± 0.05	15.1	-4.50	-8.57	1.9	0.53	0.93 ± 0.01
GABARAP	-3.97 ± 0.04	18.2	-5.42	-9.39	7.6	0.13	0.87 ± 0.01
GABARAPL1	-4.67 ± 0.06	10.9	-3.25	-7.92	0.6	1.66	1.00 ± 0.09
GABARAPL2	-0.67 ± 0.01	26.6	-8.93	-8.60	1.96	0.51	0.95 ± 0.01

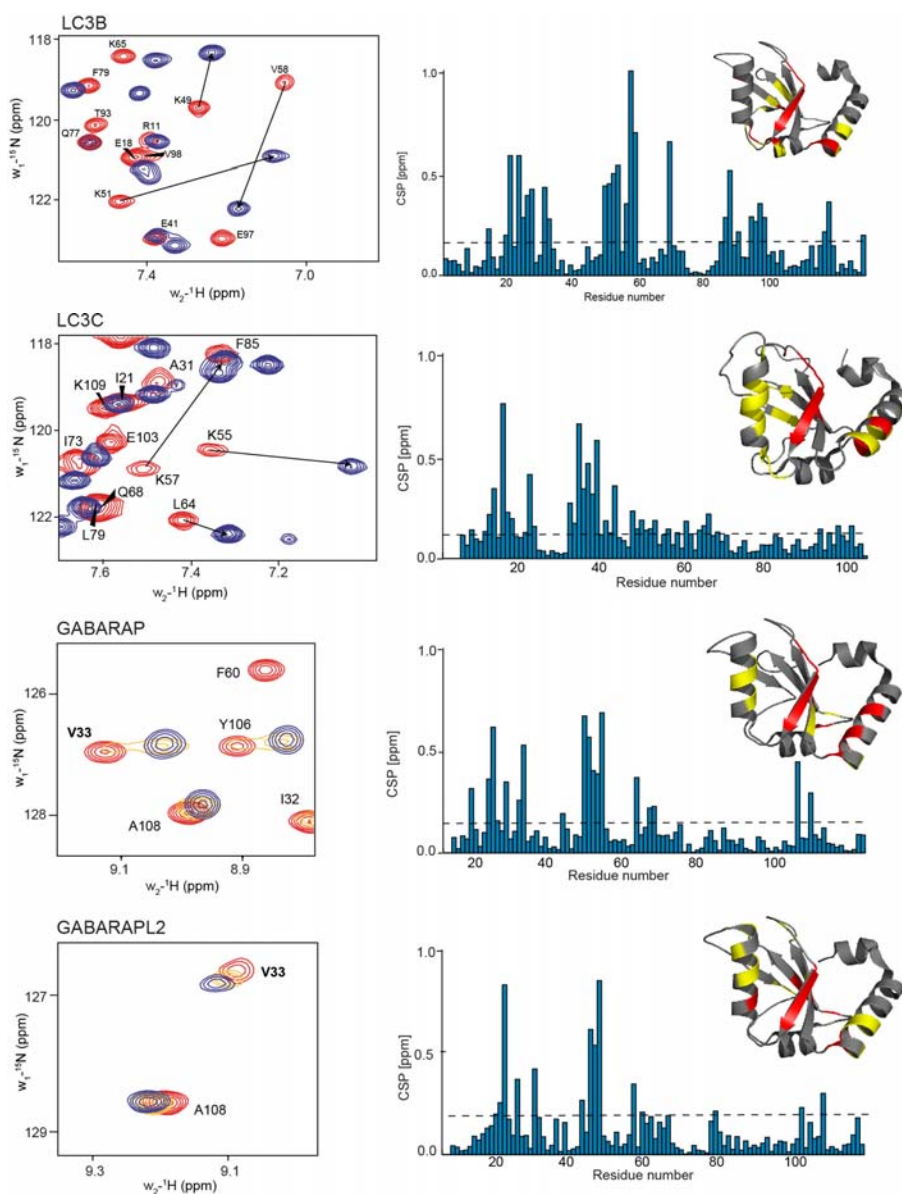


Figure 3-10: NMR titration analysis of TECPR2 LIR binding to human ATG8 proteins.

Left panel: Overlay of representative areas in ^1H - ^{15}N -HSQC spectra of ^{15}N -LC3B in the free form (red) and after saturation with the TECPR LIR peptide (blue). Chemical shift perturbations (CSP) for each residue within each protein were evaluated (right plot). The dashed line represents the standard deviation (σ) over all residues. CSP were additionally mapped on the protein structures for LC3B (PDB: 3VTU), LC3C (PDB: 3VWV, upper), GABARAP (PDB: 1GNU, left) and GABARAPL2 (PDB: 1E06, right) and residues with small ($\Delta\delta < \sigma$), intermediate ($\Delta\delta > \sigma$) or strong ($\Delta\delta > 2\sigma$) CSPs were marked in grey, yellow and red, respectively. Residues with small ($\Delta\delta < \sigma$), intermediate ($\Delta\delta > \sigma$) or strong ($\Delta\delta > 2\sigma$) CSPs were marked on the ribbon diagrams of corresponding structures in grey, yellow and red, respectively. For LC3C the K55, and for GABARAP and GABARAPL2 V33 backbone HN resonances are shown upon addition of the TECPR2 LIR peptide in molar ratios of 1:0 (red), 1:0.5 (orange) and 1:2 (blue). The GABARAP V33 HN resonance exhibits an intermediate to slow exchange modes - two peak positions (free and bound) are seen at each titration step; whereas GABARAPL2 V33 HN resonance shows the fast to intermediate exchange modes - gradual shifts of peak maxima, proportional to the TECPR2 LIR concentration.

To further validate the interaction between TECPR2 LIR and ATG8 family members, the crystal structure of TECPR2 LIR in complex with LC3B was determined by using a previously reported fusion protein strategy (Suzuki et al., 2014). Crystallization was successfully performed in collaboration with Dr. Masato Akutsu.

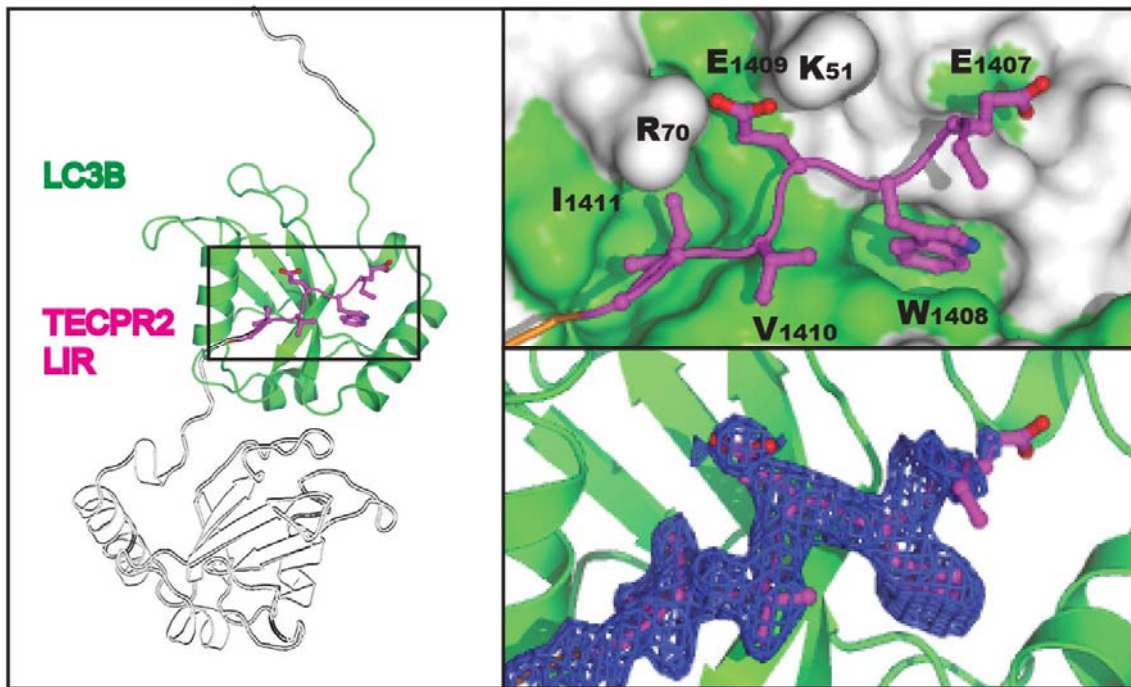


Figure 3-11: Crystal structure of TECPR2-LIR in complex with LC3B.

Ribbon and surface representation model of the TECPR2-LIR (magenta) - LC3B (green) interaction and crystallographic symmetry related molecule (white). $2F_o - F_c$ electron density (blue mesh) of TECPR2-LIR (amino acids 1406–1411), contoured at 1σ and with ball-and-stick model.

In the crystals, TECPR2 LIR interacts with crystallographic symmetry related LC3B (fig. 3-11, table 10). As indicated by NMR-based CSP mapping, the aromatic and hydrophobic residues of TECPR2 LIR, W1408 and I1411 at position 1 and 4 fit into the two hydrophobic pockets of LC3B. Additionally, two hydrogen bonds between E1409 of TECPR2 and LC3B's K51 and R70 further stabilize the binding (fig. 3-11). These results demonstrate that TECPR2 binds LC3 and GABARAP proteins via a canonical W-type LIR (fig. 3-6E).

Table 10: Crystallization data collection and refinement statistics.

Atomic coordinates of the TECPR2 LIR-LC3B crystal structure (Accession No. 5DCN). Values in parentheses are for the highest resolution shell:

	TECPR2 LIR-LC3B
Data collection statistics	
Beamline	SLS PX I
Wavelength (Å)	0.99987
Space Group	<i>P3₂21</i>
Unit Cell (Å)	$a = 60.71, b = 60.71, c = 99.95$ $\alpha = 90.00, \beta = 90.00, \gamma = 120.00$
Resolution (Å)	19.87 - 2.00 (2.11 - 2.00)
Observed reflections	289824 (40309)
Unique reflections	14950 (2141)
Redundancy	19.4 (18.8)
Completeness (%)	99.8 (99.8)
R_{merge}	0.077 (0.802)
$\langle I/\sigma I \rangle$	24.2 (4.4)
Refinement statistics	
Reflections in test set	1498
R_{cryst}	20.9
R_{free}	24.7
Number of groups	
Protein residues	126
Ions and ligand atoms	4
Water	58
Wilson B-factor	36.34
RMSD from ideal geometry	
Bond length (Å)	0.003
Bond angles (°)	0.648
Ramachandran Plot Statistics	
In Favoured Regions (%)	116 (98.31)
In Allowed Regions (%)	2 (1.69)
Outliers (%)	0 (0.00)

3.3 Association with SEC24D, BLOC-1 and HOPS requires LC3 binding of TECPR2

To assess the binding preference of TECPR2 for human ATG8 proteins in cells, immunofluorescence analysis of endogenous TECPR2 was employed in combination with a panel of cells stably expressing HA-tagged LC3 or GABARAP proteins grown in the absence and presence of Torin1 and Bafilomycin A1 (BafA1) treatment to induce and block autophagy, respectively.

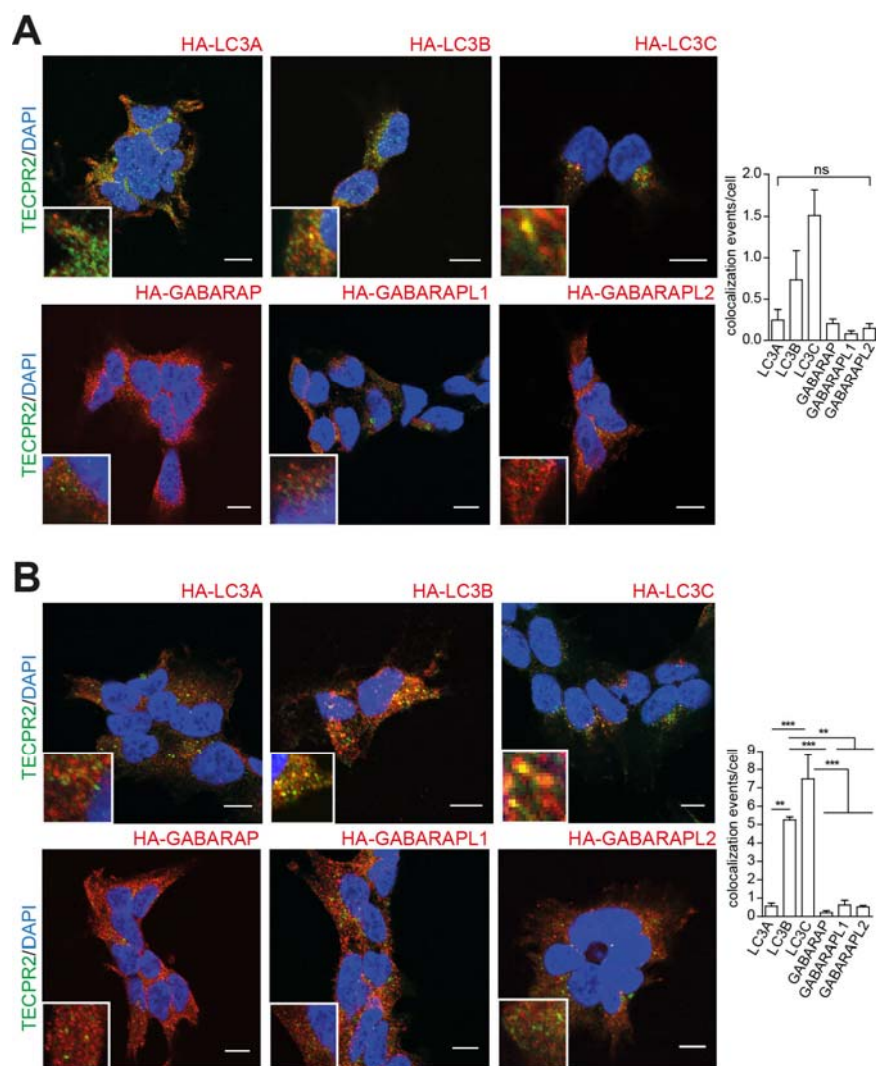


Figure 3-12: Colocalization preference of TECPR2 with LC3 subfamily members in cells.

(A-B) 293T-Rex cells expressing indicated constructs for 2 hrs were (A) left untreated or (B) treated with 250 nM Torin1 and 100 nM BafA1 for 2 hrs. Following fixation cells were labelled with α -TECPR2 and α -HA antibodies. Boxes show inset regions. Scale bar, 10 μ m. Statistical analysis of colocalization events: unpaired t-test, **= $p < 0.01$, ***= $p < 0.001$, ns=not significant. Data represent mean +SD.

Results

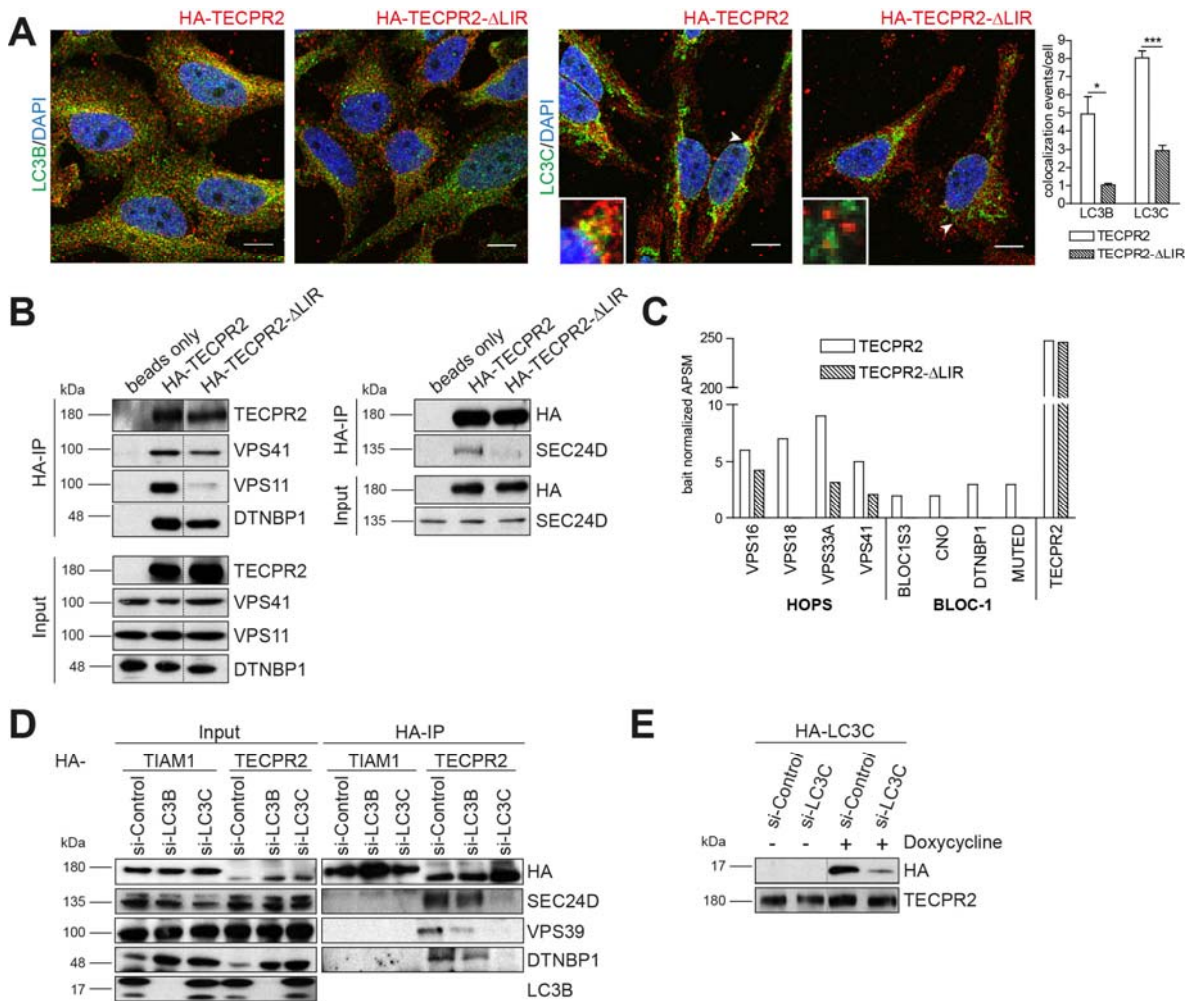


Figure 3-13: Interaction of TECPR2 with SEC24D, HOPS and BLOC-1 is LC3-dependent.

(A) HeLa Flp-IN cells stably expressing HA-TECPR2 or -TECPR2-ΔLIR for 2 hrs were fixed and labelled with α -HA and -LC3B or α -LC3C antibodies. Boxes, inset regions marked with arrowheads. Scale bar, 10 μ m. Statistical analysis of correlation coefficient: unpaired t-test $*=p<0.05$, $***=p<0.001$. Data represent mean +SD. (B) Immunoblotting of α -HA immunoprecipitates from HeLa cells expressing HA-TECPR2 or -TECPR2-ΔLIR. Dashed lines, removal of irrelevant lanes from blots. (C) Lysates from 293T-Rex cells expressing HA-TECPR2 or HA-TECPR2-ΔLIR were subjected to IP-MS analysis. Bait normalized average peptide spectral matches (APSM) are shown for BLOC-1 and HOPS subunits. (D) HeLa cells expressing HA-TECPR2 or -TIAM1 and transfected with indicated siRNAs were subjected to α -HA IP. 5 mM DTBP was used as cross linker. (E) Knockdown control for LC3C. Immunoblot analysis of lysates from HA-LC3C expressing 293T-Rex cells transfected with indicated siRNAs. Notably, the α -LC3C antibody was not specific on immunoblot.

In this experimental setting, TECPR2 partially colocalized with LC3B and LC3C in untreated cells (fig. 3-12A) and this colocalization substantially increased when cells were treated with Torin1 and BafA1 (fig. 3-12B).

Notably, no substantial colocalization of TECPR2 with the remaining ATG8 family members was detected irrespectively of the treatment (fig. 3-12A, 3-12B). TECPR2 lacking the LIR (Δ LIR) colocalized to a significantly lesser extent with endogenous LC3B and LC3C (fig. 3-

Results

13A). The observation that two different parts of TECPR2 (i.e. the N-terminal part and the C-terminal LIR) are employed in association with the trafficking components HOPS, BLOC-1 and SEC24D on the one hand and in binding to ATG8 family members LC3B and LC3C on the other hand raised the question whether these two binding events are dependent on each other. IP-MS and -Western analyses of lysates derived from cells stably expressing HA-tagged wildtype and Δ LIR TECPR2 revealed that association of HOPS and BLOC-1 subunits as well as of SEC24D with TECPR2 required its binding to ATG8 proteins (Fig. 3-13B, 3-13C). Consistently, depletion of LC3B or LC3C decreased association of HA-TECPR2 with VPS39, DTNBP1 and SEC24D (Fig. 3-13D). Interestingly, this effect was most pronounced when LC3C was depleted, which was confirmed in a parallel knockdown experiment using cells stably expressing HA-LC3C (Fig. 3-13E).

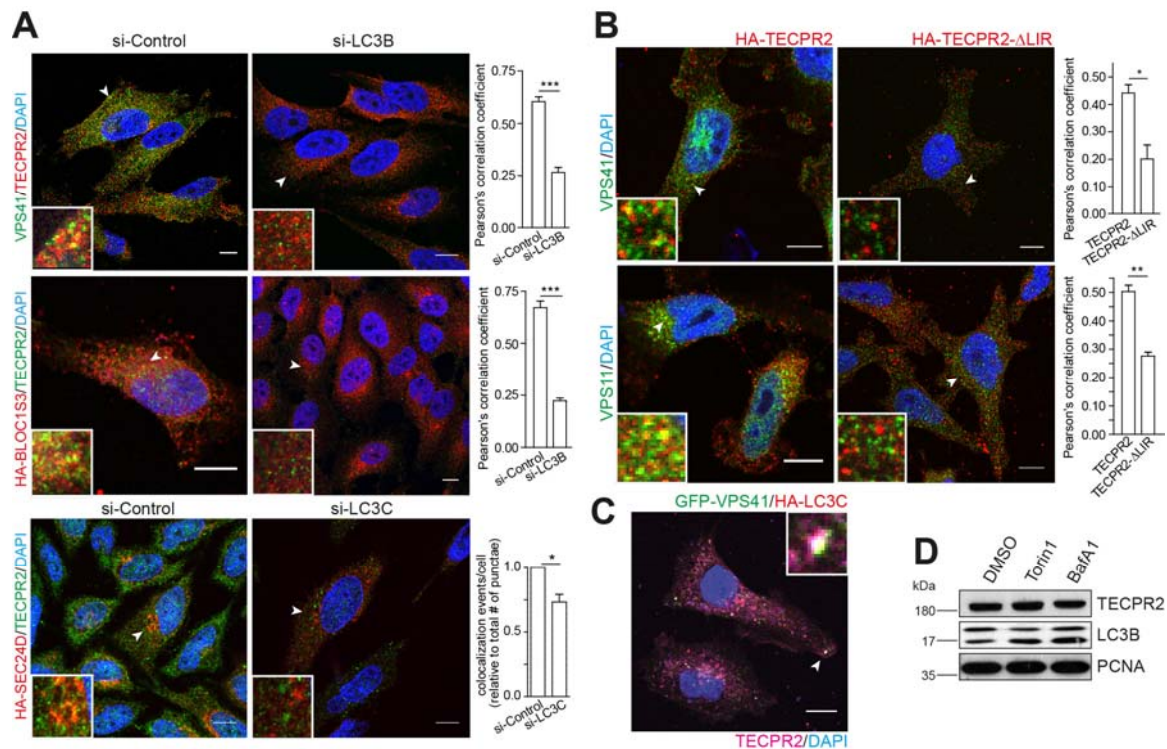


Figure 3-14: Colocalization of TECPR2 with SEC4D, HOPS and BLOC-1 is LC3-dependent.

(A) Empty or stably HA-BLOC1S3 or -SEC24D expressing HeLa cells transfected with indicated siRNAs were fixed and labelled with α -VPS41 or α -HA and -TECPR2 antibodies. Boxes, inset regions marked with arrowheads. Scale bar, 10 μ m. Statistical analysis of correlation coefficient or colocalization events: unpaired t-test $*=p<0.05$, $***=p<0.001$. Data represent mean +SD. (B) HeLa Flp-in cells expressing HA-TECPR2 or -TECPR2- Δ LIR for 2 hrs were fixed and labelled with α -HA and -VPS41 or -VPS11 antibodies. Boxes, inset regions marked with arrowheads. Scale bar, 10 μ m. Statistical analysis of correlation coefficient: unpaired t-test $*=p<0.05$, $**=p<0.01$. Data represent mean +SD. (C) HeLa cells expressing GFP-VPS41 and HA-LC3C were fixed followed by labeling with α -HA and -TECPR2 antibodies. Box, inset region marked with arrowhead. Scale bar, 10 μ m. (D) HeLa cells grown for 2 hrs in the absence or presence of BafA1 or Torin1 were analyzed by immunoblot.

Consistently, colocalization of endogenous TECPR2 with VPS41, BLOC1S3 and SEC24D (fig. 3-14A) was substantially decreased upon knockdown of LC3B and LC3C. In addition, TECPR2-ΔLIR showed significantly reduced colocalization with VPS41 and VPS11 (fig. 3-14B) compared to wild-type TECPR2. Concurrent with the LC3 binding requirement of TECPR2 to engage its interaction partners, endogenous TECPR2 was found to partially colocalize with tagged variants of VPS41 and LC3C (fig. 3-14C). To examine whether TECPR2 operates as autophagy cargo receptor mediating the selective degradation of its binding partner, the protein abundance of TECPR2 in cells treated with Torin1 or BafA1 was monitored. However, protein levels of TECPR2 were unchanged (fig. 3-14D). These findings indicate that TECPR2 requires binding to LC3B or LC3C to associate and colocalize with HOPS, BLOC-1 and SEC24D without being targeted into the autophagosome.

3.4 TECPR2 depletion destabilizes SEC24D, HOPS and BLOC-1

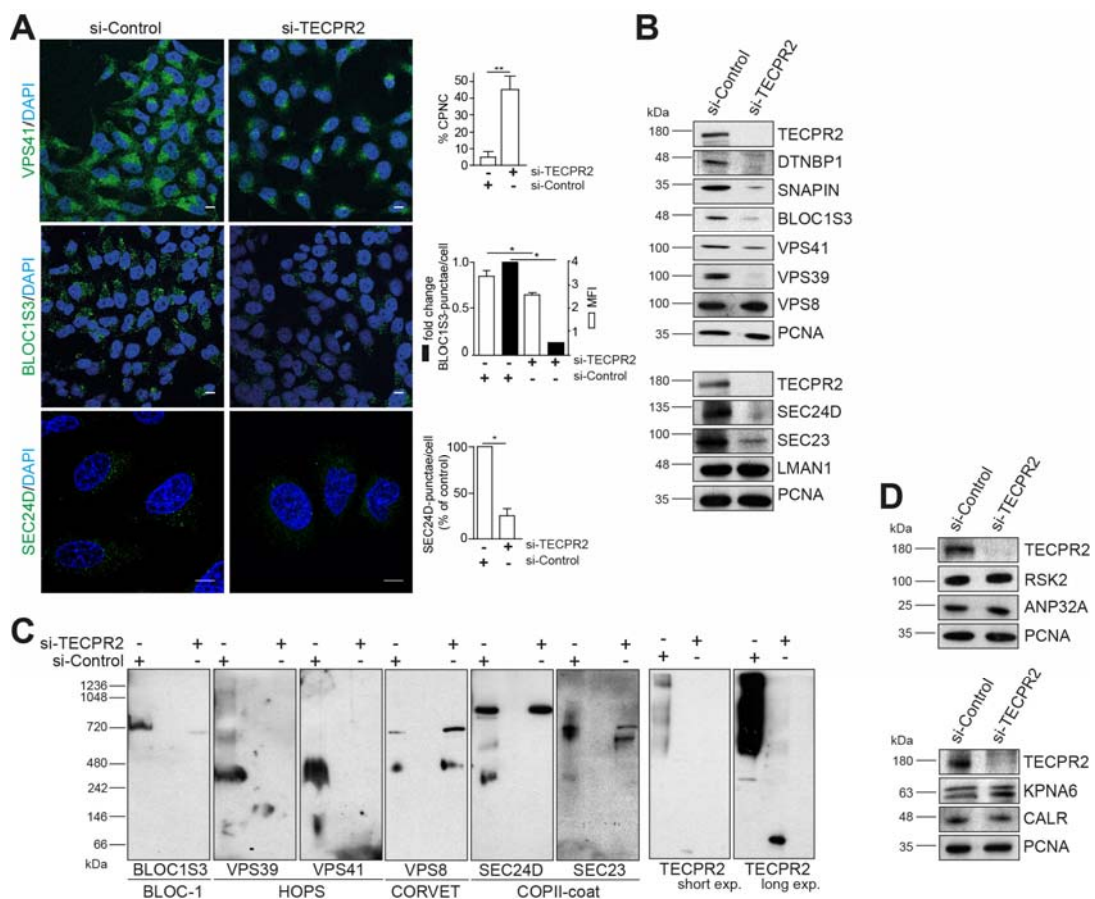


Figure 3-15: Effect of TECPR2 depletion on the protein abundance of SEC24D, HOPS and BLOC-1.

(A-B, D) HeLa cells transfected with si-Control or -TECPR2 were (A) fixed and labelled with indicated antibodies or (B, D) lysed and subjected to immunoblotting. (A) Scale bar, 10 μ m. Statistical analysis of mean fluorescence intensity (MFI), fold change of BLOC1S3-punctae/cell, condensed perinuclear cluster (CPNC) and SEC24D-punctae/cell: unpaired t-test $*=p<0.05$, $**=p<0.01$. Data represent mean +SD. (C) Native PAGE of HeLa cell lysates transfected with si-Control or -TECPR2.

Results

To start examining the relevance of TECPR2 for the function of its interaction partners, the effect of TECPR2 depletion on the subcellular distribution and abundance of SEC24D, HOPS and BLOC-1 was analyzed.

Intriguingly, TECPR2 depletion led to a condensation of VPS41 into the perinuclear region and a reduction in the number of SEC24D and BLOC1S3 positive punctae (fig. 3-15A). Protein abundance of SEC24D and of its dimer partner SEC23, of several BLOC-1 subunits and of the HOPS specific components VPS41 and VPS39 decreased upon depletion of TECPR2 whereas the protein levels of the related class C core vacuole/endosome tethering (CORVET) specific subunit VPS8 was unchanged (fig. 3-15B).

Native PAGE analysis revealed that HOPS and BLOC-1 complexes were completely absent from TECPR2 depleted cells while the CORVET complex increased in abundance (fig. 3-15C), indicating that in absence of HOPS specific subunits the core subunits shared by HOPS and CORVET might be employed as building blocks to promote assembly of CORVET. SEC24D and SEC23 co-migrated in Native PAGE between 242 and 480 kDa, possibly resembling SEC24D-SEC23 dimers. However, depletion of TECPR2 fully ablated SEC24D-SEC23 dimer formation (fig. 3-15C).

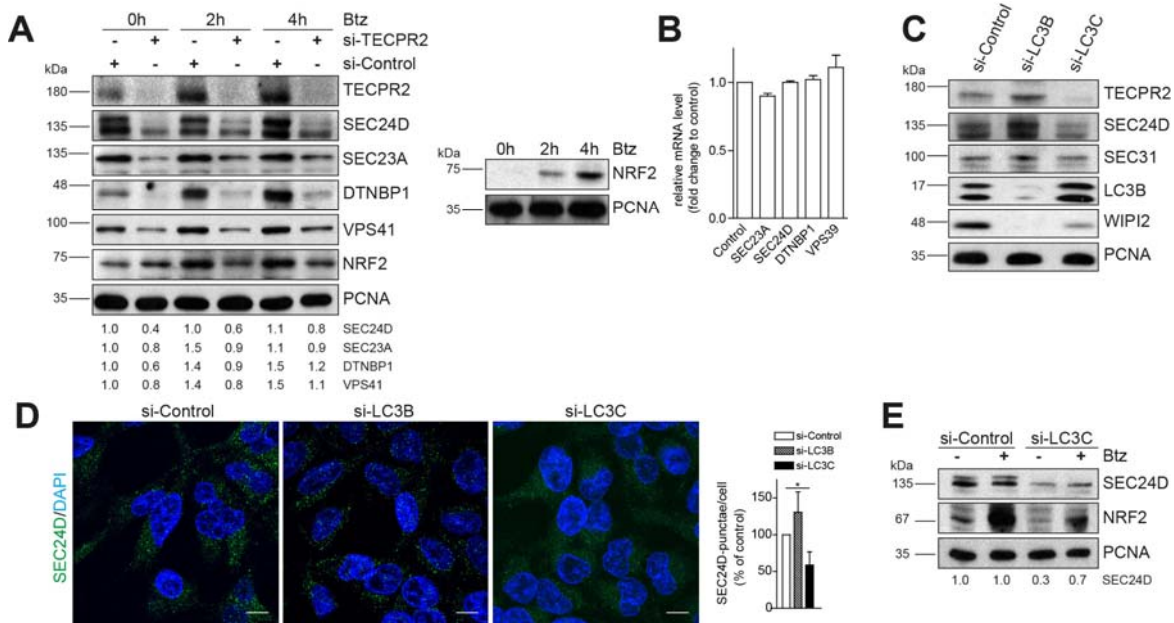


Figure 3-16: TECPR2 and LC3C are required to stabilize SEC24D.

(A) Lysates of HeLa cells grown for up to 4 hrs in absence or presence of Btz analyzed by immunoblotting. Quantification was performed with ImageJ. NRF2 served as a control of Btz-treatment. (B) qPCR of indicated genes. (C) Immunoblotting of lysates from HeLa cells transfected with indicated siRNAs. (D-E) HeLa cells transfected with indicated siRNAs and siRNA-resistant LC3C were grown for 4 hrs in the absence or presence of Btz, (D) fixed and labelled with α -SEC24D antibody or (E) lysed and subjected to immunoblotting. (D) Statistical analysis: one-way ANOVA, $*=p<0.05$. Data represent mean +SD. Scale bar 10 μ m. (E) NRF2 served as a control. Quantification was performed with ImageJ.

Importantly, the protein levels of several other TECPR2 HCIPs such as the nuclear proteins ANP32A and the importin subunit alpha-7 (KPNA6) and the calcium-binding chaperone calreticulin (CALR) were not altered upon TECPR2 knockdown (fig. 3-15D). These results indicate that the abundance changes observed for SEC24D, HOPS and BLOC-1 were specific for this subset of TECPR2 binding partners. Consistent with this finding, inhibition of the proteasome was able to partially revert the decline in VPS41, DTNBP1, SEC24D and SEC23A protein levels in response to TECPR2 depletion (fig. 3-16A), suggesting that upon loss of TECPR2 these binding partners may become subjected to proteasomal degradation. Notably, NRF2 is degraded via the proteasome and serves as positive control (Zhang et al., 2005). In addition, the mRNA levels of SEC24D, SEC23A, DTNBP1 and VPS39 were not altered upon TECPR2 knockdown, demonstrating that the abundance changes occurred post-translationally (fig. 3-16B).

Since TECPR2 colocalization with SEC24D was more frequent than with VPS41 (fig. 3-4A) the focus for further functional studies was set on SEC24D to decipher the requirements for SEC24D stabilization by TECPR2.

Consistent with the observations in the previous experiments (fig. 3-13D, 3-14A) that the presence of LC3C is important for SEC24D rather than LC3B, depletion of LC3C but not LC3B decreased protein abundance (fig. 3-16C) and punctae formation (fig. 3-16D) of SEC24D. Finally, Btz treatment partially reverted the reduction in SEC24D protein levels induced by loss of LC3C (fig. 3-16E), meaning that SEC24D is degraded via proteasome in dependence of LC3C as well as TECPR2 (fig. 3-16A).

While re-expression of wild-type TECPR2 and of the C-terminal TECPR2 fragment (751-1411aa) was able to rescue the decline in SEC24D punctae in TECPR2 depleted cells, the TECPR2 LIR-mutant (W1408A) and the N-terminal TECPR2 fragment (1-750aa) failed to revert this phenotype (fig. 3-17A). Expression of TECPR2 fragments was confirmed with α -TECPR2 staining (fig. 3-17B). These findings implicate the possibility that TECPR2 possess a secondary alternative binding site for SEC24D in the C-terminal part of TECPR2 and highlight the importance of the TECPR2-LC3 binding for SEC24D stabilization.

Re-introduction of wild-type LC3C rescued the latter phenotype in contrast to LC3C lacking the C-terminal Glycine (Δ G) (fig. 3-17C). These results suggest that TECPR2 is required for stabilization of SEC24D, HOPS, and BLOC-1 possibly contributing to their complex assembly. In the case of SEC24D, this stabilization depends on the binding of TECPR2 to lipidated LC3C.

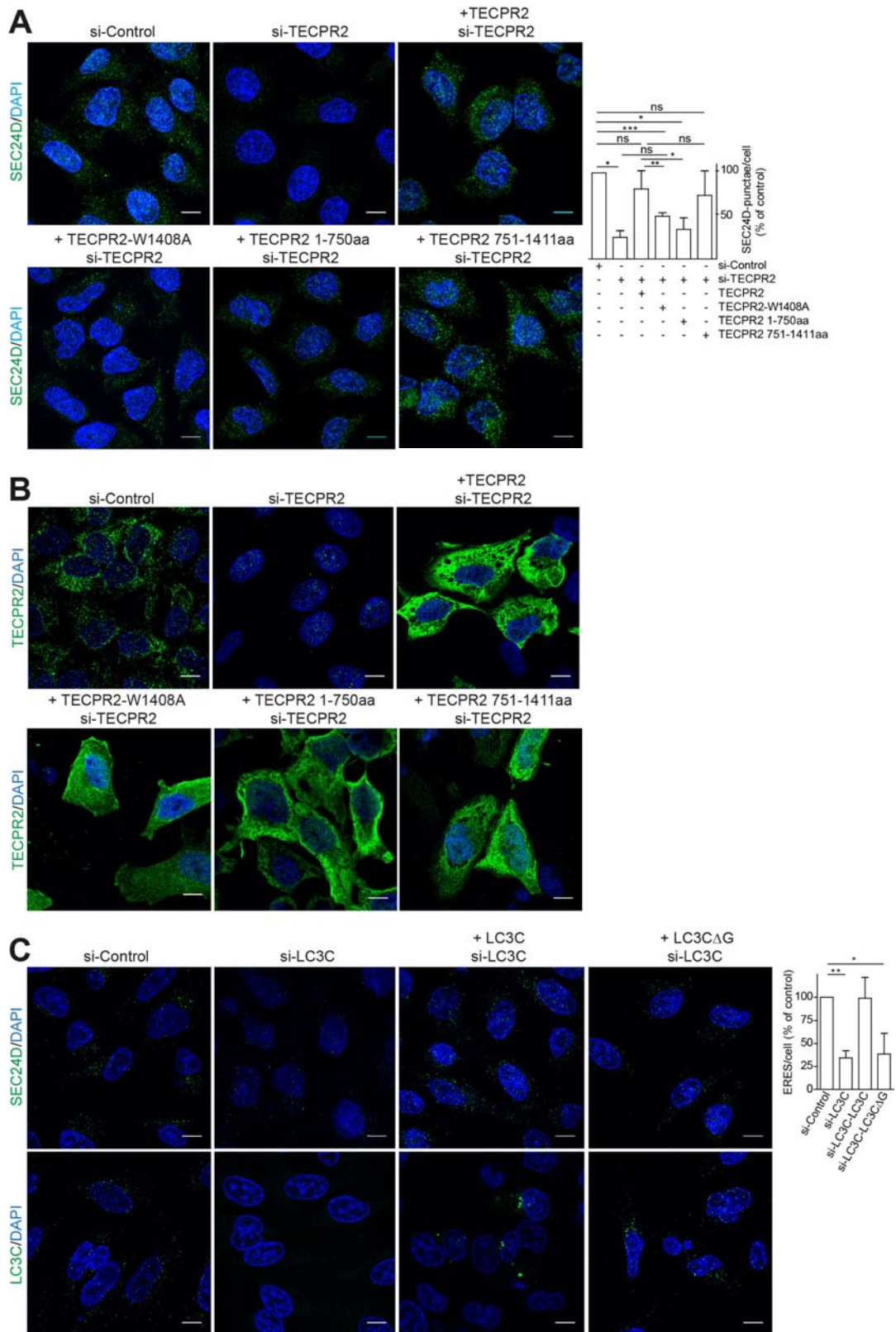


Figure 3-17: Stabilization of SEC24D levels requires the C-terminal part of TECPR2 encompassing its LIR.

(A-C) HeLa cells transfected with siRNA-resistant variants and indicated siRNAs were fixed and labelled with α -SEC24D, -TECPR2 or -LC3C antibodies. Scale bar, 10 μ m. Statistical analysis of (A): one-way ANOVA, ***= $p < 0.001$, **= $p < 0.01$, *= $p < 0.05$, ns=not significant. Data represent mean +SD.

3.5 Loss of TECPR2 compromises ERES

Since the human genome encodes for four different SEC24 isoforms, phenotypes observed for a single isoform (i.e. SEC24D) might not reflect global changes in ERES. Therefore, two complementary approaches to examine the effects of TECPR2 depletion on ERES were employed in close collaboration with Valentina Millarte and Kerstin Tillmann from the group of Dr. Hesso Farhan. First, the dynamics of SEC24D using fluorescence recovery after photo bleaching (FRAP) were determined to monitor the recruitment of SEC24D to ERES.

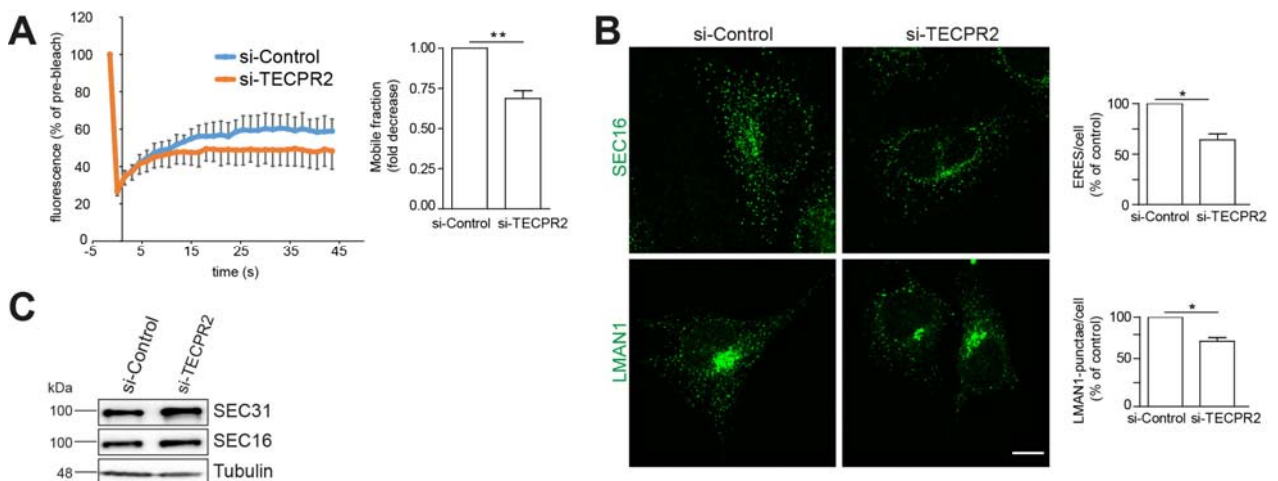


Figure 3-18: ERES are impaired upon TECPR2 depletion.

(A) FRAP curves recorded from HeLa cells expressing YFP-SEC24D and transfected with si-Control or -TECPR2 were employed for quantification of mobile SEC24D fraction. Statistical analysis: paired t-test $**=p<0.01$. Data represent mean +SD. (B) HeLa cells transfected with si-Control or -TECPR2 were fixed and labelled with α -SEC16 and -LMAN1 antibodies. Scale bar, 10 μ m. Statistical analysis: unpaired t-test $*=p<0.05$. Data represent mean +SD. (C) Immunoblotting of lysates from HeLa cells transfected with si-Control or -TECPR2. Tubulin served as loading control.

Compared to control cells, recovery and mobile fraction of YFP-tagged SEC24D was decreased in TECPR2 depleted cells (fig. 3-18A), indicating a general ERES defect resulting in reduced recruitment of SEC24D. Second, ERES number were assessed by immunostaining for SEC16, a component of the outer COPII coat that was previously shown to regulate ERES homeostasis (Sprangers and Rabouille, 2015). Consistent with compromised SEC24D-SEC23A dimer formation, it was observed that depletion of TECPR2 generally reduced ERES number (fig. 3-18B). Moreover, the number of peripheral LMN1 (ERGIC-53) positive structures were also monitored, as these are well known to reflect the function of ERES (Ben-Tekaya et al., 2005). Silencing TECPR2 reduced the number of LMN1 punctae, indicating that ERES function is probably affected (fig. 3-18B). Notably, TECPR2 depletion did not alter the protein levels of LMN1 (fig. 3-15B), SEC31 and SEC16 (fig. 3-18C).

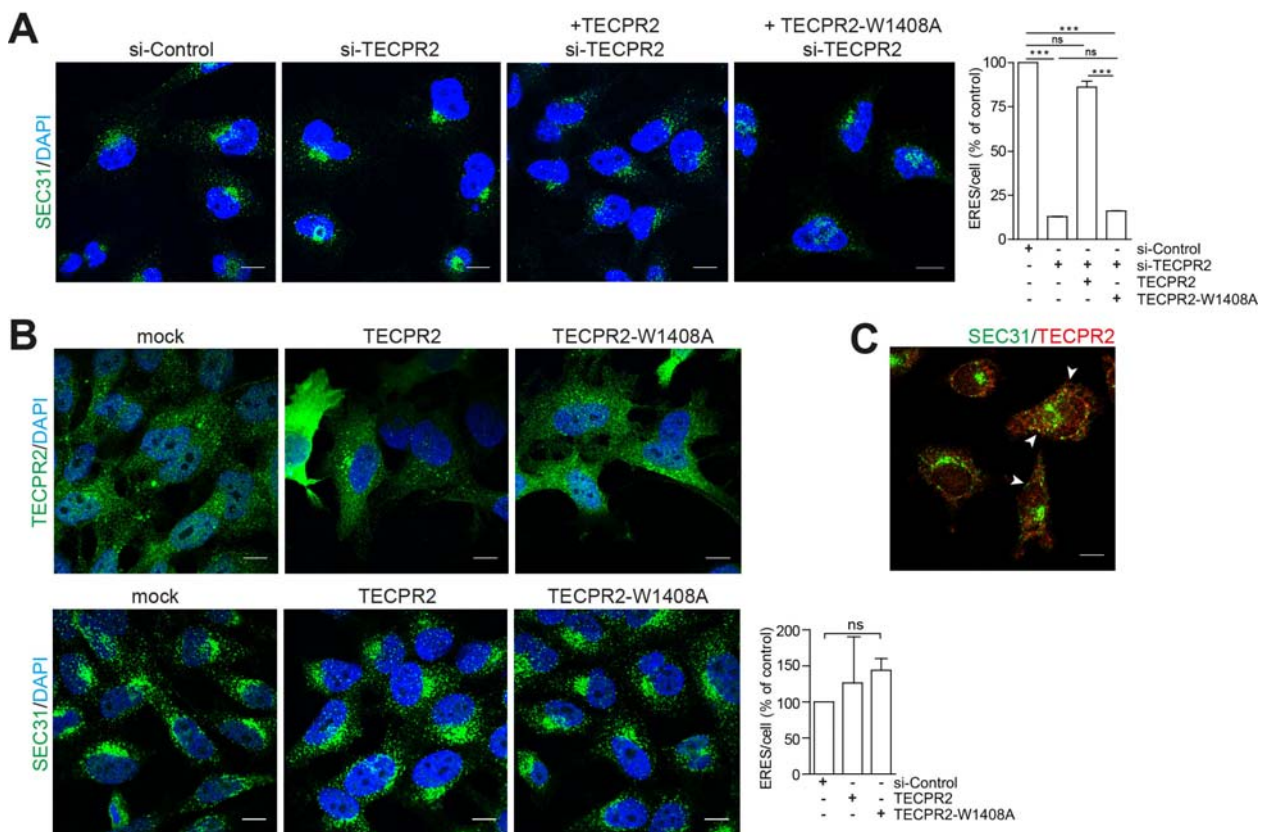


Figure 3-19: Maintenance of ERES depends on the ability of TECPR2 to bind ATG8 proteins.

(A-B) HeLa cells transfected with siRNA-resistant TECPR2 variants and indicated siRNAs were fixed and labelled with α -SEC31 or α -TECPR2 antibodies. Scale bar, 10 μ m. Statistical analysis: one-way ANOVA, ***= $p < 0.001$, ns=not significant. Data represent mean +SD. (C) HeLa cells were fixed and labelled with α -TECPR2 and α -SEC31 antibodies. Scale bar, 10 μ m.

To analyze the role of TECPR2 in maintaining efficient ERES, RNAi rescue experiments with TECPR2 were performed and ERES were monitored by SEC31 immunostaining.

While re-introducing wildtype TECPR2 rescued TECPR2 depleted cells from reduced ERES number, TECPR2 LIR-mutant (W1408A) failed to reverse this phenotype (fig. 3-19A). Notably, overexpression of TECPR2 wild-type or LIR-mutant alone did not affect ERES (fig. 3-19B). Consistent with its role in maintaining ERES, endogenous TECPR2 was detected in SEC31 positive structures (fig. 3-19C).

Results

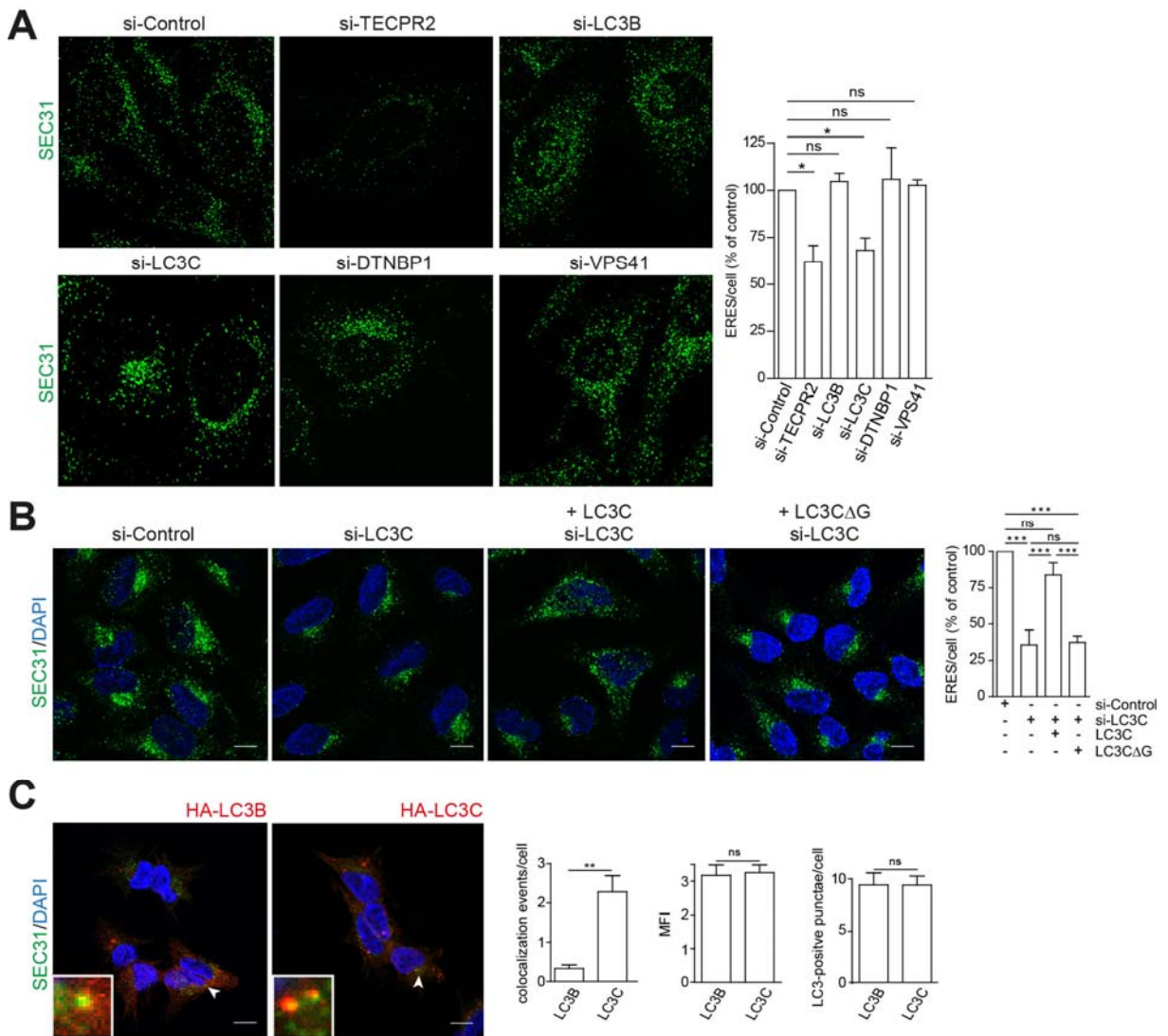


Figure 3-20: Maintenance of ERES depends on TECPR2 and LC3C.

(A) HeLa cells transfected with indicated siRNAs were fixed and labelled with α -SEC31 antibody. Scale bar, 10 μ m. Statistical analysis of ERES: unpaired t-test $*=p<0.05$, ns=not significant. Data represent mean +SD. (B) HeLa cells transfected with siRNA-resistant LC3C variants and indicated siRNAs were fixed and labelled with α -SEC31 antibody. Scale bar, 10 μ m. Statistical analysis: one-way ANOVA, $***=p<0.001$, ns=not significant. Data represent mean +SD. (C) 293Trex HEK cells expressing HA-LC3B or -LC3C were fixed and labelled with α -SEC31 antibody. Boxes, inset regions marked with arrowheads. Scale bar, 10 μ m. Statistical analysis of colocalization events (left), MFI (middle) and LC3 positive punctae (right): unpaired t-test $**=p<0.01$, ns=not significant. Data represent mean +SD.

Since maintenance of ERES by TECPR2 was LIR-dependent, the question arose whether depletion of LC3B or LC3C results in a similar phenotype than TECPR2 knockdown. Intriguingly, only knockdown of LC3C but not LC3B led to a decrease in ERES number (fig. 3-20A) without overt changes in SEC31 protein levels (fig. 3-16C). Likewise, loss of VPS41 or DTNBP1 did also not influence the number of ERES (fig. 3-20A). Importantly, re-expression of wildtype LC3C but not LC3C Δ G was able to rescue the ERES phenotype (fig. 3-20B).

Results

Consistent with a role of LC3C in maintaining ERES, colocalization between SEC31 and LC3C was detected with much higher occurrence than between SEC31 and LC3B although punctae formed by both LC3 proteins did not differ in number or intensity (fig. 3-20C).

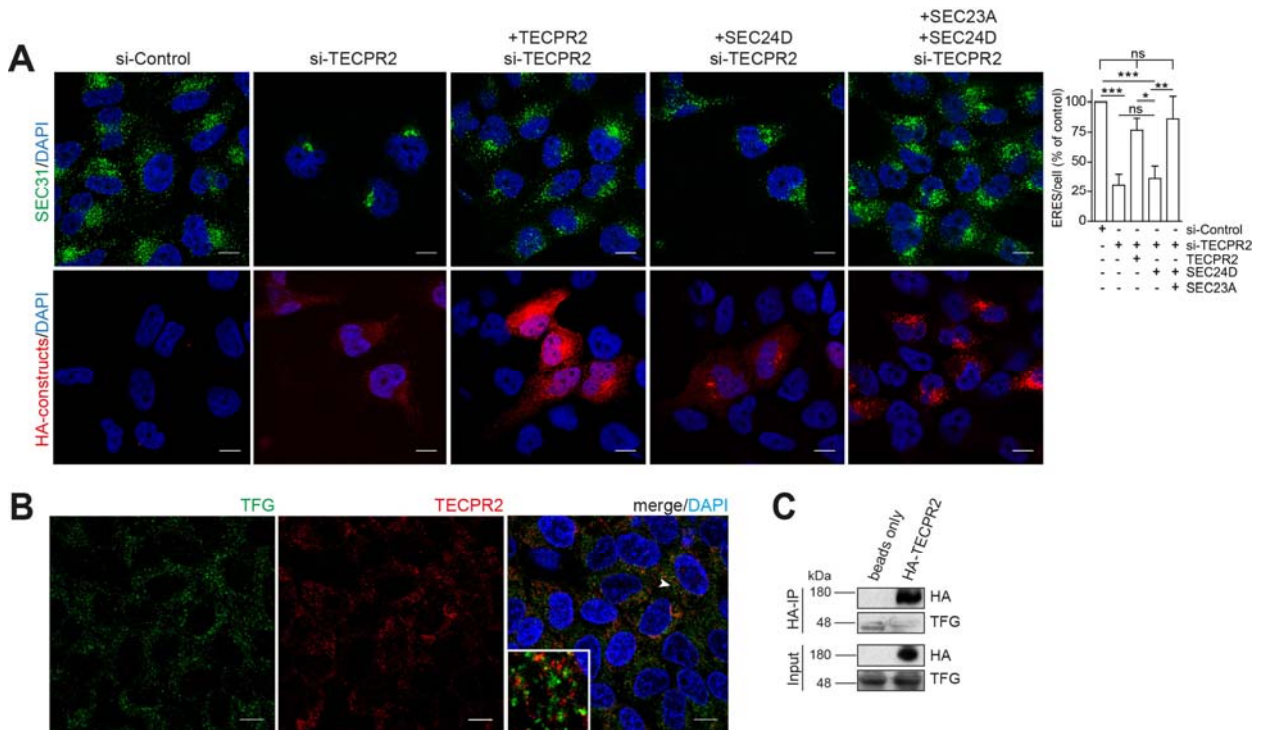


Figure 3-21: Maintenance of ERES by TECPR2 depends on SEC23A and SEC24D.

(A) HeLa cells transfected with HA-SEC24D and -SEC23A and indicated siRNAs were fixed and labelled with α -SEC31 or -HA antibodies. Scale bar, 10 μ m. Statistical analysis: one-way ANOVA, ***= $p < 0.001$, **= $p < 0.01$, *= $p < 0.05$, ns=not significant (B) HeLa cells were fixed and labelled with α -TECPR2 and α -TFG antibodies. Box show inset region marked with arrowhead. Scale bar, 10 μ m. (C) Immunoblot analysis of α -HA immunoprecipitates from HeLa cells transiently expressing HA-TECPR2 or empty lysate. 5mM DTBP was used as cross linker.

Finally, the question was addressed, whether the reduction of ERES in response to loss of TECPR2 is indeed mediated by diminished SEC24D and SEC23A protein levels. Overexpression of SEC24D and SEC23A together but not of SEC24D alone reversed the ERES phenotype in TECPR2 depleted cells (fig. 3-21A). These results demonstrate that TECPR2 positively regulates ERES in an LC3C-binding dependent manner. Notably, TECPR2 did not colocalize (fig. 3-21B) or associate (fig. 3-21C) with the COPII regulator and HSP linked protein TFG, indicating that both factors possible operate at different stages of ERES formation.

3.6 TECPR2 is required for ER export

To examine whether loss of TECPR2 also affects ER-to-Golgi transport, the retention using selective hooks (RUSH) approach (Boncompain et al., 2012) was employed in collaboration with Valentina Millarte and Kerstin Tillmann from the group of Dr. Hesso Farhan and Franck Perez. In this system secretory cargo is retained in the ER through streptavidin-based retention and released to the secretory pathway upon biotin addition. Since glycosylphosphatidylinositol (GPI) anchored proteins were exhibit to preferentially depend on SEC24C and SEC24D for their export from the ER (Bonnon et al., 2010), cells stably expressing streptavidin-binding peptide (SBP)-GFP-GPI were used.

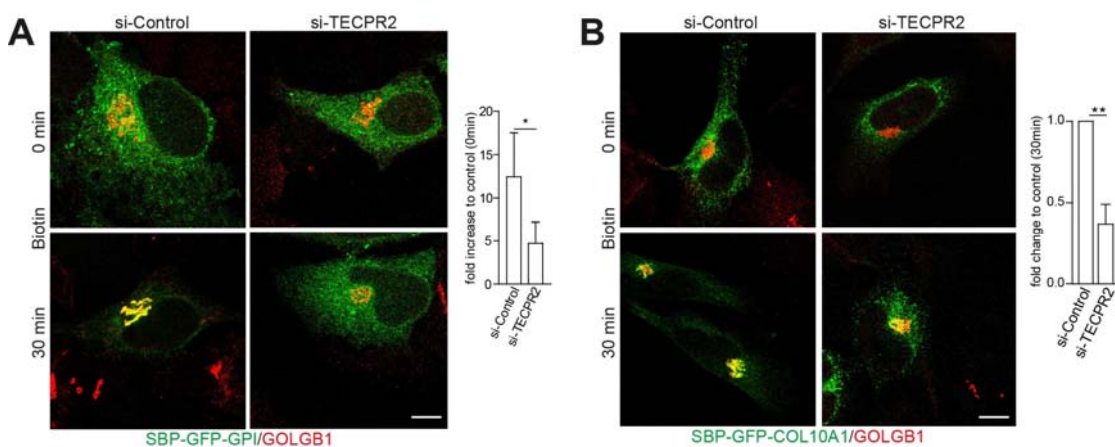


Figure 3-22: Export of cargo from ER is impaired upon TECPR2 depletion.

(A-B) HeLa cells stably expressing SBP-GFP-GPI or -COL10A1 and transfected with si-Control, -TECPR2 for 72 hrs were fixed at indicated time points post biotin addition and labelled with α -GOLGB1 antibody. Statistical significance of fold change to control: paired t-test $*=p<0.05$, $**=p<0.01$. Data represent mean +SD.

While the reporter clearly left the ER and reached the Golgi as its target compartment after biotin addition in control cells, TECPR2 knockdown caused a substantial block in the arrival of SBP-GFP-GPI from the ER to the Golgi (fig. 3-22A). To test whether other types of cargo similarly require TECPR2, the ER export of collagen 10 α 1 (COL10A1) was monitored. Depletion of TECPR2 led to a marked delay in the arrival of SBP-GFP-COL10A1 at the Golgi (fig. 3-22B).

Consistently, human fibroblasts depleted of TECPR2 displayed a dramatic reduction in the number of peripheral punctae positive for endogenous alpha-1 type I collagen (COL1A1) concurrent with a change from an elongated to a rounded morphology, which both can partially be rescued by re-introducing TECPR2 (fig. 3-23A). While decreased collagen levels were detected in the supernatant of TECPR2 depleted fibroblasts, the amount of intracellular collagen increased (fig. 3-23B). Notably, similar results were also obtained in HeLa cells (fig. 3-

Results

23C, 3-23D). To test whether LC3C knockdown phenocopies the ER export defect caused by loss of TECPR2, cells stably expressing the type II transmembrane protein mannosidase II (MAN2A1) fused to the SFB-GFP tandem were employed.

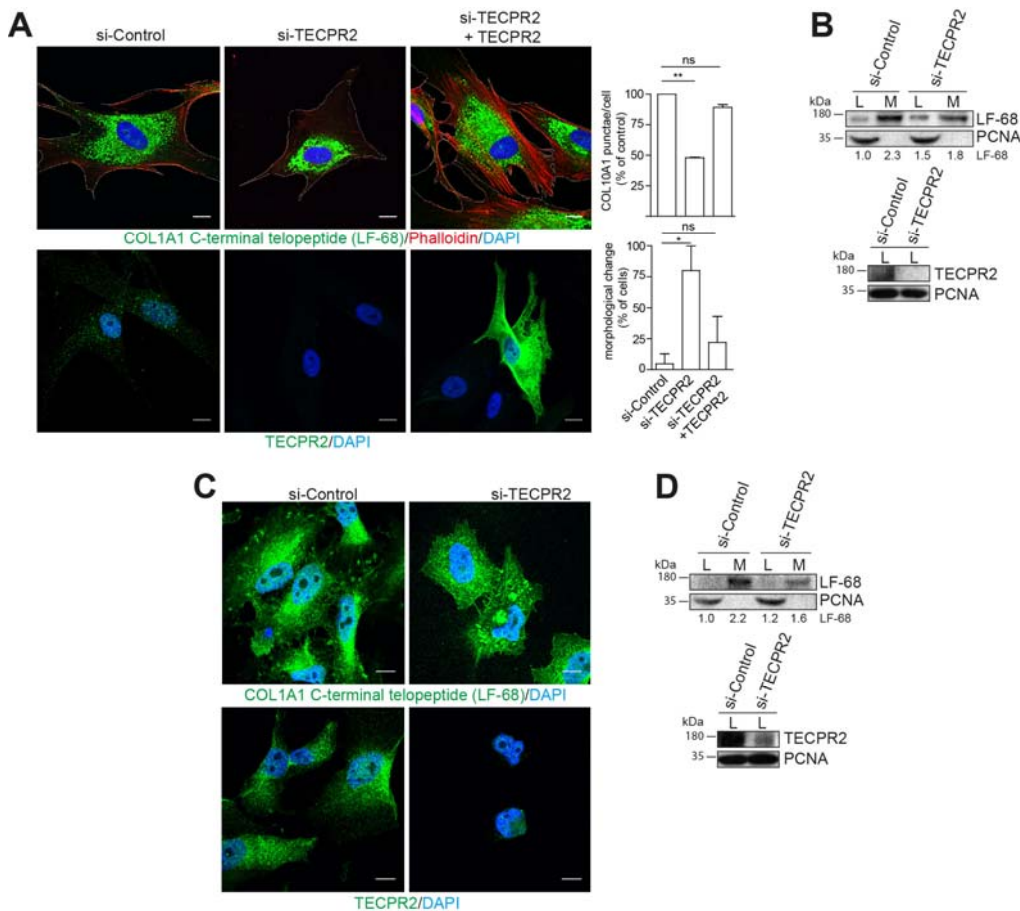


Figure 3-23: Loss of TECPR2 affects collagen secretion in human fibroblasts and HeLa cells.

(A) Human skin fibroblasts (CCD-1117sk) transfected with siRNA-resistant TECPR2 and indicated siRNAs were fixed and labelled with phalloidin and α -COL1A1 C-terminal telopeptide (LF-68) or α -TECPR2 antibodies. Scale bar, 10 μ m. Statistical significance of peripheral collagen punctae/cell and morphological change: one-way ANOVA, $*=p<0.05$, $**=p<0.01$, ns=not significant. Data represent mean +SD. (B) Lysates (L) or culture medium (M) from CCD-1117sk cells were analyzed by immunoblotting. Quantification was performed with ImageJ. (C) HeLa cells transfected with si-Control or si-TECPR2 were fixed and labelled with α -TECPR2 or α -COL1A1 C-terminal telopeptide (LF-68) antibodies. Scale bar, 10 μ m. (D) Lysates (L) or culture medium (M) from HeLa cells were analyzed by immunoblotting. Quantification was performed with ImageJ.

Intriguingly, a significant delay in trafficking of MAN2A1-SFB-GFP in TECPR2 or LC3C depleted cells but not upon knockdown of LC3B was observed (fig. 3-24). This phenotype was rescued by re-introduction of LC3C (fig. 3-25A). In a further set of experiments HeLa cells were depleted of ATG12 (fig. 3-25B), which is required for LC3 lipidation, and subjected to RUSH assays following MAN2A1-SFB-GFP. Remarkably, ATG12 depletion mimicked the phenotype of TECPR2 and LC3C knockdown, suggesting that TECPR2 requires binding to lipidated LC3C to allow efficient export from ER (fig. 3-25C).

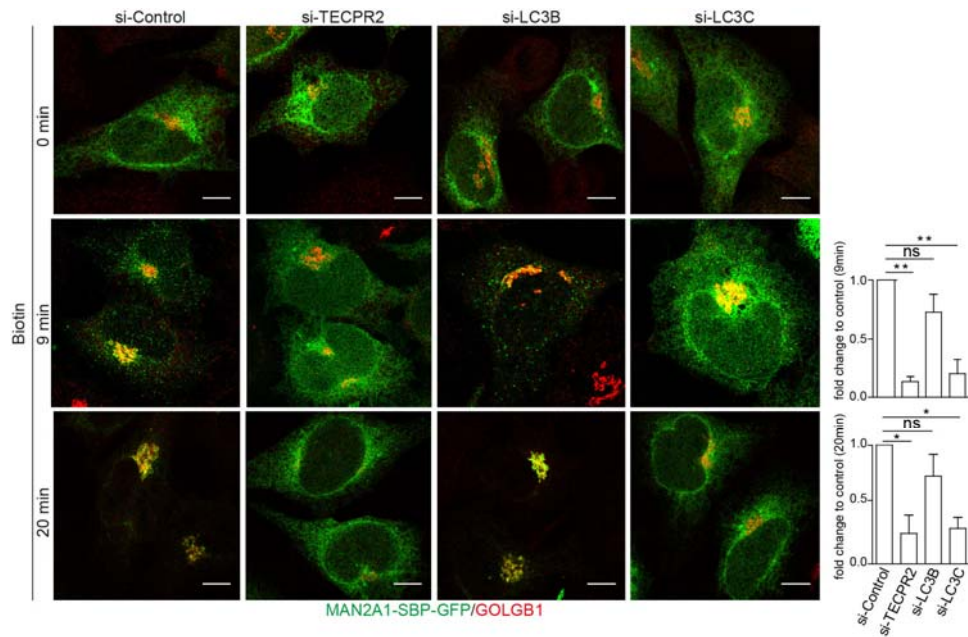


Figure 3-24: Export of mannosidase II is delayed upon knockdown of TECPR2 or LC3C.

HeLa cells stably expressing MAN2A1-SBP-GFP and transfected with si-Control, -TECPR2, -LC3B or -LC3C for 72 hrs were fixed at indicated time points post biotin addition and labelled with α -GOLGB1 antibody. Statistical significance of fold change to control: paired t-test $*=p<0.05$, $**=p<0.01$. Data represent mean +SD.

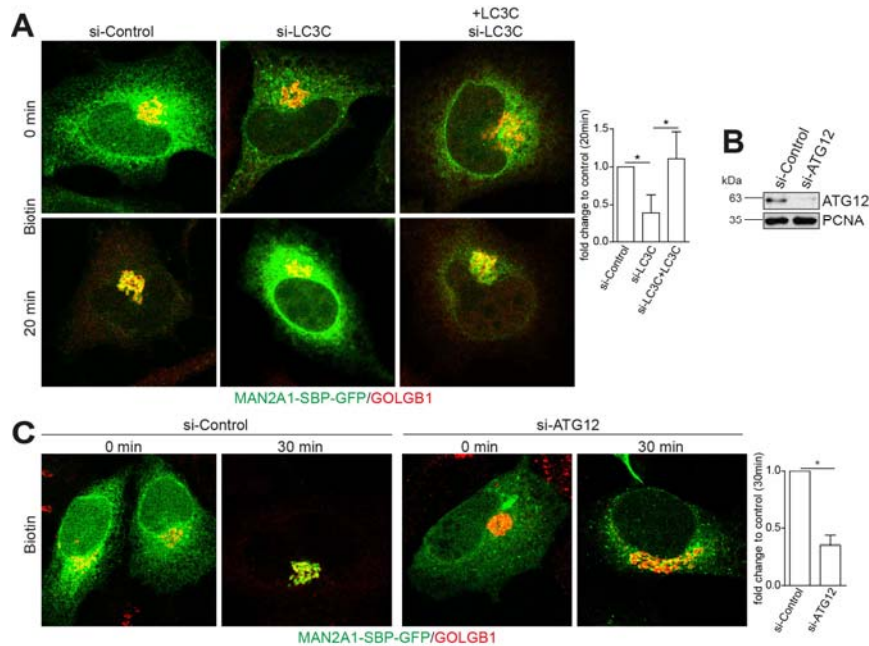


Figure 3-25: Loss of LC3C or ATG12 impairs export of cargo from ER.

(A) HeLa cells stably expressing MAN2A1-SBP-GFP transfected with si-Control or si-LC3C for 72 hrs and siRNA-resistant LC3C for the last 24 hrs were fixed post biotin addition and labelled with α -GOLGB1 antibody. Scale bar, 10 μ m. Statistical significance of fold change to control: paired t-test, $*=p<0.05$. Data represent mean +SD. (B) kd-control for ATG12 of (C). (C) HeLa cells expressing MAN2A1-SBP-GFP and transfected with indicated siRNAs were fixed post biotin addition and labelled with α -GOLGB1 antibody. Scale bar, 10 μ m. Statistical analysis of fold change to control: one-way ANOVA, $*=p<0.05$, ns=not significant. Data represent mean +SD.

Results

To investigate whether this ER export defect contributes to the mechanism underlying pathogenesis caused by the recessive c.3416delT mutation of *TECPR2* in HSP patients, MAN2A1-SBP-GFP in skin fibroblasts isolated from affected and unrelated control individuals were monitored in close collaboration with Bat-Chen Tamin-Yecheskel and Alik Demisthein from the group of Prof. Zvulun Elazar and two medical doctors Yair Anikster and Bruria Ben-Zeev. Remarkably, ER export of MAN2A1 was largely delayed in HSP patient cells (Ex-16; (Oz-Levi et al., 2012)) compared to control cells (Healthy) (fig. 3-26A) concurrent with a reduction in SEC24D protein levels while those of DTNBP1 and VPS41 were unchanged (fig. 3-276B).

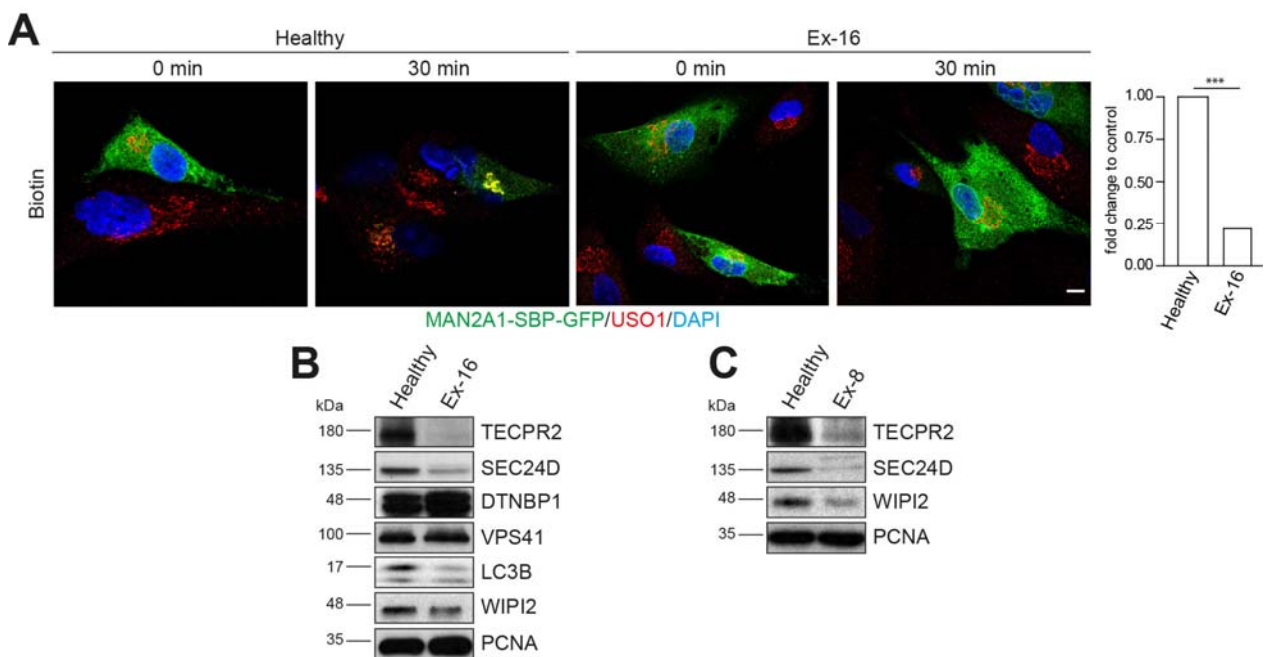


Figure 3-26: HSP patient cells show decreased SEC24D protein levels and impaired ER-to-Golgi transport.

(A) Skin fibroblasts of an HSP affected individual (Ex-16) and a healthy control (Healthy) were transfected for 24 hrs with MAN2A1-SBP-GFP. Cells were fixed at 30 min post biotin addition and labelled with α -USO1 antibody (Golgi resident protein, alias p115). Scale bar, 10 μ m. (B-C) Immunoblot analysis of skin fibroblasts isolated from HSP affected individuals (Ex-16), (Ex-8) and a healthy control (Healthy).

Importantly, fibroblasts from a patient with a new homozygous frameshift mutation in *TECPR2* (Heimer et al., 2015) showed a similar reduction in SEC24D protein abundance (fig. 3-26C). These results display that binding of TECPR2 to lipidated LC3C is required for efficient ER export of several types of secretory cargo and that deregulation of SEC24D protein levels and ER export due to impairment of TECPR2 function may contribute to HSP pathogenesis.

3.7 TECPR2 depletion affects ER morphology

Given the impact of TECPR2 on ERES and ER export, the organization of secretory pathway compartments including ER, *cis*- and *trans*-Golgi was examined by monitoring the levels and distribution of endogenous CKAP4 (alias CLIMP63), GOLGA2 (alias GM130) and TGOLN2 (alias TGN46), respectively. The intensity of the CKAP4 immunofluorescence staining markedly increased in TECPR2 depleted cells while CKAP4 protein levels were unchanged (fig. 3-27A, 3-27B).

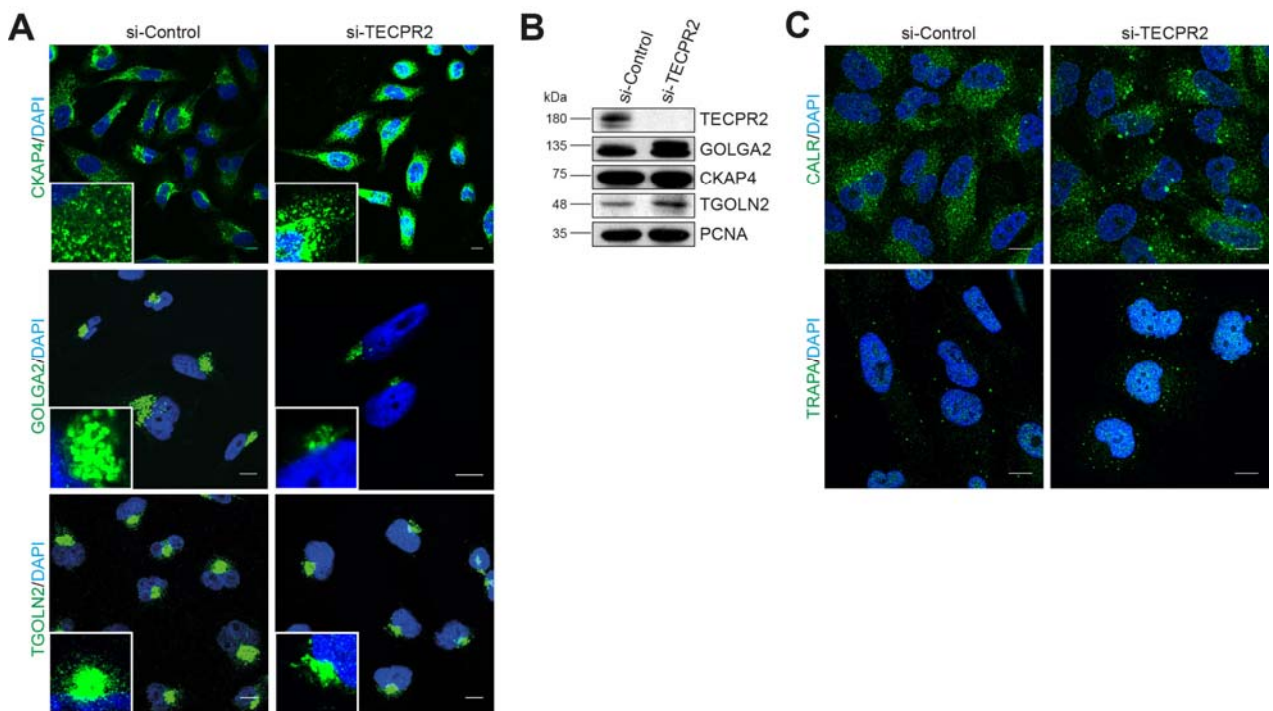


Figure 3-27: ER and Golgi proteins cluster in absence of TECPR2.

(A-C) HeLa cells were (A, C) fixed and labelled with indicated antibodies or (B) lysed and subjected to immunoblot analysis. (A, C) Scale bar, 10 μ m. Boxes show inset regions.

Conversely, these cells displayed a condensed *cis*- and *trans*-Golgi as well as increased protein abundance of GOLGA2, a protein located in the membrane of *cis*-Golgi stacks, and TGOLN2, a *trans*-Golgi network marker (fig. 3-27A, 3-27B). Testing of the calcium-binding ER chaperones Calregulin (CALR) and TRAPA exhibit a similar elevation in protein levels upon TECPR2 depletion (fig. 3-27C).

To further explore the changes in ER morphology observed with the ER sheet marker CKAP4, we monitored SEC61B and ZFYVE27 (alias protrudin) as general and tubule-specific ER markers, respectively.

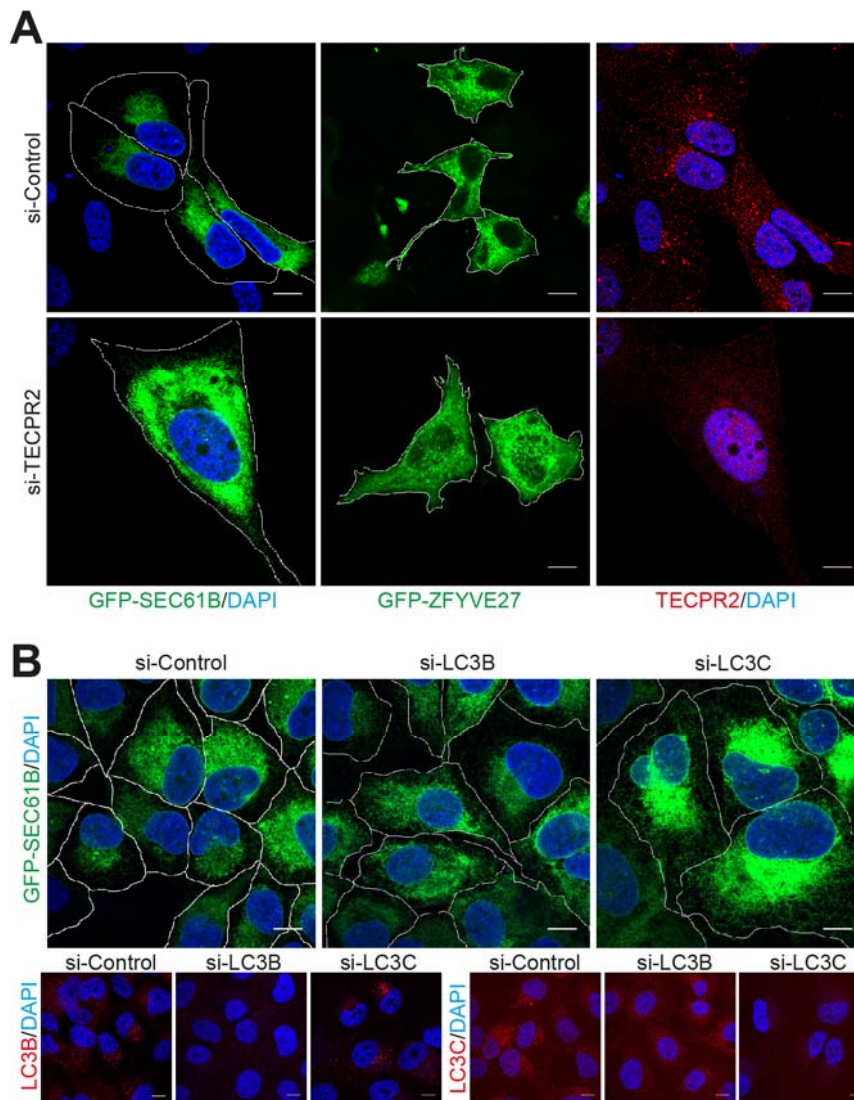


Figure 3-28: Loss of TECPR2 leads to altered ER morphology.

(A) U2OS cells stably expressing GFP-tagged SEC61B or ZFYVE27 and transfected with si-Control or si-TECPR2 were fixed and for control labelled with α -TECPR2 antibody. (B) U2OS cells stably expressing GFP-tagged SEC61B transfected with indicated siRNAs were fixed and labelled with α -LC3B or α -LC3C antibodies.

TECPR2 depleted cells expressing GFP-SEC61B or GFP-ZFYVE27 (fig. 3-28A) showed a marked expansion of the respective ER sub-compartment. Consistent with the cooperative function of TECPR2 and LC3C, depletion of LC3C but not LC3B led to a similar expansion of ER sheets as observed for TECPR2 depletion (fig. 3-28B).

Finally, to assess whether the impact of TECPR2 knockdown on ERES and ER morphology are accompanied with ER stress induction, the abundance of the ER stress markers BIP and HERP were monitored.

Results

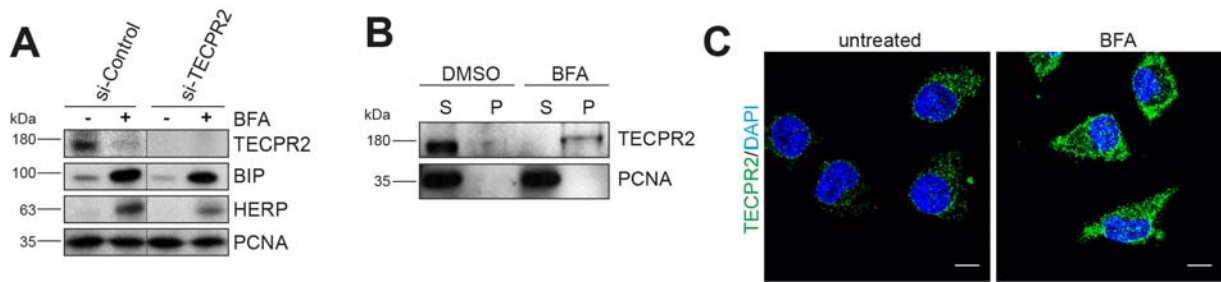


Figure 3-29: Absence of TECPR2 does not induce ER stress response.

(A-B) HeLa cells transfected with si-Control or si-TECPR2 or left untreated were incubated with BFA for 24 hrs and analyzed by immunoblotting. (B) S: soluble fraction; P: pellet (21.000x g) fraction. (C) HeLa cells treated with DMSO or BFA for 2 hrs were fixed and labelled with α -TECPR2 antibody. Scale bar, 10 μ m.

While TECPR2 depleted cells did not show signs of ER stress response, the stress responsiveness of these cells to Brefeldin A (BFA) was slightly reduced (fig. 3-29A). Surprisingly, ER stress seems to induce aggregation or membrane binding of TECPR2, since BFA treatment led to a redistribution of TECPR2 from the soluble to the pellet fraction (fig. 3-29B) concurrent with an increase in fluorescence intensity of TECPR2 (fig. 3-29C). These results suggest that TECPR2 contributes to maintenance of ER morphology and stress responsiveness.

3.8 TECPR2 contributes to autophagosome formation

The findings that TECPR2 operates in the early secretory pathway and the emerging evidence that link ERES to autophagosome formation (Ge et al., 2014; Graef et al., 2013; Zoppino et al., 2010) prompted to revisit the autophagy phenotype observed in TECPR2-deficient cells (Behrends et al., 2010; Oz-Levi et al., 2012).

Knockdown of TECPR2 decreased the amount of lipidated LC3B (fig. 3-30A) and reduced the number of LC3B positive punctae in absence and presence of BafA1 (fig. 3-30B). However, LC3B positive punctae still increased in response to BafA1 treatment in control and TECPR2 depleted cells (fig. 3-30B), suggesting that autophagosome formation but not autophagy flux is impaired upon TECPR2 deficiency. Consistent with reduced autophagosomal engulfment, the protein levels of the cargo receptor SQSTM1 (alias p62) (fig.3-30A) and the number of SQSTM1 positive punctae (fig. 3-30B) elevated in cells depleted of TECPR2.

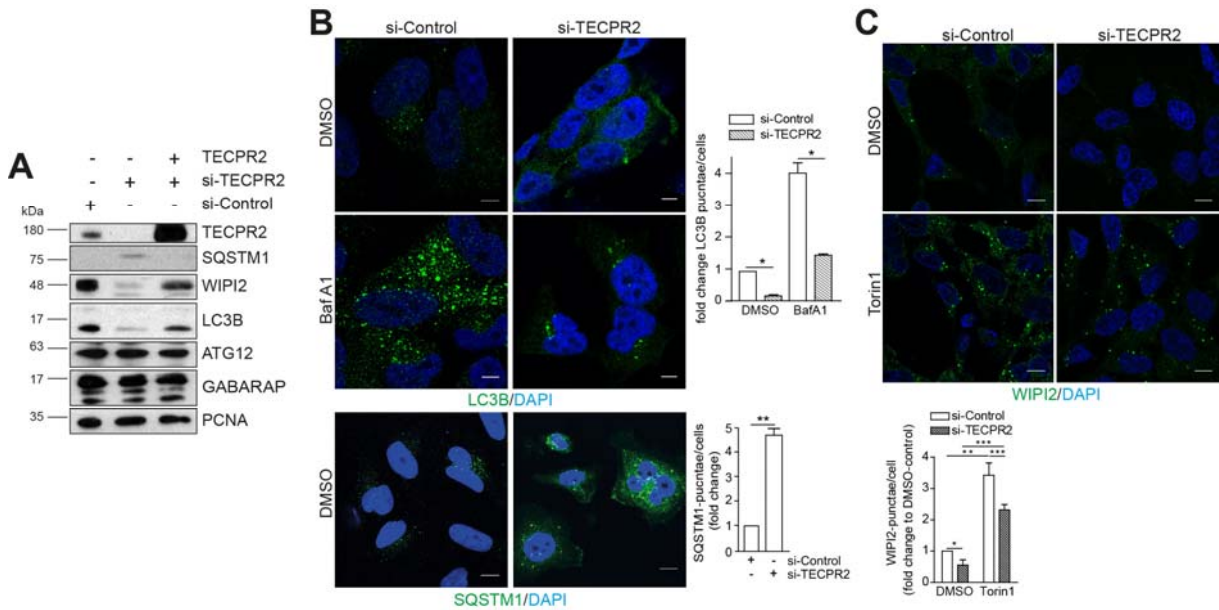


Figure 3-30: TECPR2 is required for autophagosome biogenesis.

(A) Immunoblotting of lysates derived from HeLa cells transfected with a siRNA-resistant TECPR2 variant and indicated siRNAs. (B) HeLa cells transfected with si-Control or -TECPR2 and treated with DMSO or BafA1 for 2 hrs were fixed and labelled with indicated antibodies. Scale bar, 10 μ m. Statistical analysis of fold change of punctae: unpaired t-test $*=p<0.05$, $**=p<0.01$. Data represent mean +SD. (C) HeLa cells transfected with si-Control or -TECPR2 and treated with DMSO or Torin1 for 2 hrs were fixed and labelled with α -WIPI2 antibody. Scale bar, 10 μ m. Statistical analysis of fold change of WIPI2-punctae: unpaired t-test $*=p<0.05$, $**=p<0.01$, $p<0.001$. Data represent mean +SD.

To start deciphering which step during autophagosome formation is impaired in the absence of TECPR2, the abundance of several core autophagy proteins was monitored. While GABARAP and ATG12 were unaffected, the protein levels of the PI(3)P effector protein WIPI2 substantially decreased in TECPR2-deficient cells (fig. 3-30A). Consistent with this finding, WIPI2 punctae were reduced in conditions of basal and Torin1 induced autophagy as well as in HSP patient cells (fig. 3-30C, 3-26B, 3-26C). Importantly, re-introducing TECPR2 rescued the protein abundance phenotypes of LC3B, SQSTM1 and WIPI2 caused by TECPR2 depletion (fig. 3-30A). Since TECPR2 appears to be a regulator of functional ERES and efficient ER export, it was tested whether other conditions of ER export deficiency similarly affect autophagosome formation. To this end, a constitutively inactive form of SAR1 that disrupts ERES was employed (Ward et al., 2001).

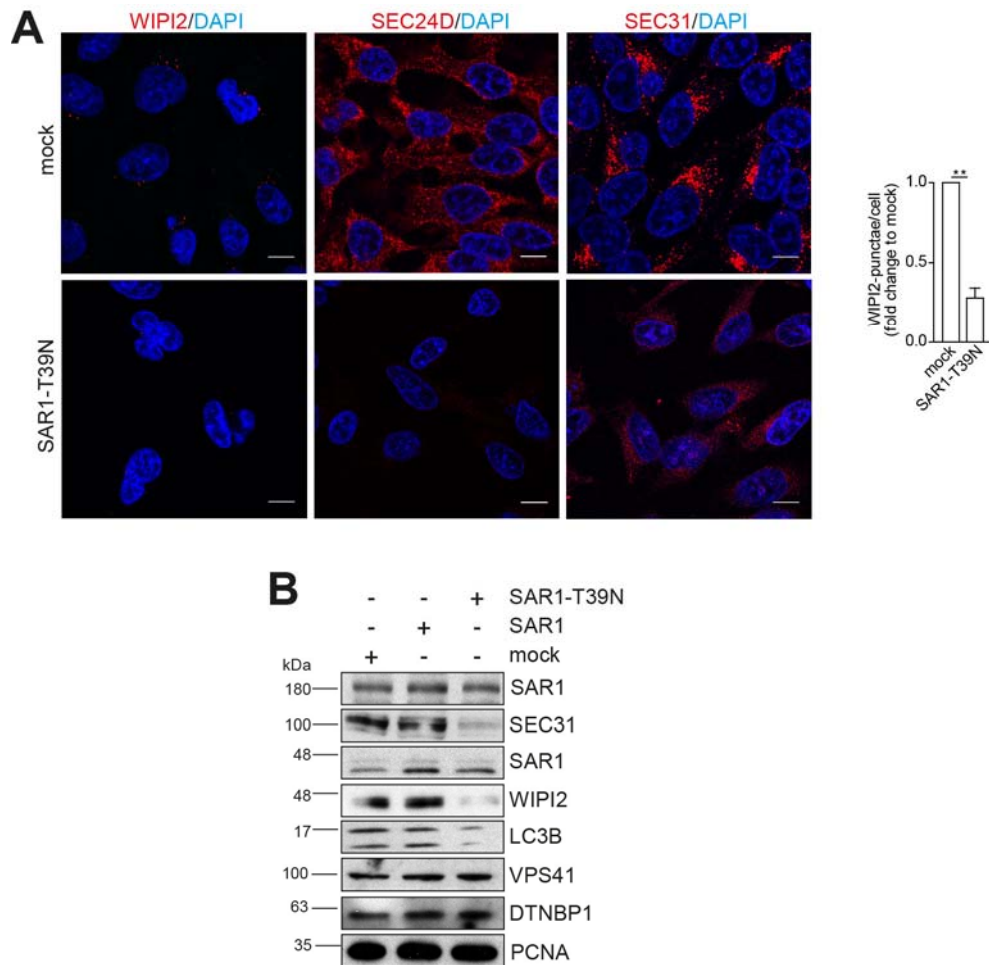


Figure 3-31: Functional ERES are required for formation of autophagosomes.

(A-B) HeLa cells expressing SAR1 or SAR1-T39N were (A) treated with Torin1 for 2 hrs, fixed and labelled with α -WIPI2, -SEC24D or -SEC31 antibodies or (B) lysed and subjected to immunoblotting. (A) Statistical analysis: Fold change of punctae: unpaired t-test $**=p<0.01$. Data represent mean +SD.

SAR1-T39N overexpression (fig. 3-31A) displayed a reduction in the protein levels of WIPI2 and those of lipidated LC3B (fig. 3-31B). The number of WIPI2 and SEC24D punctae likewise declined in SAR1-T39N overexpressing cells treated with Torin1 (fig. 3-31A), suggesting that factors that are required for the maintenance of functional ERES such as TECPR2 or SAR1 critically contribute to autophagosome formation.

In line with the cooperativity of TECPR2 and LC3C in regulating ERES, depletion of LC3C reduced WIPI2 punctae in untreated and Torin1 treated cells (fig. 3-32A, 3-32B, and 3-16C). Surprisingly, LC3B depletion caused a similar WIPI2 phenotype.

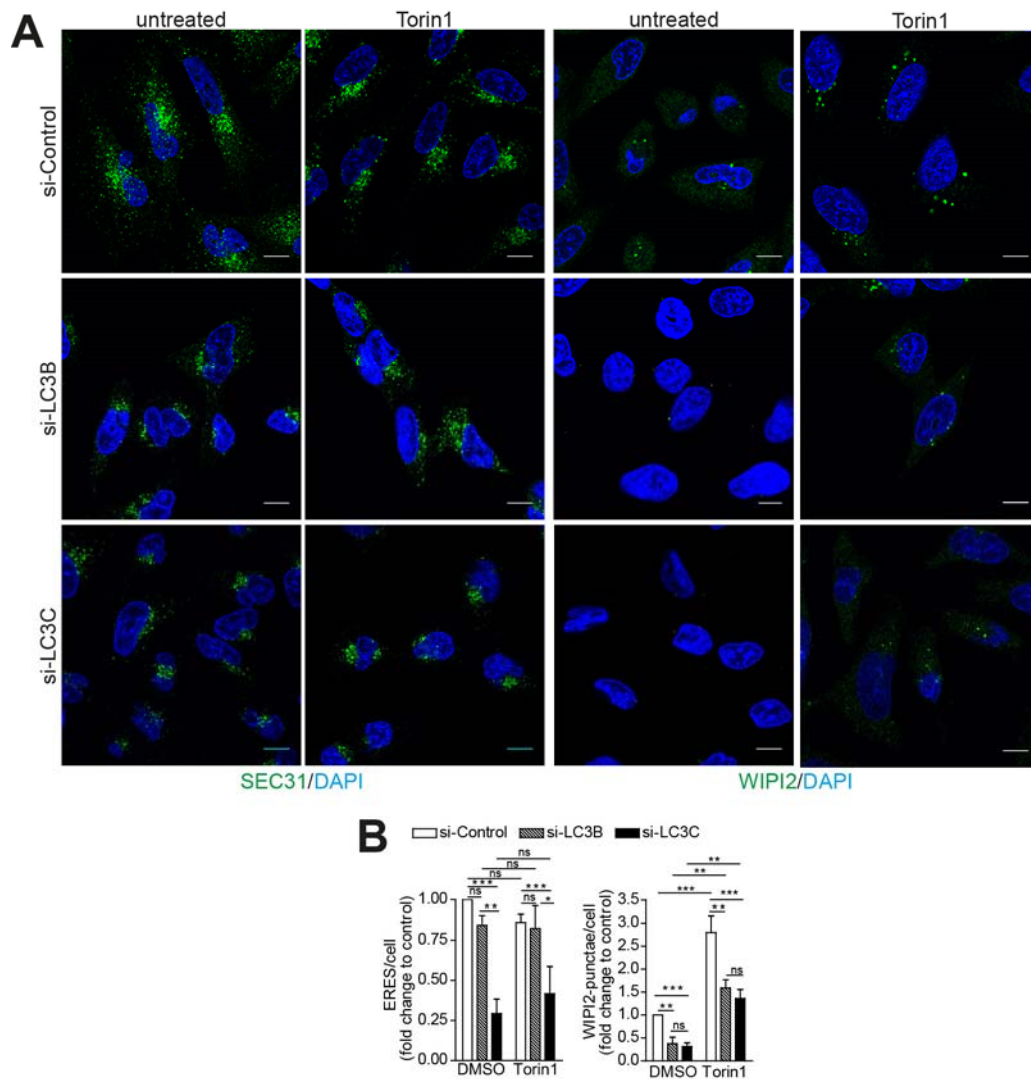


Figure 3-32: WIPI2 punctae formation is controlled by LC3B and LC3C.

(A) HeLa cells transfected with indicated siRNAs and treated with DMSO or Torin1 for 2 hrs were fixed and labelled with indicated antibodies. Scale bar, 10 μ m. (B) Statistical analysis of (A). Fold change of punctae/cell: unpaired t-test *= p <0.05, **= p <0.01, ***= p <0.0001, ns=not significant. Data represent mean +SD.

While LC3B lipidation was shown to depend on recruitment of the ATG12~ATG5-ATG16L1 ligase scaffold by WIPI2 (Dooley et al., 2014), LC3B might affect upstream core autophagy components such as WIPI2 via negative feedback loops. In support of this hypothesis, LIR-dependent binding of LC3B and GABARAP to ULK1 was found to be required for starvation induced association of ULK1 with autophagosomes (Alemu et al., 2012; Kraft et al., 2012). To further explore how TECPR2 and LC3C contribute to autophagosome formation the colocalization of both proteins with markers of early autophagosome intermediates were probed. However, neither TECPR2 nor LC3C were detected in GFP-DFCP1, -WIPI1 or -WIPI2 positive structures in basal growth conditions or in response to Torin1 treatment (fig. 3-33A, 3-33B).

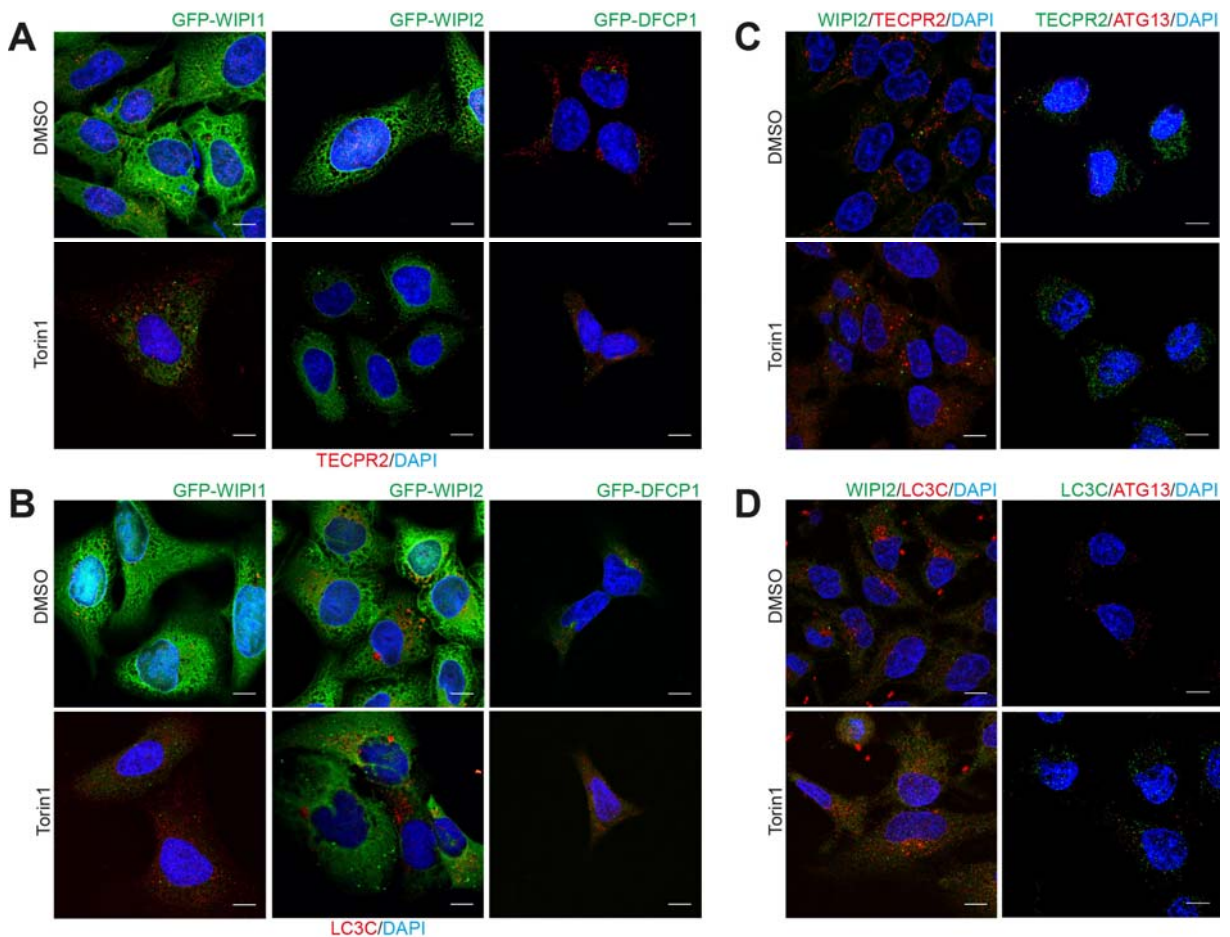


Figure 3-33: TECPR2 does not colocalize with early autophagic machinery components.

(A-B) U2OS cells stable expressing GFP-WIPI1, -WIPI2 or -DFCP1 were treated with DMSO or Torin1 for 2 hrs, fixed and labelled with α -TECPR2 or α -LC3C antibodies. Scale bar, 10 μ m. (C-D) HeLa cells treated with DMSO or Torin1 for 2 hrs were fixed and labelled with indicated antibodies. Scale bar, 10 μ m.

Furthermore, the colocalization of endogenous TECPR2 or LC3C with the early autophagy markers WIPI2 and ATG13 was determined (fig. 3-33C, 3-33D). In both cases, no distinct overlap was observed, suggesting that TECPR2 and LC3C might be locally restricted to allow ERES formation without being permanent components of autophagosome formation sites. Without direct interacting to the mentioned early autophagy markers, still an influence of TECPR2 to omegasome formation was obtained. In immunofluorescence microscopy, the levels of the omegasome marker DFCP1 significantly increased upon depletion of TECPR2, pointing to the assumption that an accumulation of omegasomes occurs under these conditions (fig. 3-34A). Further, a contribution of neither LC3B nor LC3C was observed for DFCP1 (fig. 3-34B).

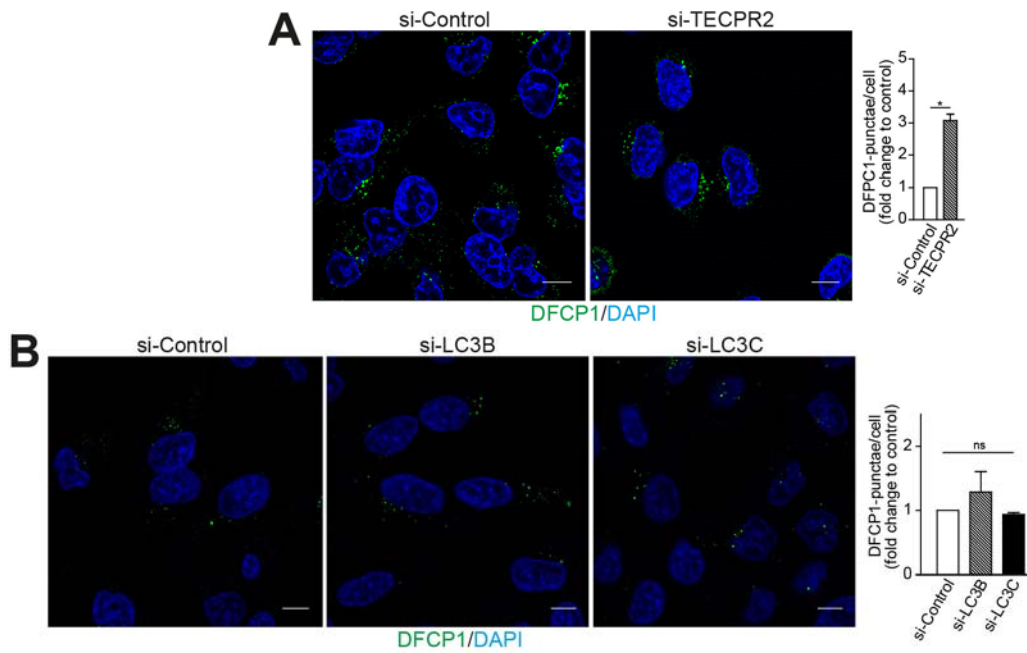


Figure 3-34: Influence of TECPR2 or LC3B/LC3C on DFCP1 on omegasomes in the ER. (A, B) HeLa cells transfected with indicated siRNAs and were fixed and labelled with α -DFCP1 antibody. Scale bar, 10 μ m. Statistical analyses: Fold change of punctae/cell: unpaired t-test $*=p<0.05$, ns=not significant. Data represent mean +SD.

Since TECPR2 depletion also affects the integrity of HOPS and BLOC-1, the question was addressed whether disruption of either trafficking complex impairs autophagy in a similar manner than depletion of TECPR2. Intriguingly, knockdown of the HOPS specific subunit VPS41 blocked autophagy flux (fig. 3-35A, 3-35B), as reported previously for the HOPS specific subunit VPS39 (Jiang et al., 2014). Depletion of the BLOC-1 component DTNBP1 led to a slight decrease in the amounts of lipidated LC3B, which did not accelerate considerably upon BafA1 (fig. 3-35A). Interestingly, autolysosomes were almost absent from DTNBP1 depleted cells (fig. 3-35B), indicating a block in lysosomal fusion or degradation in response to loss of BLOC-1.

Thus, HOPS or BLOC-1 disruption is unlikely to contribute to the autophagosome formation phenotype caused by ERES deficiency. Conversely, functional ERES are not required for maintaining HOPS and BLOC-1 integrity, since SAR1-T39N had no effect on the abundance of HOPS or BLOC-1 components as observed for TECPR2 depletion (fig. 3-31B, 3-15B). Moreover, additional knockdown of PIK3C3, the catalytic subunit of the lipid kinase responsible for PI(3)P production, in TECPR2 depleted cells did not further decrease the levels of VPS41 compared to TECPR2 depletion alone (fig. 3-35C), suggesting that ERES and autophagy impairment are unlikely responsible for the disruption of HOPS and BLOC-1.

Results

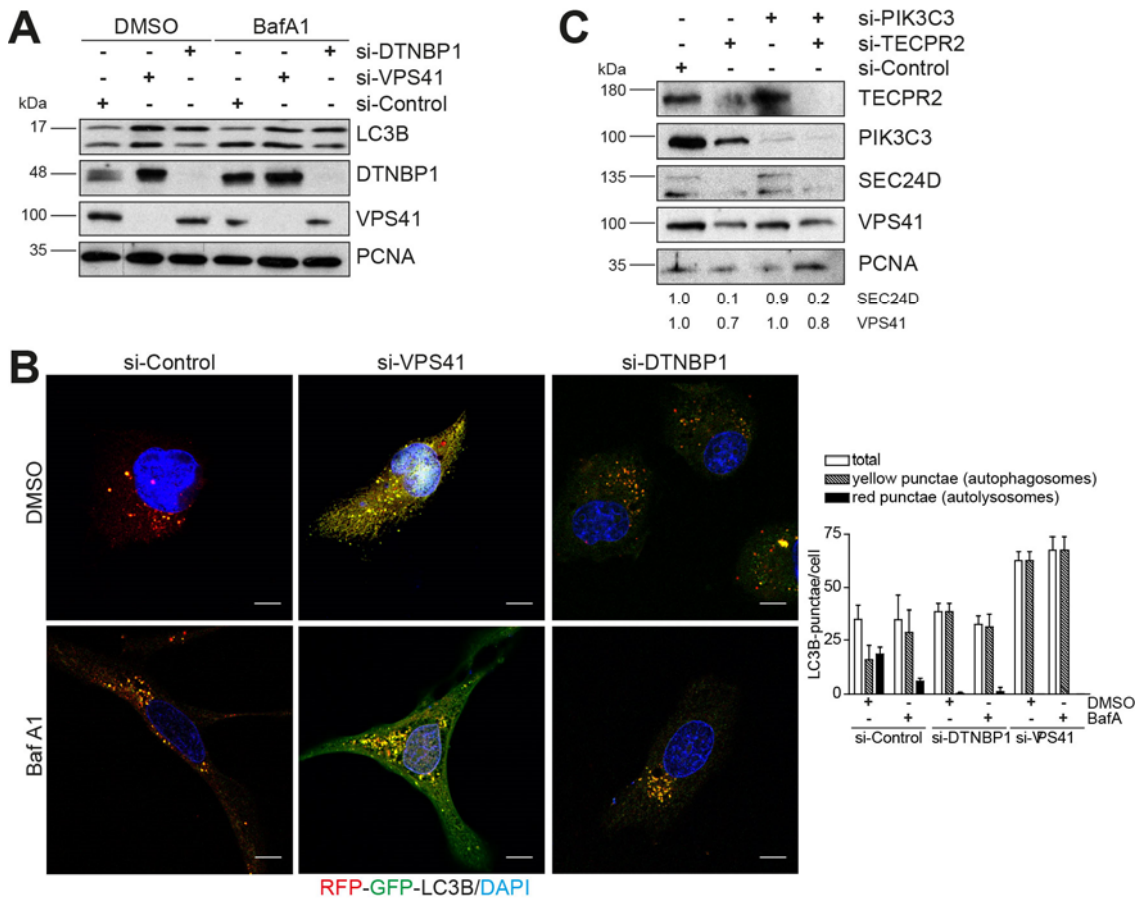


Figure 3-35: Loss of HOPS or BLOC-1 does not affect formation but maturation of autophagosomes.

(A) HeLa cells transfected with indicated siRNA were treated with DMSO or BafA1 for 2 hrs, lysed and subjected to immunoblot. (B) U2OS cells stable expressing RFP-GFP-LC3B were transfected with indicated siRNAs and treated with DMSO or BafA1 for 2 hrs. LC3B-punctae were analyzed with ImageJ and quantifications of autophagosomes (yellow punctae) and autolysosomes (red punctae) are presented. Data represent mean +SD. (C) HeLa cells were transfected with indicated siRNAs and subjected to immunoblot analysis. Quantification was performed with ImageJ.

These results indicate that TECPR2 and LC3C are required for autophagosome formation possibly through regulation of functional ERES and that TECPR2 is a multifunctional scaffolding protein that separately engages several different trafficking proteins.

4. Discussion

4.1 Model: TECPR2 as scaffold for endomembrane signaling

This study established TECPR2 as a positive regulator of COPII-dependent secretion and a subsequent maintenance of the endocytic and autophagic pathways. Depletion of TECPR2 leads to degradation of COPII coat proteins required for ERES formation and ER export. Thus, TECPR2 coordinates secretory trafficking and therefore displays broad implications in neurodegenerative diseases, since axons are in particular dependent on efficient secretory vesicle trafficking.

Based on the results the most plausible role of TECPR2 might be to serve as a multifunctional scaffold protein. Common to the three characterized interactors, namely SEC24D, HOPS and BLOC-1, is their operation at endomembranes. Since so far a lipid-binding domain has not been identified in TECPR2, LC3 proteins could anchor TECPR2 at endomembranes to locally stabilize its binding partners and to prevent their proteasomal degradation. Through this mechanism, TECPR2 would contribute to the spatial organization of its binding partners.

The finding that HSP patient cells carrying mutated *TECPR2* show decreased SEC24D protein levels and defective ER-to-Golgi transport underlines the relevance of this study. Together with TFG, TECPR2 represents the second HSP associated protein being involved in regulation of ERES, ER export and ER morphology. In addition, TECPR2 was reported to be a positive autophagy regulator (Oz-Levi et al., 2012). Since disruption of ERES by overexpressing SAR1-T39N affected early autophagosome intermediates marked by the PI(3)P effector WIPI2 in a similar manner as TECPR2 and LC3C depletion, the role of TECPR2 in autophagosome formation seems mechanistically linked to the maintenance of ERES. Future work is needed to dissect whether compromised ERES affect PI(3)P production or other factors stabilizing WIPI2 at the ER. While the autophagy defect upon TECPR2 deficiency might be caused by the impairment of the early secretory pathway, the relative contribution of defective secretion, altered ER morphology and affected autophagy to the progressive degeneration of axons in HSP remains to be addressed. The combination of these altered cellular processes might explain why the recessive mutation in *TECPR2* gives rise to a set of neurodegenerative diseases including HSP, hereditary sensory-autonomic neuropathy (HSAN), and neuroaxonal dystrophy (NAD). In future studies the list might be expanded by determining TECPR2's contribution to various types of neuronal disorders by a common disturbance of trafficking pathways. Deeper insight into the mechanistic function of TECPR2 might shed light in the field of neurodegeneration in general, as TECPR2 acts as a multifunctional protein contributing to several trafficking pathways and bridges endocytosis, autophagy and secretory pathways.

The present work demonstrated the association of TECPR2 with human ATG8 proteins in a manner dependent on a canonical LIR motif in TECPR2. In addition, SEC24D was identified as novel association partner of TECPR2.

The proposed model illustrates that TECPR2 associates with the inner COPII protein SEC24D to potentially enable its dimerization with SEC23A. The TECPR2-SEC24D interaction is dependent on TECPR2's binding to the human ATG8 family member LC3C but does not lead to autophagosomal degradation of the binding partners. On the contrary, TECPR2 regulates protein abundance and subsequently complex formation of SEC24D, presumably by preventing its proteasomal degradation.

This observation is strongly supported by the fact that TECPR2 binds to the inner COPII coat protein SEC24D and by this means stabilizes the protein, which leads to correct formation of COPII coated vesicles and subsequently efficient ER export of different types of secretory cargo. Budding of functional COPII vesicles involves LIR-dependent binding of TECPR2 to lipidated LC3C, suggesting that TECPR2 and LC3C cooperatively function as positive regulators of COPII-dependent ER export.

TECPR2 and LC3C also positively influence the generation of omegasomes, suggesting that maintenance of functional ERES through TECPR2 and LC3C critically contributes to autophagosome formation. Thus, this work supports the emerging concept that ERES might function in the biogenesis of autophagosomes (Sanchez-Wandelmer et al., 2015) (fig. 4-1). This hypothesis will be discussed in detail in chapter 4.6.

In addition, HOPS and BLOC-1 were also identified as interaction partners of TECPR2. Likewise, TECPR2 stabilizes these protein complexes possibly by preventing their proteasomal degradation and facilitating their assembly. For both complexes it has been reported that their disruption result in accumulation of LC3B-positive autophagosomes (Cai et al., 2010; Itakura et al., 2012; Yuzaki, 2010). These observations were confirmed in the present study. Given the role of HOPS and BLOC-1 in endosomal fusion and sorting, it is very likely that loss of TECPR2 also affects other vesicle trafficking routes in the cell. Complementary, a loss of the BLOC-1 complex by depletion of the subunit SNAPIN drives an accumulation of autophagosomes (Cai et al., 2010; Yuzaki, 2010), which emphasizes the assumption that autophagic pathway is diminished upon TECPR2 depletion. Therefore, TECPR2 also contributes to the function of those complexes, which has some effects on autophagy but not in the same way as TECPR2 itself has.

Furthermore, the positive effect of TECPR2 on lipidated LC3B turned out to be rather a secondary effect of TECPR2's regulatory function on ER export of cargo along the COPII vesicle secretion pathway.

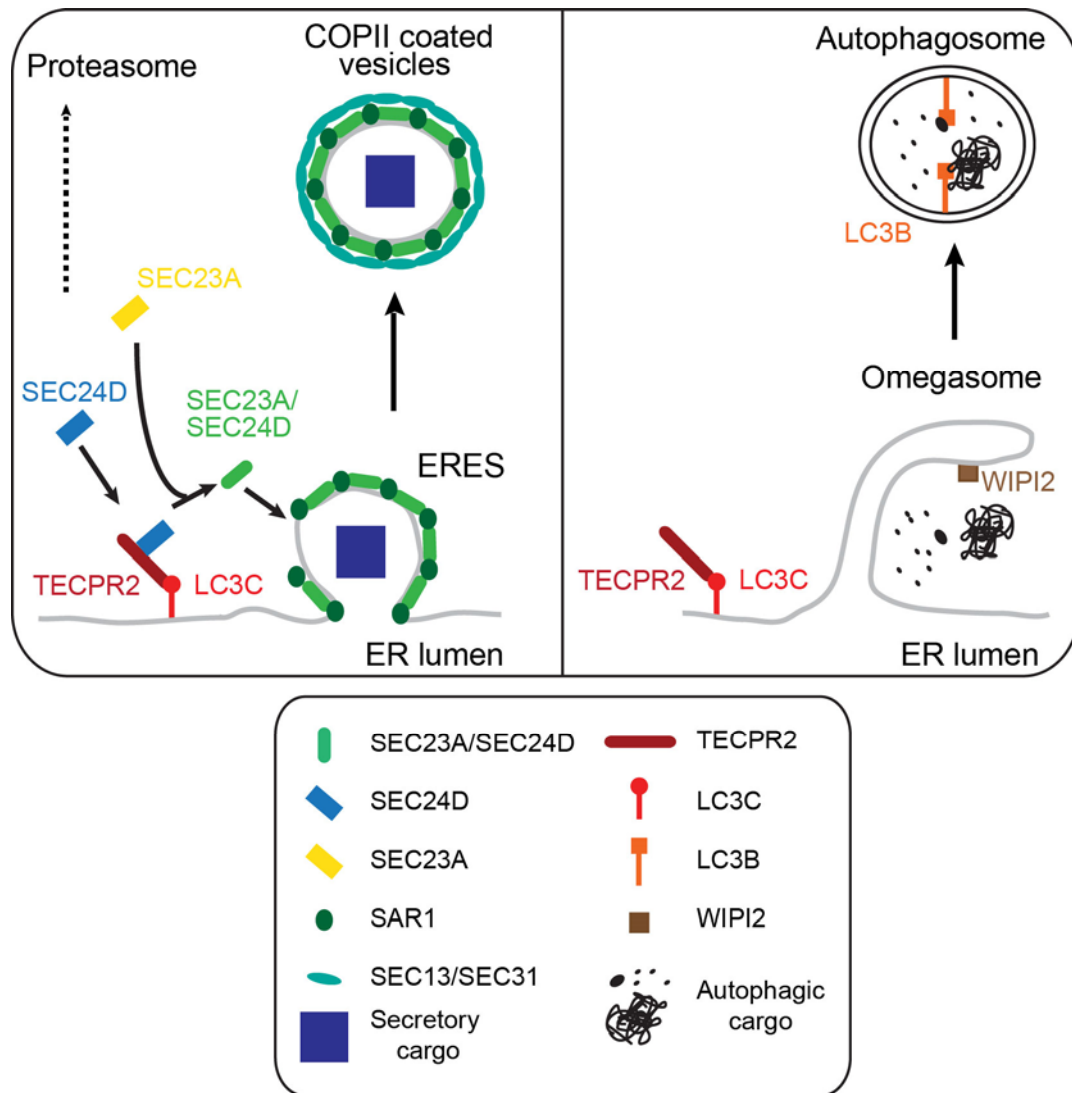


Figure 4-1: Working model for the role of TECPR2 in COPII-dependent ER export and autophagy.

Left: TECPR2 interacts with LC3C via its LIR motif, stabilizes and recruits SEC24D to the ERES. By heterodimerization of SEC24D with SEC23A the inner COPII coat forms and subsequently the COPII vesicles accurately bud from ERES. SEC24D is proteasomal degraded in absence of TECPR2-LC3C. Right: TECPR2 and LC3C positively influence protein levels of WIPI2 and therefore contribute to omegasome development at ER, enabling autophagosome formation.

4.2 Assembly of the inner COPII coat

TECPR2 positively regulates ER export of cargo from ERES by associating with the inner COPII coat protein SEC24D. Taken into account that TECPR2 also interacts with other endomembrane trafficking components (i.e. HOPS and BLOC-1) and stabilizes the protein levels of these binding partners, this work proposes TECPR2 serving as a multifunctional scaffold protein. To accomplish this function in a highly localized manner TECPR2 is anchored

to the endomembrane systems through binding to LC3B and/or LC3C. Consequently, TECPR2 and LC3B/C jointly regulate the respective vesicle trafficking pathway.

In line with such a scenario, TECPR2 and LC3C are both found at ERES. Since TECPR2 binds SEC24D in the absence of its heterodimer partner SEC23A, TECPR2 might be required to prime SEC24D for efficient heterodimer formation with SEC23A at the site of COPII coat assembly. Consistent with this hypothesis, TECPR2 depletion also affects the protein abundance of SEC23. Thus, in the absence of TECPR2, SEC24D might not be competent to dimerize with SEC23A and subsequently both seemingly superfluous monomers are subjected to proteasomal degradation.

This presumably indirect stabilization effect of TECPR2 on SEC23 could also explain the broad range of cargo that is affected by loss of TECPR2 given that SEC24D only has a reported preference for GPI anchored proteins (Lord et al., 2013). Therefore, TECPR2 and LC3C are proposed to cooperate and spatially organize unassembled SEC24D at ERES, potentially in a conformation ready to bind its heterodimer partner SEC23 as well as cargo or cargo adaptors. This model is supported by the observation that TECPR2 depletion, besides affecting protein abundance and assembly of its binding partners, also alters their subcellular distribution. The finding that TECPR2 binds SEC24D in the absence of its heterodimer partner SEC23 suggests that TECPR2 interacts with SEC24D before the COPII coat is formed or after its disassembly. Anchoring SEC24D in close proximity to ERES through interaction with LC3C-bound TECPR2 might not only prevent proteasomal degradation of cytosolic free SEC24D but might also accelerate the efficiency of SEC23/SEC24 dimer formation at the site of COPII coat formation. Notably, ERES localization of TECPR2 and SEC24D might additionally be coordinated by the accessory COPII coat formation factor SEC23IP (p125A) (Ong et al., 2010), which was found associated with both TECPR2 and SEC24D (fig. 3-1). However, it remains to be examined whether this spatially scaffolding is unique for SEC24D or whether the other SEC24 isoforms are controlled by similar machineries. Collectively, this model provides a basic mechanism of how coat proteins might be recycled and primed for the next round of coating (fig. 4-1).

Besides the WD40 repeat propeller, TECPR2 contains six TECPR repeats in the C-terminal part of the protein. Since each of these repeats is predicted to give rise to β -strands, all six repeats might form one additional β -propeller-like domain. TECPR repeat have also been found in the protein TECPR1 (Behrends et al., 2010), which is implicated in selective autophagy of bacterial pathogens and autophagosome maturation (Chen et al., 2012; Ogawa et al., 2011). However, the function of TECPR repeats remained elusive. For this reason further research is required to elucidate the distinct binding mechanism of TECPR2 to various different binding partners.

However, this study revealed the binding of the COPII-coat protein SEC24D to the N-terminal part of TECPR2. Depletion of TECPR2 led to a reduction of SEC24D protein level and

subsequently a diminished recruitment of SEC24D to the ERES. Consequently, correct assembly of ERES is prevented, followed by an impairment of ER-to-Golgi trafficking and accumulation of secretory cargo proteins such as mannosidase II and collagen in the ER. Loss of LC3C, but not LC3B, causes similar ERES maintenance and ER export defects, supporting the concept that TECPR2 functions particularly together with LC3C at ER exit sites. The present study demonstrated that only lipidated LC3C cooperates with TECPR2 in regulating ER export. This finding implicates that LC3C is located at the ER membrane and anchors TECPR2 to the ER. Therefore, TECPR2 possibly serves as a stabilizing factor of COPII coat proteins in a LC3C-dependent manner. However, evidence for the incorporation of LC3C-PE conjugates into the ER membrane is still missing. Furthermore, it remains unclear whether factors regulating COPII coat assembly such as SAR1, lipid kinases and phosphatases or the lipid composition of the ER are affected by TECPR2 depletion.

Of note, TECPR2-mediated ERES stabilization does not occur as a classical ER-stress response, since the ER-stress markers HERP and BIP are not upregulated upon TECPR2 knockdown. Which kind of signaling pathway mediates this process needs to be further investigated. Common for all affected pathways is the supply of endomembranes and lipids. A possible scenario would be that TECPR2 acts as control center, distributing lipids derived from ER to proteins responsible for formation of different vesicles, which then shuttle cargo via the intended pathway. In this scenario the LC3 proteins could serve as connective elements to support the lipid binding. As TECPR2 binds at least to two different members of the LC3 subfamily of ATG8 proteins, it is possible, that these members recruit lipids destined for the different endomembrane-mediated pathways. In further studies the connection of TECPR2 to lipids could be investigated to decipher a possible role in lipid recruitment and distribution.

Beyond that, it is even conceivable that TECPR2 regulates the transcription of its interaction partner. Possibly, TECPR2 controls the mRNA levels of some of its association partners as well as of specific inner-cellular trafficking proteins like cargo for ER export. Assuming a role for TECPR2 as a transcription factor, its absence might lead to a negative feedback loop on the secretory pathway components. By a lack of TECPR2 the processing of mRNA could be influenced in a way, that pathways are activated to suppress the transcription of interaction partners or affected protein groups, mediating TECPR2-dependent ER export; for instance collagens. For this purpose, TECPR2 might enter the nucleus by itself or is even potent to activate a cascade of other proteins to influence the transcription of genes. This hypothesis is supported by the fact, that TECPR2 comprise a nuclear localization sequence and encompass several association partners connected to nuclear function (chapter 3.1, fig. 3-1). It will be of special interest to investigate the contribution of TECPR2 to transcriptional processes to unravel possible novel roles of this versatile protein.

4.3 HOPS

In addition to SEC24D, TECPR2 was also found to bind to HOPS, which is a crucial tethering factor in the endocytic pathway. Moreover, depletion of TECPR2 completely disrupted the HOPS complex. Yeast HOPS forms a seahorse shaped structure in which the core subunits that are shared with the related CORVET complex mainly occupy the center region and where the HOPS specific subunits VPS39 and VPS41 are located at opposing ends (Balderhaar and Ungermann, 2013). Given the conservation of HOPS and CORVET subunits in higher eukaryotes, HOPS is thought to adapt a similar subunit arrangement in human cells. Intriguingly, the finding that the marked decrease of HOPS upon TECPR2 depletion is accompanied by a robust increase of CORVET suggests that binding of HOPS to TECPR2 is mainly mediated by VPS39 and VPS41. In the absence of TECPR2 both subunits might not be able to efficiently assemble with the HOPS/CORVET core and subsequently are degraded as supernumerary complex members. It will be interesting to investigate whether CORVET assembly requires a similar scaffolding factor that binds to the CORVET specific subunits. Finally, in analogy to SEC24D it remains to be carefully addressed whether the scaffolding function of TECPR2 is similarly required for the function of HOPS or BLOC-1.

Through binding to LC3B or LC3C, TECPR2 might recruit HOPS to distinct membrane compartments. Given the role of HOPS in mediating lysosomal fusion (Balderhaar and Ungermann, 2013) and the observation that TECPR2 colocalized with LC3C and the HOPS-specific subunit VPS41, it is tempting to speculate that TECPR2 associates with HOPS while bound to LC3B or LC3C on the surface of a closed autophagosome. Consistent with a previous report that the autophagosomal SNARE STX17 binds HOPS and promotes the autophagosome-lysosome fusion (Jiang et al., 2014), the present work identified STX17 as an interacting partner of VPS41. Intriguingly, STX17 and HOPS were recently shown to be bound by the RAB7A-interacting protein PLEKHM1 which is recruited to autophagosomes through binding with LC3 and GABARAP proteins (McEwan et al., 2015). Moreover, depletion of the HOPS complex-specific subunit VPS41 led to a blockage of autophagic turnover and thereby to an acceleration of lipidated LC3B, which represents the opposing phenotype compared to loss of TECPR2. TECPR2 stabilizes the HOPS complex in a LC3-dependent manner and, despite of its localization in punctuate structures, only partially coincide with autophagosomes. It is possible that only a fraction of TECPR2 punctae resides at autophagosomes. Given that HOPS is known to participate in the early-to-late endosome maturation (Balderhaar and Ungermann, 2013), LC3-bound TECPR2 might support the recruitment of HOPS to autophagosomes and thereby positively influence autophagosome maturation. Further evidence for the involvement of HOPS in autophagy was provided by recent work on LGG-2, the *C.elegans* homolog of LC3, which facilitates tethering of autophagosomes with lysosomes through binding with the HOPS subunits VPS39 (Manil-Segalen et al., 2014) and VPS18 (Peng

et al., 2012). Notably, the latter plays a critical role in autophagic clearance in mouse brains and therefore contributes to neurodegeneration (Peng et al., 2012). While the individual contribution of TECPR2, LC3, and STX17 to recruitment and regulation of HOPS at the autophagosomal membrane remains to be determined, it is clear that a network of protein interaction seems to be required to facilitate autophagosome-lysosome fusion.

4.4 BLOC-1

TECPR2 positively influences BLOC-1 by binding with and stabilizing of the complex in a similar fashion as the HOPS complex. TECPR2 might also recruit BLOC-1 to distinct membrane compartments in a LC3-dependent manner. BLOC-1 which is responsible for endosome to melanosomes trafficking was disrupted upon loss of TECPR2 similarly as HOPS. Comparable to its function on SEC24D and possibly HOPS, TECPR2 might scaffold the complex assembly of BLOC-1. BLOC-1 was recently shown to form a flexible linear chain consisting of eight globular domains that are unlikely to correspond to the eight individual subunits (Lee et al., 2012). Instead these domains might be constituted by inter-subunit interactions potentially mediated by extensive regions of predicted coiled-coil in each of the subunits. Such a structure would almost certainly require stepwise assembly of partially folded subunits on a scaffolding protein. However, the question remains whether the scaffolding function of TECPR2 is sufficient for BLOC-1 assembly or whether additional factors are involved in this process. A good candidate for the latter scenario is the protein BCAS4, which was identified as common binding partner of TECPR2 and the most of the BLOC-1 subunits (fig. 3-1).

Conversely, the function of BLOC-1 in the context of autophagy remained mostly elusive. BLOC-1 is known to support early endosome maturation by facilitating endosome-to-lysosome fusion (Setty et al., 2007). Since TECPR2 regulates the stability of BLOC-1 it is expected that TECPR2 deficiency also affect BLOC-1-mediated trafficking. In the context of BLOC-1 function in autophagy, it needs to be determined whether BLOC-1 is similarly present on autophagosomes and whether its cargo sorting function contributes to autophagosome maturation.

Interestingly, HOPS and BLOC-1 are connected by ATG14, an essential autophagy-specific regulator of the class III phosphatidylinositol 3-kinase complex, which is involved in formation and maturation of autophagosomes (Simonsen and Tooze, 2009). The fusion of autophagosomes to lysosomes is supported by ATG14 (Diao et al., 2015) and the HOPS complex (Jiang et al., 2014). In addition, ATG14 also binds the fusogenic SNARE effector protein SNAPIN (Kim et al., 2012), which is part of the BLOC-1 complex and regulates fusion of endosomal membranes (Lee et al., 2012). Further studies are required to investigate the

functional significance of the link between HOPS and BLOC-1 complexes for their role in autophagy and the potential coordination of these two complexes by TECPR2.

4.5 LIR motif of TECPR2 and binding preference

TECPR2 was described as an interactor of the human ATG8-family and a positive regulator of autophagy (Behrends et al., 2010). By mapping the canonical LIR motif W-E-V-I at the C-terminus of TECPR2 and by revealing almost exclusive colocalization of endogenous TECPR2 with LC3B- and LC3C-positive structures under basal and autophagy-induced conditions the present work firmly established TECPR2 as a specific LC3B/C-binding protein.

LIR motifs usually consist of an aromatic amino acid and a hydrophobic amino acid at the position 1 and 4 (F/W/Y₁-X₂-X₃-I/L/V₄). Restricted by hydrophobic residues at position 4, there exist only a limited numbers of possible LIR sequences. However, combination of subtle different sequences of both LIR and ATG8 proteins confers LIR-containing proteins with a great diversity of specificity in the recognition of ATG8 proteins. For example, the LC3C-specific LIR (termed CLIR; I₁₃₃-L-V-V₁₃₆) of the autophagy receptor nuclear domain 10 protein 52 (NDP52) lacks an aromatic residue at position 1 but encompasses three hydrophobic residues that mainly contribute to the association with LC3C. Hydrophobic interactions between CLIR V136 and the HP2 of LC3C (L64 and F69) and between CLIR V135 and F33 of LC3C compensate for the absence of an aromatic residue in CLIR (von Muhlinen et al., 2012). A second LC3C-specific LIR is found in the autophagy adaptor protein ALFY (autophagy-linked FYVE protein) (Lystad et al., 2014). The LIR of ALFY (KD₃₃₄₄G F-I-F-V NY₃₃₅₁) has additional ionic interactions with both GABARAP and LC3C through residues surrounding the LIR (mainly D3344 and Y3351), thereby providing exclusive binding to both the GABARAPs and LC3C. Although the LIR motif of TECPR2 was shown to associate with ATG8 family members with a slight preference for LC3-family proteins and GABARAP *in vitro*, the LIR motif (W1408-E-V-I1411) in the very C-terminus of TECPR2 is a canonical and non-specific type of LIR. The aromatic and hydrophobic residues W1408 and I1411 at position 1 and 4 should fit into the HP1 and HP2 of all LC3 and GARABAP proteins.

However, in cells, the favored binding partners of TECPR2 within the ATG8 family are LC3B and LC3C. Since there were no significant differences observed between the binding mode for LC3B and LC3C by both, ITC and NMR experiments, other cellular factors or residues preceding the C-terminal LIR might contribute to the observed preference in cells. The present study exhibits that LC3C preferentially localizes at ERES in contrast to LC3B, the basis of this specific subcellular distribution remains unclear. Strikingly, impaired ERES number and disrupted ER export correlate with depletion of LC3C but not LC3B. While the exact functions still have to be elucidated, abundance and localization of each ATG8 protein and the

observation that TECPR2 requires binding to LC3C to positively regulate ER export raises the possibility that LC3 and GABARAP proteins might in general serve as docking sites on endomembranes and have roles beyond autophagy. This notion is supported by the recent finding that GABARAP proteins recruit an ubiquitin E3 ligase to membranes to spatially restrict RAC1 signaling (Genau et al., 2015).

4.6 ER export and autophagy

Recent advances identified ERES as important hubs for autophagosomal biogenesis (Carlsson and Simonsen, 2015; Graef et al., 2013; Suzuki et al., 2013; Wang et al., 2014). For instance, the assembly of autophagic machinery was linked to ERES function (Sanchez-Wandelmer et al., 2015). These sites might not only allow COPII vesicle secretion but further operate as building hubs for omegasomes and assembly platform for phagophore structures. Assuming ERES are also involved in recruiting of several autophagic factors; these sites could not only provide a scaffold for assembly of vesicles destined for different pathways but also coordinate required factors such as lipids. ERES could also be engaged in the budding of autophagosomes from the ER and therefore contribute to autophagosome formation by facilitating the fusion events with lysosomes (Graef et al., 2013).

Another aspect represents the localization of Atg9 positive vesicles at ERES (Mari et al., 2010). Initially, it was shown in yeast that vesicles originating from the secretory pathway, re-translocate from the plasma membrane towards pre-autophagosomal structures at the ER, where they supply lipids and contribute to the expansion of autophagosomes (Graef et al., 2013). This model depicts that autophagosomes form at ERES dependent on Atg9-positive membranes, whereby the formation and recruitment of Atg9-positive vesicles to PAS relies on functional ERES. Further, the process of Atg9 vesicle recruitment is regulated by the kinase Atg1 and ERES, while Atg9 and Atg1 together facilitate the recruitment of PI3K. In mammalian cells ULK1, which is the homolog of Atg1, induces the activation of LC3 lipidation and consequently facilitates autophagosome generation and COPII-vesicles recruitment to the ERGIC, which represents another source for membranes (Ge et al., 2014). Moreover, depletion of SAR1, which inhibits assembly of ERES, leads to a loss of autophagosome formation and decrease in LC3-punctae (Zoppino et al., 2010). Thus, both COPII vesicles as well as the formation of ERES appear to be important for appropriate autophagosome formation.

Based on these recent findings two models on how ERES contribute to the formation of early autophagosome intermediates such as omegasomes emerged (Sanchez-Wandelmer et al., 2015), which will be discussed in the following sections.

In the first model, ERES deliver membranous and proteinaceous components to the phagophore or pre-autophagosomal structures (PAS) via trafficking of COPII-coated vesicles, thereby supporting the formation of autophagosomes (fig. 4-2). In addition, Atg9-positive vesicles derived from the plasma membrane are recruited to the autophagosome assembly site and also provide lipids as building blocks for autophagosome biogenesis. In yeast, these vesicles are captured by Atg1-Atg13 (human: ULK1-ATG13) conjunction with the transport protein particle (TRAPP) III and active Ypt1 (human RAB1A). At the PAS the TRAPPIII-Ypt1 complex is also required for recruitment of COPII-vesicles derived from ERES. Ypt1 and Atg17 could also be involved in this process. Ypt1 contributes to autophagosome formation and is strictly regulated by TRAPPIII which acts as GEF for Ypt1 and RAB1A, respectively (Cai et al., 2007; Cai et al., 2005). Interestingly, in yeast it has been demonstrated that TRAPPIII interacts with Sec23 (Tan et al., 2013) and in mammals the TRAPPIII complex was found associated with the ERES marker SEC31 (Bassik et al., 2013). In this model, TECPR2 could allow the COPII vesicles to bud from ERES and hand them over to TRAPPIII complex.

In the second concept, the ERES themselves provide the scaffold for autophagosome biogenesis (fig. 4-2). Atg9-positive and other early autophagic components could be recruited to the COPII-vesicle assembly site in a TRAPPIII-Ypt1-dependent manner. Here, the phagophore is directed from ERES, which may or may not be competent to bud off COPII vesicles (Carlsson and Simonsen, 2015; Proikas-Cezanne et al., 2015; Sanchez-Wandelmer et al., 2015). In this scenario, it is feasible that both Atg9-vesicles and the ER could serve as membrane source and supply lipids for the generation and elongation of the phagophore membrane. The hierarchically recruited core autophagy components stabilize each other and provide an extended scaffold for the formation of the omegasome which serves as early autophagosome intermediate.

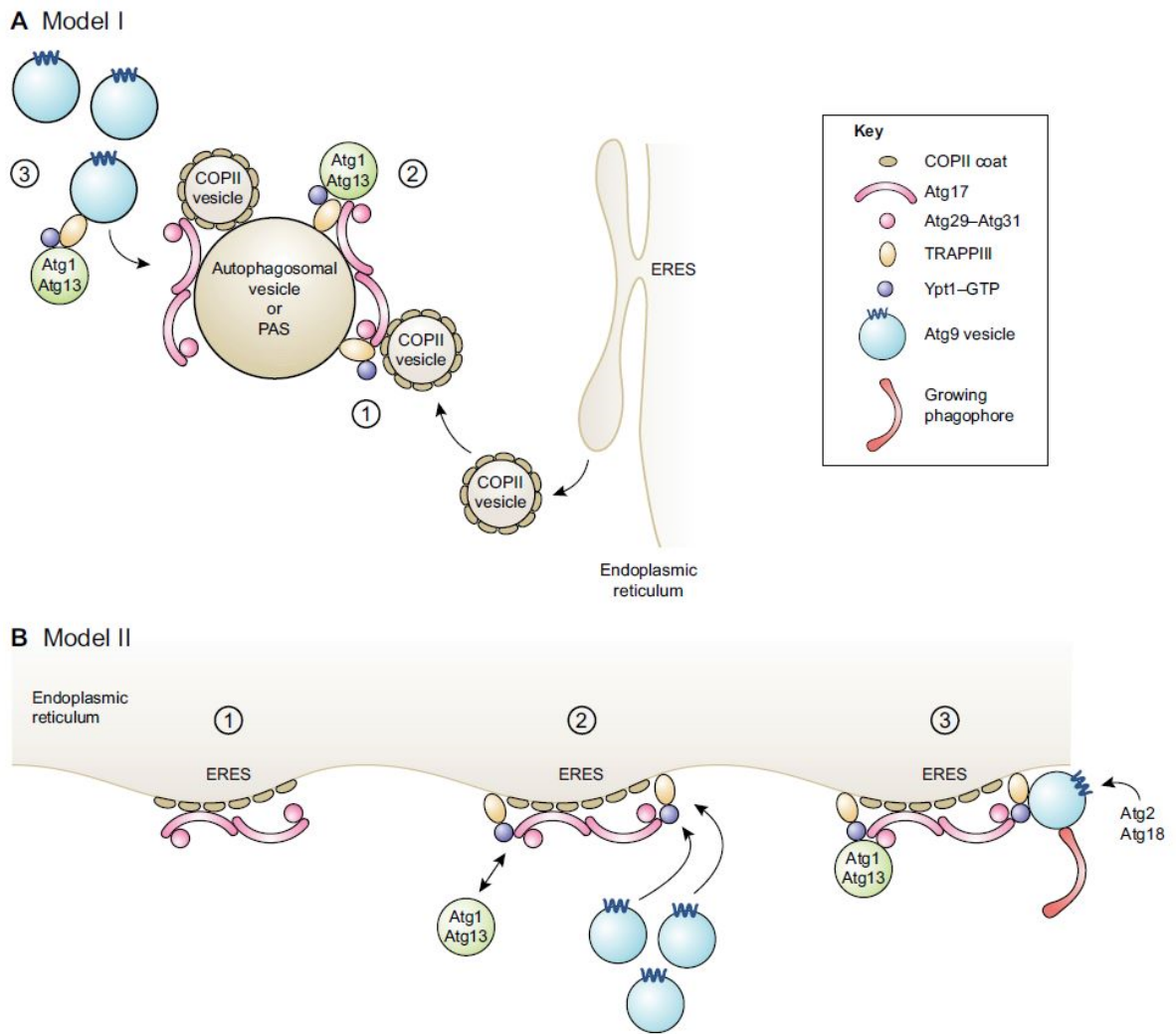


Figure 4-2: Models for involvement of ERES in autophagosome formation.

(A) Model I: COPII-vesicles deliver membranes and factors essential for formation of autophagosomes to the preautophagosomal structure (PAS) in a TRAPPIII-Ypt1 and ATG17-29-31 dependent fashion. ATG9 vesicles are recruited independently of the COPII machinery. (B) Model II: ERES serve as scaffold for the autophagosome biogenesis. ATG17 interacts with COPII structures. Subsequently, the other components are assembled at these regions and the phagophore expands from the ERES. From (Sanchez-Wandelmer et al., 2015)

The results of the present study could fit into the second model as well due to the fact that TECPR2 is required to maintain the protein levels of the omegasome marker WIPI2 and thereby directly affects autophagosome formation. Furthermore, the levels of the omegasome marker DFCP1 increased upon TECPR2 depletion, strengthening the idea of a disturbance of the autophagic pathway at the ER membrane and in particular at the omegasome levels. DFCP1 as well as WIPI2 are PI(3)P effector proteins, both contributing to the lipidation events of LC3. It is known, that upon WIPI2 depletion the protein levels of DFCP1 accelerate and those of LC3B decelerate (Polson et al., 2010). This implies that autophagosome formation is disrupted by impairment of LC3 lipidation and an accumulation of omegasomes. By this means,

WIPI2 supports the biogenesis of autophagosomes at the omegasomes in a PI(3)P-dependent fashion. This notion is supported by direct interaction of WIPI2 with the early autophagy marker ATG16L1, which is important for PI(3)P-dependent LC3 lipidation and autophagosome formation (Dooley et al., 2014). In the light of these reports the results of the present work suggest that TECPR2 regulates autophagosome and omegasome formation through WIPI2. Further, work in *C.elegans* exhibited that WD40 domain proteins bind to PI(3)P to regulate omegasome and autophagosome formation (Lu et al., 2011). As TECPR2 comprise three N-terminal WD40 domains, it might be interesting to probe the association of TECPR2 with lipids such as PI(3)P (compare with chapter 5.1).

In summary, TECPR2 positively regulates the budding of COPII vesicles from the ER, which then could be shuttled back toward the autophagosome formation site at ERES from the plasma membrane or recycling endosomes. In another possible scenario, the ERES might distinguish between the different cargos or other marking proteins for autophagy and the secretory pathway and switch from secretion of COPII-coated vesicles to formation of omegasomes by so far unknown factors. In both cases TECPR2 serves as stabilizing element providing a scaffold for both COPII vesicle and autophagosome formation.

4.7 ER maintenance and neurodegeneration

In hereditary spastic paraparesis neurodegeneration is related to the maintenance of ER architecture. The ER network pattern contributes to membrane bending, microtubule development and vesicle biogenesis. As mentioned in the introduction (see chapter 1.1.1 and 1.2.5) TFG, a protein highly expressed in the central nervous system and the eye, is linked to HSP. Depletion of TFG inhibits cargo secretion and leads to fragmentation of the ER. Thus, TFG regulates protein secretion from ER and maintains ER morphology by stabilizing the ER network. This regulation is mediated by direct interaction with SEC16 at ERES (Witte et al., 2011). Besides, other HSP-associated proteins are involved in the regulation of ER architecture. For instance, spastin contributes to regulation of ER network pattern by disassembling microtubules (Connell et al., 2009). Spastin directly associates with atlastin-1, another protein contributing to HSP (Zuchner et al., 2006) (fig. 1-1), which was also shown to positively influence ER structure (Bian et al., 2011). Moreover, REEP1, known to be HSP-connected as well, generates and maintains curved ER membranes (Friedman and Voeltz, 2011).

Similar to TFG, depletion of TECPR2 altered the morphology of the ER. Since ERES and COPII are implicated in autophagosome biogenesis (Ge et al., 2014; Graef et al., 2013; Zoppino et al., 2010), the autophagy defect observed in HSP patients with mutated TECPR2 (Oz-Levi et al., 2012) might be a consequence of the impairment of ERES caused by the

absence of TECPR2. In this context it might be interesting to examine TFG-deficient cells with regard to autophagy defects.

Based on the results of the present work, TECPR2 (SPG49) should be re-grouped into the category of HSP-associated genes that are required for maintaining proper architecture and function of the ER. However, it remains to be addressed whether defective secretion, altered ER morphology or both contribute to the progressive degeneration of axons in HSP. Given the established function of HOPS and BLOC-1 as endosomal multisubunit tethering and sorting factors it is likely that destabilization of these two complexes due to the absence of TECPR2 leads to modulation of cellular processes regulated by HOPS and BLOC-1. Deciphering the individual contribution of defective HOPS and BLOC-1 versus impaired ER export and altered ER architecture might be complicated based on the fact that ER and endosomes are interconnected by ER contact sites (Rowland et al., 2014). However, this potential mixture of phenotypes might explain why the recessive mutation in *TECPR2* (c.3416delT) gives rise to a complicated form of HSP.

In a recent study TECPR2 was related to hereditary sensory-autonomic neuropathy (HSAN) (Heimer et al., 2015). Exome sequencing of patients unraveled two novel mutations (c.1319delT, c.C556T) in the *TECPR2* gene. Loss of TECPR2 could be associated to several subtypes of HSAN in its autosomal recessive form and therefore TECPR2 seems also involved in this second neurodegenerative disease. HSAN patients show a common decrease in pain and temperature sensitivity, while more specific characteristics are chubbiness, short stature and progressive microcephaly (Heimer et al., 2015). Moreover, this disease is characterized by chronic respiratory defects and autonomic dysfunctions. In general, symptoms of HSAN patients are similar to those suffering from HSP. The ER-related autophagy receptor FAM134B was recently linked to HSAN due to alterations of the *cis*-Golgi compartment and ERphagy (Khaminets et al., 2015; Kurth et al., 2009). FAM134B is critical for long-term survival of autonomic ganglion neurons and therefore contributes to HSAN. This example supports the hypothesis that TECPR2 contributes to neurodegenerative disorders in general by affecting ER maintenance and the secretory pathway.

Another aspect was provided by a study on Spanish water dogs, which emerged as valuable model organisms to explore neurodegenerative disease and connect those to human pathology, as the canine nervous system is similar to the one in humans and the genomes share remarkable homologies as well (Hahn et al., 2015). Hahn and colleagues detected that the loss of function of TECPR2 protein was related to neuroaxonal dystrophy (NAD) and described the association of TECPR2 to NAD-typical phenotypes in immunohistochemistry. Moreover, in this study TECPR2 was also linked to autophagy failure. NAD is defined by the formation of spheroids without the accumulation of iron in the basal ganglion. An example for an NAD causing gene is *PLA2G6*, encoding a calcium-independent phospholipase, which is

responsible for remodeling membrane phospholipids in axons and synapses (Sumi-Akamaru et al., 2015). Patients carrying mutations in the *PLA2G6* gene exhibit disruption of Golgi morphology and NAD in combination with other neurodegenerations like Parkinson's disease (Davids et al., 2015).

Considering that fibroblast from HSP patients with mutated *TECPR2* showed reduced SEC24D protein levels in the present study, defective ER export, and ER morphology changes, further analyses are required to address whether these phenotypes also manifest themselves in *TECPR2*-deficient neuronal cell types. Possibly, *TECPR2*, which acts as a general scaffold protein to facilitate endomembrane transport pathways, contributes to neurodegenerative diseases in a more constitutive mode. Therefore it is of common interest to investigate *TECPR2* in a more global context of neurodegenerative diseases rather than keeping up solely with the HSP linkage. Furthermore, with aid of *TECPR2* the classification of the mentioned neurodegenerative diseases could carefully be remodeled.

4.8 Concluding remarks and future perspectives

In this work *TECPR2* was identified as a multifunctional scaffold protein, which is essential for the stabilization and correct function of its association partners SEC24D, HOPS and BLOC-1. This raises the question how *TECPR2* accomplishes binding to these three seemingly different trafficking components. Interaction of *TECPR2* with the monomeric SEC24D as well as with subunits of the HOPS and BLOC-1 complex involves the N-terminal part of *TECPR2* that encompasses the WD40 repeat β -propeller. Intriguingly, in a larger number of very different proteins this domain has been exhibited to mediate binding to ubiquitin (Pashkova et al., 2010). Furthermore, the HOPS subunit VPS41 and the BLOC-1 member DTNBP1 increased in their abundance when proteasomal degradation was inhibited. The fact that ubiquitylation sites are mapped in SEC24D, HOPS and BLOC-1 (Kim et al., 2011) strengthens the possibility that the association between *TECPR2* and these binding partners is mediated by ubiquitin.

Thus, *TECPR2* may not engage its binding partners directly but rather their ubiquitylated form through ubiquitin-mediated binding of the WD40 repeat β -propeller of *TECPR2*. In an alternative scenario, the N-terminal part of *TECPR2* might encompass multiple distinct binding sites for SEC24D, HOPS and BLOC-1. To test this former hypothesis, *TECPR2* overexpressing cell lysates were assayed in GST pulldowns with purified mono-, di- or tetra-ubiquitin.

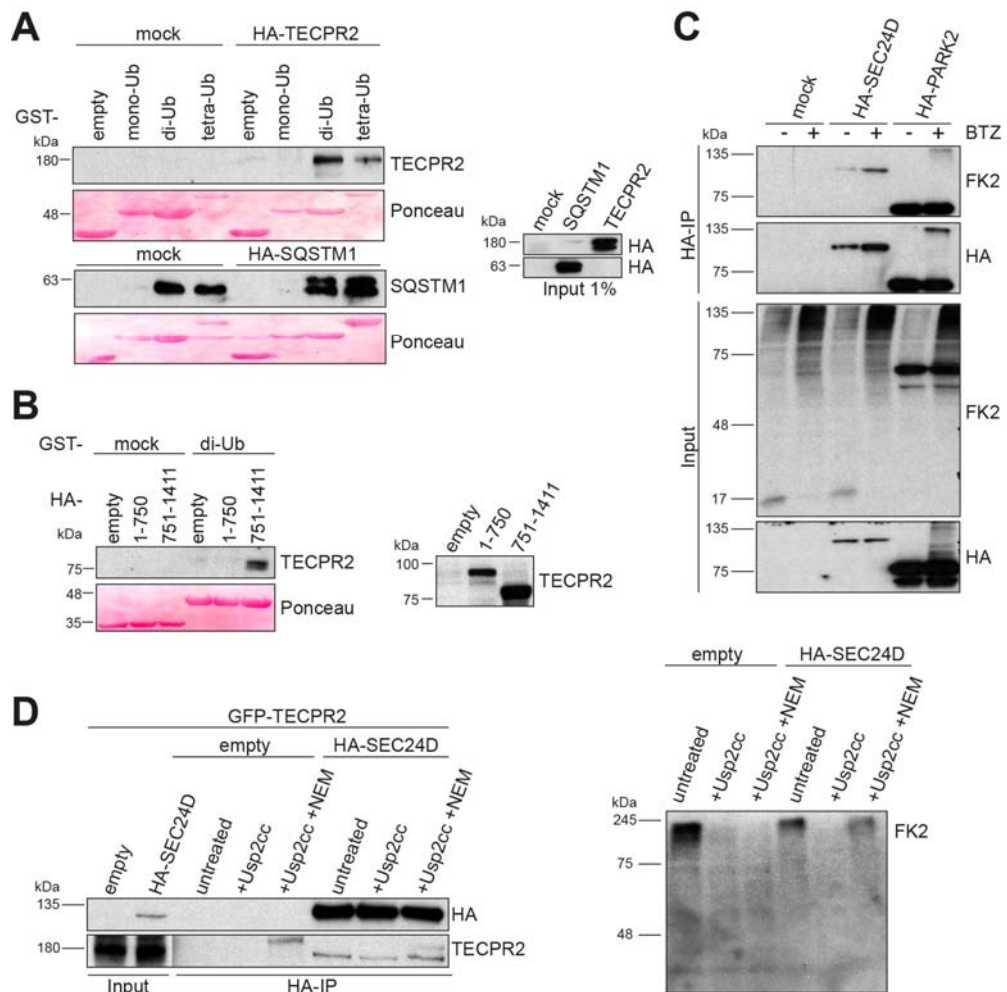


Figure 4-3: Contribution of ubiquitin to interaction of TECPR2 with SEC24D.

(A-B) Pull-downs using purified GST-ubiquitin variants and 293T cell lysate (empty or transiently overexpressing HA-TECPR2 fragments) analyzed by immunoblotting and Ponceau staining. SQSTM1 served as positive control. Overexpression of proteins was monitored by HA-antibody. (C) Denaturing IP of HA-SEC24D and -PARK2 overexpressing cells grown for 8 hrs in absence or presence of Btz. Ubiquitylation was detected with FK2-antibody. (D) Immunoprecipitation of HeLa cells overexpressing HA-SEC24D and treated with Usp2cc and NEM (left). FK2 recognizes ubiquitin. Control of DUB and NEM function was conducted by detection of ubiquitin with FK2-antibody in lysates prior IP (right).

Intriguingly, TECPR2 associated mainly with di- and moderately with tetra-ubiquitin. SQSTM1, as a known ubiquitin binding protein, served as positive control (fig. 4-3A). By applying TECPR2 variants in pull-down assays the C-terminal part of the protein, comprising the TECPR repeats, was identified as the region responsible for ubiquitin binding (fig. 4-3B). Next, denaturing HA-IPs of SEC24D were conducted to assess the ubiquitylation status of SEC24D (fig. 4-3C). Note that the ubiquitin E3 ligase PARK2/Parkin was used as positive control due to its known auto-ubiquitylation activity. Intriguingly, covalently bound ubiquitin was detected on SEC24D, which accumulated upon inhibition of the proteasome by Bortezomib (Btz). To directly examine whether the interaction between TECPR2 and SEC24D is mediated by

ubiquitin, cells overexpressing HA-SEC24D and GFP-TECPR2 were subjected to denaturing HA-IPs in the absence and presence of catalytic domain of the de-ubiquitinating enzyme (DUB) USP2 (Usp2cc) and the broad DUB inhibitor N-Ethylmaleimide (NEM) (fig. 4-3D). While the amount of TECPR2 precipitated with SEC24D was markedly reduced in Usp2cc treated lysates, inhibition of Usp2cc by NEM was able to fully restore SEC24D binding to TECPR2. Collectively, these findings strongly support the idea of ubiquitin contributing to the binding of TECPR2 to SEC24D. Given that this work showed that TECPR2 employs its N-terminal part to bind SEC24D, it is possible that the ubiquitin- and TECPR repeat-mediated binding additionally stabilizes the interaction of TECPR2 to SEC24D. Further investigations are necessary to clarify the issue. Moreover, future studies are required to address whether HOPS and/or BLOC-1 are engaged in a similar binding mode by TECPR2. Follow up research in this direction provides high potential to gain deeper insights into mechanistic functions of TECPR2 and its ability to operate with and regulate so many different proteins.

5. References

Adams, P.D., Afonine, P.V., Bunkoczi, G., Chen, V.B., Davis, I.W., Echols, N., Headd, J.J., Hung, L.W., Kapral, G.J., Grosse-Kunstleve, R.W., *et al.* (2010). PHENIX: a comprehensive Python-based system for macromolecular structure solution. *Acta crystallographica. Section D, Biological crystallography* **66**, 213-221.

Alemu, E.A., Lamark, T., Torgersen, K.M., Birgisdottir, A.B., Larsen, K.B., Jain, A., Olsvik, H., Overvatn, A., Kirkin, V., and Johansen, T. (2012). ATG8 family proteins act as scaffolds for assembly of the ULK complex: sequence requirements for LC3-interacting region (LIR) motifs. *The Journal of biological chemistry* **287**, 39275-39290.

Axe, E.L., Walker, S.A., Manifava, M., Chandra, P., Roderick, H.L., Habermann, A., Griffiths, G., and Ktistakis, N.T. (2008). Autophagosome formation from membrane compartments enriched in phosphatidylinositol 3-phosphate and dynamically connected to the endoplasmic reticulum. *The Journal of cell biology* **182**, 685-701.

Balderhaar, H.J., and Ungermann, C. (2013). CORVET and HOPS tethering complexes - coordinators of endosome and lysosome fusion. *Journal of cell science* **126**, 1307-1316.

Bassik, M.C., Kampmann, M., Lebbink, R.J., Wang, S., Hein, M.Y., Poser, I., Weibezahn, J., Horlbeck, M.A., Chen, S., Mann, M., *et al.* (2013). A systematic mammalian genetic interaction map reveals pathways underlying ricin susceptibility. *Cell* **152**, 909-922.

Beetz, C., Johnson, A., Schuh, A.L., Thakur, S., Varga, R.E., Fothergill, T., Hertel, N., Bomba-Warczak, E., Thiele, H., Nurnberg, G., *et al.* (2013). Inhibition of TFG function causes hereditary axon degeneration by impairing endoplasmic reticulum structure. *Proceedings of the National Academy of Sciences of the United States of America* **110**, 5091-5096.

Behrends, C., Sowa, M.E., Gygi, S.P., and Harper, J.W. (2010). Network organization of the human autophagy system. *Nature* **466**, 68-76.

Ben-Tekaya, H., Miura, K., Pepperkok, R., and Hauri, H.P. (2005). Live imaging of bidirectional traffic from the ERGIC. *Journal of cell science* **118**, 357-367.

Bi, X., Corpina, R.A., and Goldberg, J. (2002). Structure of the Sec23/24-Sar1 pre-budding complex of the COPII vesicle coat. *Nature* **419**, 271-277.

Bian, X., Klemm, R.W., Liu, T.Y., Zhang, M., Sun, S., Sui, X., Liu, X., Rapoport, T.A., and Hu, J. (2011). Structures of the atlastin GTPase provide insight into homotypic fusion of endoplasmic reticulum membranes. *Proceedings of the National Academy of Sciences of the United States of America* **108**, 3976-3981.

Bielli, A., Haney, C.J., Gabreski, G., Watkins, S.C., Bannykh, S.I., and Aridor, M. (2005). Regulation of Sar1 NH2 terminus by GTP binding and hydrolysis promotes membrane deformation to control COPII vesicle fission. *The Journal of cell biology* **171**, 919-924.

Bjorkoy, G., Lamark, T., Brech, A., Outzen, H., Perander, M., Overvatn, A., Stenmark, H., and Johansen, T. (2005). p62/SQSTM1 forms protein aggregates degraded by autophagy and has a protective effect on huntingtin-induced cell death. *The Journal of cell biology* **171**, 603-614.

Blackstone, C. (2012). Cellular pathways of hereditary spastic paraplegia. *Annu Rev Neurosci* **35**, 25-47.

References

- Bolte, S., and Cordelieres, F.P. (2006). A guided tour into subcellular colocalization analysis in light microscopy. *Journal of microscopy* 224, 213-232.
- Boncompain, G., Divoux, S., Gareil, N., de Forges, H., Lescure, A., Latreche, L., Mercanti, V., Jollivet, F., Raposo, G., and Perez, F. (2012). Synchronization of secretory protein traffic in populations of cells. *Nature methods* 9, 493-498.
- Bonifacino, J.S., and Glick, B.S. (2004). The mechanisms of vesicle budding and fusion. *Cell* 116, 153-166.
- Bonnon, C., Wendeler, M.W., Paccaud, J.P., and Hauri, H.P. (2010). Selective export of human GPI-anchored proteins from the endoplasmic reticulum. *Journal of cell science* 123, 1705-1715.
- Borgese, N., and Fasana, E. (2011). Targeting pathways of C-tail-anchored proteins. *Biochimica et biophysica acta* 1808, 937-946.
- Brocker, C., Kuhlee, A., Gatsogiannis, C., Balderhaar, H.J., Honscher, C., Engelbrecht-Vandre, S., Ungermann, C., and Raunser, S. (2012). Molecular architecture of the multisubunit homotypic fusion and vacuole protein sorting (HOPS) tethering complex. *Proceedings of the National Academy of Sciences of the United States of America* 109, 1991-1996.
- Cai, H., Yu, S., Menon, S., Cai, Y., Lazarova, D., Fu, C., Reinisch, K., Hay, J.C., and Ferro-Novick, S. (2007). TRAPPI tethers COPII vesicles by binding the coat subunit Sec23. *Nature* 445, 941-944.
- Cai, H., Zhang, Y., Pypaert, M., Walker, L., and Ferro-Novick, S. (2005). Mutants in *trs120* disrupt traffic from the early endosome to the late Golgi. *The Journal of cell biology* 171, 823-833.
- Cai, Q., Lu, L., Tian, J.H., Zhu, Y.B., Qiao, H., and Sheng, Z.H. (2010). Snapin-regulated late endosomal transport is critical for efficient autophagy-lysosomal function in neurons. *Neuron* 68, 73-86.
- Carlsson, S.R., and Simonsen, A. (2015). Membrane dynamics in autophagosome biogenesis. *Journal of cell science* 128, 193-205.
- Chang, K.W., Yang, P.Y., Lai, H.Y., Yeh, T.S., Chen, T.C., and Yeh, C.T. (2006). Identification of a novel actin isoform in hepatocellular carcinoma. *Hepatology* 43, 33-39.
- Chen, D., Fan, W., Lu, Y., Ding, X., Chen, S., and Zhong, Q. (2012). A mammalian autophagosome maturation mechanism mediated by TECPR1 and the Atg12-Atg5 conjugate. *Molecular cell* 45, 629-641.
- Chen, W.R., Xiong, W., and Shepherd, G.M. (2000). Analysis of relations between NMDA receptors and GABA release at olfactory bulb reciprocal synapses. *Neuron* 25, 625-633.
- Collins, K.M., and Wickner, W.T. (2007). Trans-SNARE complex assembly and yeast vacuole membrane fusion. *Proceedings of the National Academy of Sciences of the United States of America* 104, 8755-8760.
- Connell, J.W., Lindon, C., Luzio, J.P., and Reid, E. (2009). Spastin couples microtubule severing to membrane traffic in completion of cytokinesis and secretion. *Traffic* 10, 42-56.
- D'Arcangelo, J.G., Stahmer, K.R., and Miller, E.A. (2013). Vesicle-mediated export from the ER: COPII coat function and regulation. *Biochimica et biophysica acta* 1833, 2464-2472.

References

- Davids, M., Kane, M.S., He, M., Wolfe, L.A., Li, X., Raihan, M.A., Chao, K.R., Bone, W.P., Boerkoel, C.F., Gahl, W.A., *et al.* (2015). Disruption of Golgi morphology and altered protein glycosylation in PLA2G6-associated neurodegeneration. *J Med Genet*.
- Di Pietro, S.M., and Dell'Angelica, E.C. (2005). The cell biology of Hermansky-Pudlak syndrome: recent advances. *Traffic* 6, 525-533.
- Di Pietro, S.M., Falcon-Perez, J.M., Tenza, D., Setty, S.R., Marks, M.S., Raposo, G., and Dell'Angelica, E.C. (2006). BLOC-1 interacts with BLOC-2 and the AP-3 complex to facilitate protein trafficking on endosomes. *Molecular biology of the cell* 17, 4027-4038.
- Diamant, G., Amir-Zilberstein, L., Yamaguchi, Y., Handa, H., and Dikstein, R. (2012). DSIF restricts NF-kappaB signaling by coordinating elongation with mRNA processing of negative feedback genes. *Cell Rep* 2, 722-731.
- Diao, J., Liu, R., Rong, Y., Zhao, M., Zhang, J., Lai, Y., Zhou, Q., Wilz, L.M., Li, J., Vivona, S., *et al.* (2015). ATG14 promotes membrane tethering and fusion of autophagosomes to endolysosomes. *Nature*.
- Dion, P.A., Daoud, H., and Rouleau, G.A. (2009). Genetics of motor neuron disorders: new insights into pathogenic mechanisms. *Nat Rev Genet* 10, 769-782.
- Dooley, H.C., Razi, M., Polson, H.E., Girardin, S.E., Wilson, M.I., and Tooze, S.A. (2014). WIPI2 links LC3 conjugation with PI3P, autophagosome formation, and pathogen clearance by recruiting Atg12-5-16L1. *Molecular cell* 55, 238-252.
- Emsley, P., Lohkamp, B., Scott, W.G., and Cowtan, K. (2010). Features and development of Coot. *Acta crystallographica. Section D, Biological crystallography* 66, 486-501.
- Evans, K., Keller, C., Pavur, K., Glasgow, K., Conn, B., and Luring, B. (2006). Interaction of two hereditary spastic paraplegia gene products, spastin and atlastin, suggests a common pathway for axonal maintenance. *Proceedings of the National Academy of Sciences of the United States of America* 103, 10666-10671.
- Farhan, H., Reiterer, V., Korkhov, V.M., Schmid, J.A., Freissmuth, M., and Sitte, H.H. (2007). Concentrative export from the endoplasmic reticulum of the gamma-aminobutyric acid transporter 1 requires binding to SEC24D. *The Journal of biological chemistry* 282, 7679-7689.
- Farhan, H., Weiss, M., Tani, K., Kaufman, R.J., and Hauri, H.P. (2008). Adaptation of endoplasmic reticulum exit sites to acute and chronic increases in cargo load. *The EMBO journal* 27, 2043-2054.
- Fink, J.K. (1993). Hereditary Spastic Paraplegia Overview. In *GeneReviews(R)*, R.A. Pagon, M.P. Adam, H.H. Ardinger, S.E. Wallace, A. Amemiya, L.J.H. Bean, T.D. Bird, C.R. Dolan, C.T. Fong, R.J.H. Smith, and K. Stephens, eds. (Seattle (WA)).
- Fink, J.K. (2006). Hereditary spastic paraplegia. *Current neurology and neuroscience reports* 6, 65-76.
- Fink, J.K. (2014). Hereditary spastic paraplegia: clinical principles and genetic advances. *Seminars in neurology* 34, 293-305.
- Friedman, J.R., and Voeltz, G.K. (2011). The ER in 3D: a multifunctional dynamic membrane network. *Trends Cell Biol* 21, 709-717.

References

- Ganley, I.G., Lam du, H., Wang, J., Ding, X., Chen, S., and Jiang, X. (2009). ULK1.ATG13.FIP200 complex mediates mTOR signaling and is essential for autophagy. *The Journal of biological chemistry* 284, 12297-12305.
- Ge, L., Zhang, M., and Schekman, R. (2014). Phosphatidylinositol 3-kinase and COPII generate LC3 lipidation vesicles from the ER-Golgi intermediate compartment. *eLife* 3, e04135.
- Genau, H.M., Huber, J., Baschieri, F., Akutsu, M., Dotsch, V., Farhan, H., Rogov, V., and Behrends, C. (2015). CUL3-KBTBD6/KBTBD7 Ubiquitin Ligase Cooperates with GABARAP Proteins to Spatially Restrict TIAM1-RAC1 Signaling. *Molecular cell* 57, 995-1010.
- Goyal, U., and Blackstone, C. (2013). Untangling the web: mechanisms underlying ER network formation. *Biochimica et biophysica acta* 1833, 2492-2498.
- Graef, M., Friedman, J.R., Graham, C., Babu, M., and Nunnari, J. (2013). ER exit sites are physical and functional core autophagosome biogenesis components. *Molecular biology of the cell* 24, 2918-2931.
- Gutierrez, M.G., Munafo, D.B., Beron, W., and Colombo, M.I. (2004). Rab7 is required for the normal progression of the autophagic pathway in mammalian cells. *Journal of cell science* 117, 2687-2697.
- Hahn, K., Rohdin, C., Jagannathan, V., Wohlsein, P., Baumgartner, W., Seehusen, F., Spitzbarth, I., Grandon, R., Drogemuller, C., and Jaderlund, K.H. (2015). TECPR2 Associated Neuroaxonal Dystrophy in Spanish Water Dogs. *PLoS One* 10, e0141824.
- Hazan, J., Fonknechten, N., Mavel, D., Paternotte, C., Samson, D., Artiguenave, F., Davoine, C.S., Cruaud, C., Durr, A., Wincker, P., *et al.* (1999). Spastin, a new AAA protein, is altered in the most frequent form of autosomal dominant spastic paraplegia. *Nature genetics* 23, 296-303.
- Hegde, R.S., and Keenan, R.J. (2011). Tail-anchored membrane protein insertion into the endoplasmic reticulum. *Nature reviews. Molecular cell biology* 12, 787-798.
- Heimer, G., Oz-Levi, D., Eyal, E., Edvardson, S., Nissenkorn, A., Ruzzo, E.K., Szeinberg, A., Maayan, C., Mai-Zahav, M., Efrati, O., *et al.* (2015). TECPR2 mutations cause a new subtype of familial dysautonomia like hereditary sensory autonomic neuropathy with intellectual disability. *Eur J Paediatr Neurol*.
- Hermansky, F., and Pudlak, P. (1959). Albinism associated with hemorrhagic diathesis and unusual pigmented reticular cells in the bone marrow: report of two cases with histochemical studies. *Blood* 14, 162-169.
- Hughes, H., Budnik, A., Schmidt, K., Palmer, K.J., Mantell, J., Noakes, C., Johnson, A., Carter, D.A., Verkade, P., Watson, P., *et al.* (2009). Organisation of human ER-exit sites: requirements for the localisation of Sec16 to transitional ER. *Journal of cell science* 122, 2924-2934.
- Huh, C.G., Aldrich, J., Mottahedeh, J., Kwon, H., Johnson, C., and Marsh, R. (1998). Cloning and characterization of *Physarum polycephalum* tectonins. Homologues of *Limulus* lectin L-6. *The Journal of biological chemistry* 273, 6565-6574.
- Huizing, M., Boissy, R.E., and Gahl, W.A. (2002). Hermansky-Pudlak syndrome: vesicle formation from yeast to man. *Pigment Cell Res* 15, 405-419.

References

- Huizing, M., Sarangarajan, R., Strovel, E., Zhao, Y., Gahl, W.A., and Boissy, R.E. (2001). AP-3 mediates tyrosinase but not TRP-1 trafficking in human melanocytes. *Molecular biology of the cell* *12*, 2075-2085.
- Ichimura, Y., Kumanomidou, T., Sou, Y.S., Mizushima, T., Ezaki, J., Ueno, T., Kominami, E., Yamane, T., Tanaka, K., and Komatsu, M. (2008). Structural basis for sorting mechanism of p62 in selective autophagy. *The Journal of biological chemistry* *283*, 22847-22857.
- Itakura, E., Kishi-Itakura, C., and Mizushima, N. (2012). The hairpin-type tail-anchored SNARE syntaxin 17 targets to autophagosomes for fusion with endosomes/lysosomes. *Cell* *151*, 1256-1269.
- Itakura, E., Kishi, C., Inoue, K., and Mizushima, N. (2008). Beclin 1 forms two distinct phosphatidylinositol 3-kinase complexes with mammalian Atg14 and UVRAG. *Molecular biology of the cell* *19*, 5360-5372.
- Jager, S., Bucci, C., Tanida, I., Ueno, T., Kominami, E., Saftig, P., and Eskelinen, E.L. (2004). Role for Rab7 in maturation of late autophagic vacuoles. *Journal of cell science* *117*, 4837-4848.
- Jensen, D., and Schekman, R. (2011). COPII-mediated vesicle formation at a glance. *Journal of cell science* *124*, 1-4.
- Jiang, P., Nishimura, T., Sakamaki, Y., Itakura, E., Hatta, T., Natsume, T., and Mizushima, N. (2014). The HOPS complex mediates autophagosome-lysosome fusion through interaction with syntaxin 17. *Molecular biology of the cell* *25*, 1327-1337.
- Johansen, T., and Lamark, T. (2011). Selective autophagy mediated by autophagic adapter proteins. *Autophagy* *7*, 279-296.
- John Peter, A.T., Lachmann, J., Rana, M., Bunge, M., Cabrera, M., and Ungermann, C. (2013). The BLOC-1 complex promotes endosomal maturation by recruiting the Rab5 GTPase-activating protein Msb3. *The Journal of cell biology* *201*, 97-111.
- Juris, L., Montino, M., Rube, P., Schlotterhose, P., Thumm, M., and Krick, R. (2015). PI3P binding by Atg21 organises Atg8 lipidation. *The EMBO journal* *34*, 955-973.
- Kabeya, Y., Mizushima, N., Yamamoto, A., Oshitani-Okamoto, S., Ohsumi, Y., and Yoshimori, T. (2004). LC3, GABARAP and GATE16 localize to autophagosomal membrane depending on form-II formation. *Journal of cell science* *117*, 2805-2812.
- Kabsch, W. (2010). Xds. *Acta crystallographica. Section D, Biological crystallography* *66*, 125-132.
- Kamada, K. (2012). The GINS complex: structure and function. *Subcell Biochem* *62*, 135-156.
- Kamada, K., Kubota, Y., Arata, T., Shindo, Y., and Hanaoka, F. (2007). Structure of the human GINS complex and its assembly and functional interface in replication initiation. *Nature structural & molecular biology* *14*, 388-396.
- Khaminets, A., Heinrich, T., Mari, M., Grumati, P., Huebner, A.K., Akutsu, M., Liebmann, L., Stolz, A., Nietzsche, S., Koch, N., *et al.* (2015). Regulation of endoplasmic reticulum turnover by selective autophagy. *Nature* *522*, 354-358.

References

- Kim, H.J., Zhong, Q., Sheng, Z.H., Yoshimori, T., Liang, C., and Jung, J.U. (2012). Beclin-1-interacting autophagy protein Atg14L targets the SNARE-associated protein Snapin to coordinate endocytic trafficking. *Journal of cell science* *125*, 4740-4750.
- Kim, T.H., Lee, J.H., Park, Y.E., Shin, J.H., Nam, T.S., Kim, H.S., Jang, H.J., Semenov, A., Kim, S.J., and Kim, D.S. (2014). Mutation analysis of SPAST, ATL1, and REEP1 in Korean Patients with Hereditary Spastic Paraplegia. *J Clin Neurol* *10*, 257-261.
- Kim, W., Bennett, E.J., Huttlin, E.L., Guo, A., Li, J., Possemato, A., Sowa, M.E., Rad, R., Rush, J., Comb, M.J., *et al.* (2011). Systematic and quantitative assessment of the ubiquitin-modified proteome. *Molecular cell* *44*, 325-340.
- Kittler, J.T., Rostaing, P., Schiavo, G., Fritschy, J.M., Olsen, R., Triller, A., and Moss, S.J. (2001). The subcellular distribution of GABARAP and its ability to interact with NSF suggest a role for this protein in the intracellular transport of GABA(A) receptors. *Mol Cell Neurosci* *18*, 13-25.
- Klinkenberg, D., Long, K.R., Shome, K., Watkins, S.C., and Aridor, M. (2014). A cascade of ER exit site assembly that is regulated by p125A and lipid signals. *Journal of cell science* *127*, 1765-1778.
- Kraft, C., Kijanska, M., Kalie, E., Siergiejuk, E., Lee, S.S., Semplicio, G., Stoffel, I., Brezovich, A., Verma, M., Hansmann, I., *et al.* (2012). Binding of the Atg1/ULK1 kinase to the ubiquitin-like protein Atg8 regulates autophagy. *The EMBO journal* *31*, 3691-3703.
- Kurth, I., Pamminger, T., Hennings, J.C., Soehendra, D., Huebner, A.K., Rotthier, A., Baets, J., Senderek, J., Topaloglu, H., Farrell, S.A., *et al.* (2009). Mutations in FAM134B, encoding a newly identified Golgi protein, cause severe sensory and autonomic neuropathy. *Nature genetics* *41*, 1179-1181.
- Kuznetsov, S.A., and Gelfand, V.I. (1987). 18 kDa microtubule-associated protein: identification as a new light chain (LC-3) of microtubule-associated protein 1 (MAP-1). *FEBS letters* *212*, 145-148.
- Lamb, C.A., Yoshimori, T., and Tooze, S.A. (2013). The autophagosome: origins unknown, biogenesis complex. *Nature reviews. Molecular cell biology* *14*, 759-774.
- Lee, H.H., Nemecek, D., Schindler, C., Smith, W.J., Ghirlando, R., Steven, A.C., Bonifacino, J.S., and Hurley, J.H. (2012). Assembly and architecture of biogenesis of lysosome-related organelles complex-1 (BLOC-1). *The Journal of biological chemistry* *287*, 5882-5890.
- Lee, M.C., Miller, E.A., Goldberg, J., Orci, L., and Schekman, R. (2004). Bi-directional protein transport between the ER and Golgi. *Annual review of cell and developmental biology* *20*, 87-123.
- Li, W., Rusiniak, M.E., Chintala, S., Gautam, R., Novak, E.K., and Swank, R.T. (2004). Murine Hermansky-Pudlak syndrome genes: regulators of lysosome-related organelles. *Bioessays* *26*, 616-628.
- Liang, C., Lee, J.S., Inn, K.S., Gack, M.U., Li, Q., Roberts, E.A., Vergne, I., Deretic, V., Feng, P., Akazawa, C., *et al.* (2008). Beclin1-binding UVRAG targets the class C Vps complex to coordinate autophagosome maturation and endocytic trafficking. *Nature cell biology* *10*, 776-787.

References

- Lord, C., Ferro-Novick, S., and Miller, E.A. (2013). The highly conserved COPII coat complex sorts cargo from the endoplasmic reticulum and targets it to the golgi. *Cold Spring Harbor perspectives in biology* 5.
- Lu, Q., Yang, P., Huang, X., Hu, W., Guo, B., Wu, F., Lin, L., Kovacs, A.L., Yu, L., and Zhang, H. (2011). The WD40 repeat PtdIns(3)P-binding protein EPG-6 regulates progression of omegasomes to autophagosomes. *Developmental cell* 21, 343-357.
- Lystad, A.H., Ichimura, Y., Takagi, K., Yang, Y., Pankiv, S., Kanegae, Y., Kageyama, S., Suzuki, M., Saito, I., Mizushima, T., *et al.* (2014). Structural determinants in GABARAP required for the selective binding and recruitment of ALFY to LC3B-positive structures. *EMBO reports* 15, 557-565.
- Manil-Segalen, M., Lefebvre, C., Jenzer, C., Trichet, M., Boulogne, C., Satiat-Jeunemaitre, B., and Legouis, R. (2014). The *C. elegans* LC3 acts downstream of GABARAP to degrade autophagosomes by interacting with the HOPS subunit VPS39. *Developmental cell* 28, 43-55.
- Mann, S.S., and Hammarback, J.A. (1994). Molecular characterization of light chain 3. A microtubule binding subunit of MAP1A and MAP1B. *The Journal of biological chemistry* 269, 11492-11497.
- Mannan, A.U., Krawen, P., Sauter, S.M., Boehm, J., Chronowska, A., Paulus, W., Neesen, J., and Engel, W. (2006). ZFYVE27 (SPG33), a novel spastin-binding protein, is mutated in hereditary spastic paraplegia. *American journal of human genetics* 79, 351-357.
- Mari, M., Griffith, J., Rieter, E., Krishnappa, L., Klionsky, D.J., and Reggiori, F. (2010). An Atg9-containing compartment that functions in the early steps of autophagosome biogenesis. *The Journal of cell biology* 190, 1005-1022.
- McEwan, D.G., Popovic, D., Gubas, A., Terawaki, S., Suzuki, H., Stadel, D., Coxon, F.P., Miranda de Stegmann, D., Bhogaraju, S., Maddi, K., *et al.* (2015). PLEKHM1 regulates autophagosome-lysosome fusion through HOPS complex and LC3/GABARAP proteins. *Molecular cell* 57, 39-54.
- Merte, J., Jensen, D., Wright, K., Sarsfield, S., Wang, Y., Schekman, R., and Ginty, D.D. (2010). Sec24b selectively sorts Vangl2 to regulate planar cell polarity during neural tube closure. *Nature cell biology* 12, 41-46; sup pp 41-48.
- Michell, R.H., Heath, V.L., Lemmon, M.A., and Dove, S.K. (2006). Phosphatidylinositol 3,5-bisphosphate: metabolism and cellular functions. *Trends in biochemical sciences* 31, 52-63.
- Morgan, N.V., Pasha, S., Johnson, C.A., Ainsworth, J.R., Eady, R.A., Dawood, B., McKeown, C., Trembath, R.C., Wilde, J., Watson, S.P., *et al.* (2006). A germline mutation in BLOC1S3/reduced pigmentation causes a novel variant of Hermansky-Pudlak syndrome (HPS8). *American journal of human genetics* 78, 160-166.
- Namekawa, M., Muriel, M.P., Janer, A., Latouche, M., Dauphin, A., Debeir, T., Martin, E., Duyckaerts, C., Prigent, A., Depienne, C., *et al.* (2007). Mutations in the SPG3A gene encoding the GTPase atlastin interfere with vesicle trafficking in the ER/Golgi interface and Golgi morphogenesis. *Mol Cell Neurosci* 35, 1-13.
- Nickerson, D.P., Russell, M.R., and Odorizzi, G. (2007). A concentric circle model of multivesicular body cargo sorting. *EMBO reports* 8, 644-650.

References

- Nikonov, A.V., Hauri, H.P., Lauring, B., and Kreibich, G. (2007). Climp-63-mediated binding of microtubules to the ER affects the lateral mobility of translocon complexes. *Journal of cell science* *120*, 2248-2258.
- Novak, I., Kirkin, V., McEwan, D.G., Zhang, J., Wild, P., Rozenknop, A., Rogov, V., Lohr, F., Popovic, D., Occhipinti, A., *et al.* (2010). Nix is a selective autophagy receptor for mitochondrial clearance. *EMBO reports* *11*, 45-51.
- Ogawa, M., and Sasakawa, C. (2011). The role of Tecpr1 in selective autophagy as a cargo receptor. *Autophagy* *7*, 1389-1391.
- Ogawa, M., Yoshikawa, Y., Kobayashi, T., Mimuro, H., Fukumatsu, M., Kiga, K., Piao, Z., Ashida, H., Yoshida, M., Kakuta, S., *et al.* (2011). A Tecpr1-dependent selective autophagy pathway targets bacterial pathogens. *Cell host & microbe* *9*, 376-389.
- Ong, Y.S., Tang, B.L., Loo, L.S., and Hong, W. (2010). p125A exists as part of the mammalian Sec13/Sec31 COPII subcomplex to facilitate ER-Golgi transport. *The Journal of cell biology* *190*, 331-345.
- Oz-Levi, D., Ben-Zeev, B., Ruzzo, E.K., Hitomi, Y., Gelman, A., Pelak, K., Anikster, Y., Reznik-Wolf, H., Bar-Joseph, I., Olender, T., *et al.* (2012). Mutation in TECPR2 reveals a role for autophagy in hereditary spastic paraparesis. *American journal of human genetics* *91*, 1065-1072.
- Pagano, A., Letourneur, F., Garcia-Estefania, D., Carpentier, J.L., Orci, L., and Paccaud, J.P. (1999). Sec24 proteins and sorting at the endoplasmic reticulum. *The Journal of biological chemistry* *274*, 7833-7840.
- Pankiv, S., Clausen, T.H., Lamark, T., Brech, A., Bruun, J.A., Outzen, H., Overvatn, A., Bjorkoy, G., and Johansen, T. (2007). p62/SQSTM1 binds directly to Atg8/LC3 to facilitate degradation of ubiquitinated protein aggregates by autophagy. *The Journal of biological chemistry* *282*, 24131-24145.
- Pashkova, N., Gakhar, L., Winistorfer, S.C., Yu, L., Ramaswamy, S., and Piper, R.C. (2010). WD40 repeat propellers define a ubiquitin-binding domain that regulates turnover of F box proteins. *Molecular cell* *40*, 433-443.
- Peden, A.A., Oorschot, V., Hesser, B.A., Austin, C.D., Scheller, R.H., and Klumperman, J. (2004). Localization of the AP-3 adaptor complex defines a novel endosomal exit site for lysosomal membrane proteins. *The Journal of cell biology* *164*, 1065-1076.
- Peng, C., Ye, J., Yan, S., Kong, S., Shen, Y., Li, C., Li, Q., Zheng, Y., Deng, K., Xu, T., *et al.* (2012). Ablation of vacuole protein sorting 18 (Vps18) gene leads to neurodegeneration and impaired neuronal migration by disrupting multiple vesicle transport pathways to lysosomes. *The Journal of biological chemistry* *287*, 32861-32873.
- Perini, E.D., Schaefer, R., Stoter, M., Kalaidzidis, Y., and Zerial, M. (2014). Mammalian CORVET is required for fusion and conversion of distinct early endosome subpopulations. *Traffic* *15*, 1366-1389.
- Pieren, M., Schmidt, A., and Mayer, A. (2010). The SM protein Vps33 and the t-SNARE H(abc) domain promote fusion pore opening. *Nature structural & molecular biology* *17*, 710-717.
- Pols, M.S., ten Brink, C., Gosavi, P., Oorschot, V., and Klumperman, J. (2013). The HOPS proteins hVps41 and hVps39 are required for homotypic and heterotypic late endosome fusion. *Traffic* *14*, 219-232.

References

- Polson, H.E., de Lartigue, J., Rigden, D.J., Reedijk, M., Urbe, S., Clague, M.J., and Tooze, S.A. (2010). Mammalian Atg18 (WIPI2) localizes to omegasome-anchored phagophores and positively regulates LC3 lipidation. *Autophagy* 6, 506-522.
- Poteryaev, D., Datta, S., Ackema, K., Zerial, M., and Spang, A. (2010). Identification of the switch in early-to-late endosome transition. *Cell* 141, 497-508.
- Proikas-Cezanne, T., Takacs, Z., Donnes, P., and Kohlbacher, O. (2015). WIPI proteins: essential PtdIns3P effectors at the nascent autophagosome. *Journal of cell science* 128, 207-217.
- Proikas-Cezanne, T., Waddell, S., Gaugel, A., Frickey, T., Lupas, A., and Nordheim, A. (2004). WIPI-1alpha (WIPI49), a member of the novel 7-bladed WIPI protein family, is aberrantly expressed in human cancer and is linked to starvation-induced autophagy. *Oncogene* 23, 9314-9325.
- Rogov, V., Dotsch, V., Johansen, T., and Kirkin, V. (2014). Interactions between autophagy receptors and ubiquitin-like proteins form the molecular basis for selective autophagy. *Molecular cell* 53, 167-178.
- Rogov, V.V., Rozenknop, A., Rogova, N.Y., Lohr, F., Tikole, S., Jaravine, V., Guntert, P., Dikic, I., and Dotsch, V. (2012). A universal expression tag for structural and functional studies of proteins. *Chembiochem : a European journal of chemical biology* 13, 959-963.
- Rogov, V.V., Suzuki, H., Fiskin, E., Wild, P., Kniss, A., Rozenknop, A., Kato, R., Kawasaki, M., McEwan, D.G., Lohr, F., *et al.* (2013). Structural basis for phosphorylation-triggered autophagic clearance of Salmonella. *The Biochemical journal* 454, 459-466.
- Rowland, A.A., Chitwood, P.J., Phillips, M.J., and Voeltz, G.K. (2014). ER contact sites define the position and timing of endosome fission. *Cell* 159, 1027-1041.
- Rozenknop, A., Rogov, V.V., Rogova, N.Y., Lohr, F., Guntert, P., Dikic, I., and Dotsch, V. (2011). Characterization of the interaction of GABARAPL-1 with the LIR motif of NBR1. *Journal of molecular biology* 410, 477-487.
- Saito, K., Chen, M., Bard, F., Chen, S., Zhou, H., Woodley, D., Polischuk, R., Schekman, R., and Malhotra, V. (2009). TANGO1 facilitates cargo loading at endoplasmic reticulum exit sites. *Cell* 136, 891-902.
- Salazar, G., Craige, B., Styers, M.L., Newell-Litwa, K.A., Doucette, M.M., Wainer, B.H., Falcon-Perez, J.M., Dell'Angelica, E.C., Peden, A.A., Werner, E., *et al.* (2006). BLOC-1 complex deficiency alters the targeting of adaptor protein complex-3 cargoes. *Molecular biology of the cell* 17, 4014-4026.
- Sanchez-Wandelmer, J., Ktistakis, N.T., and Reggiori, F. (2015). ERES: sites for autophagosome biogenesis and maturation? *Journal of cell science* 128, 185-192.
- Sanderson, C.M., Connell, J.W., Edwards, T.L., Bright, N.A., Duley, S., Thompson, A., Luzio, J.P., and Reid, E. (2006). Spastin and atlastin, two proteins mutated in autosomal-dominant hereditary spastic paraplegia, are binding partners. *Hum Mol Genet* 15, 307-318.
- Seo, S.B., McNamara, P., Heo, S., Turner, A., Lane, W.S., and Chakravarti, D. (2001). Regulation of histone acetylation and transcription by INHAT, a human cellular complex containing the set oncoprotein. *Cell* 104, 119-130.

References

- Setty, S.R., Tenza, D., Truschel, S.T., Chou, E., Sviderskaya, E.V., Theos, A.C., Lamoreux, M.L., Di Pietro, S.M., Starcevic, M., Bennett, D.C., *et al.* (2007). BLOC-1 is required for cargo-specific sorting from vacuolar early endosomes toward lysosome-related organelles. *Molecular biology of the cell* 18, 768-780.
- Shirane, M., and Nakayama, K.I. (2006). Protrudin induces neurite formation by directional membrane trafficking. *Science* 314, 818-821.
- Shpilka, T., Weidberg, H., Pietrokovski, S., and Elazar, Z. (2011). Atg8: an autophagy-related ubiquitin-like protein family. *Genome biology* 12, 226.
- Sievers, F., Wilm, A., Dineen, D., Gibson, T.J., Karplus, K., Li, W., Lopez, R., McWilliam, H., Remmert, M., Soding, J., *et al.* (2011). Fast, scalable generation of high-quality protein multiple sequence alignments using Clustal Omega. *Mol Syst Biol* 7, 539.
- Simonsen, A., and Tooze, S.A. (2009). Coordination of membrane events during autophagy by multiple class III PI3-kinase complexes. *The Journal of cell biology* 186, 773-782.
- Slobodkin, M.R., and Elazar, Z. (2013). The Atg8 family: multifunctional ubiquitin-like key regulators of autophagy. *Essays in biochemistry* 55, 51-64.
- Sohda, M., Misumi, Y., Fujiwara, T., Nishioka, M., and Ikehara, Y. (1994). Molecular cloning and sequence analysis of a human 372-kDA protein localized in the Golgi complex. *Biochemical and biophysical research communications* 205, 1399-1408.
- Solinger, J.A., and Spang, A. (2013). Tethering complexes in the endocytic pathway: CORVET and HOPS. *The FEBS journal* 280, 2743-2757.
- Sowa, M.E., Bennett, E.J., Gygi, S.P., and Harper, J.W. (2009). Defining the human deubiquitinating enzyme interaction landscape. *Cell* 138, 389-403.
- Spang, A. (2015). The Road not Taken: Less Traveled Roads from the TGN to the Plasma Membrane. *Membranes (Basel)* 5, 84-98.
- Sprague, B.L., Muller, F., Pego, R.L., Bungay, P.M., Stavreva, D.A., and McNally, J.G. (2006). Analysis of binding at a single spatially localized cluster of binding sites by fluorescence recovery after photobleaching. *Biophysical journal* 91, 1169-1191.
- Sprangers, J., and Rabouille, C. (2015). SEC16 in COPII coat dynamics at ER exit sites. *Biochem Soc Trans* 43, 97-103.
- Stolz, A., Ernst, A., and Dikic, I. (2014). Cargo recognition and trafficking in selective autophagy. *Nature cell biology* 16, 495-501.
- Sumi-Akamaru, H., Beck, G., Kato, S., and Mochizuki, H. (2015). Neuroaxonal dystrophy in PLA2G6 knockout mice. *Neuropathology* 35, 289-302.
- Suzuki, H., Tabata, K., Morita, E., Kawasaki, M., Kato, R., Dobson, R.C., Yoshimori, T., and Wakatsuki, S. (2014). Structural basis of the autophagy-related LC3/Atg13 LIR complex: recognition and interaction mechanism. *Structure* 22, 47-58.
- Suzuki, K., Akioka, M., Kondo-Kakuta, C., Yamamoto, H., and Ohsumi, Y. (2013). Fine mapping of autophagy-related proteins during autophagosome formation in *Saccharomyces cerevisiae*. *Journal of cell science* 126, 2534-2544.

References

- Suzuki, T., Oiso, N., Gautam, R., Novak, E.K., Panthier, J.J., Suprabha, P.G., Vida, T., Swank, R.T., and Spritz, R.A. (2003). The mouse organellar biogenesis mutant buff results from a mutation in *Vps33a*, a homologue of yeast *vps33* and *Drosophila carnation*. *Proceedings of the National Academy of Sciences of the United States of America* *100*, 1146-1150.
- Tan, D., Cai, Y., Wang, J., Zhang, J., Menon, S., Chou, H.T., Ferro-Novick, S., Reinisch, K.M., and Walz, T. (2013). The EM structure of the TRAPP3 complex leads to the identification of a requirement for COPII vesicles on the macroautophagy pathway. *Proceedings of the National Academy of Sciences of the United States of America* *110*, 19432-19437.
- Townley, A.K., Feng, Y., Schmidt, K., Carter, D.A., Porter, R., Verkade, P., and Stephens, D.J. (2008). Efficient coupling of Sec23-Sec24 to Sec13-Sec31 drives COPII-dependent collagen secretion and is essential for normal craniofacial development. *Journal of cell science* *121*, 3025-3034.
- Van Damme, P., Lasa, M., Polevoda, B., Gazquez, C., Elosegui-Artola, A., Kim, D.S., De Juan-Pardo, E., Demeyer, K., Hole, K., Larrea, E., *et al.* (2012). N-terminal acetylome analyses and functional insights of the N-terminal acetyltransferase NatB. *Proceedings of the National Academy of Sciences of the United States of America* *109*, 12449-12454.
- Vantaggiato, C., Clementi, E., and Bassi, M.T. (2014). ZFYVE26/SPASTIZIN: a close link between complicated hereditary spastic paraparesis and autophagy. *Autophagy* *10*, 374-375.
- Vantaggiato, C., Crimella, C., Airoidi, G., Polishchuk, R., Bonato, S., Brighina, E., Scarlato, M., Musumeci, O., Toscano, A., Martinuzzi, A., *et al.* (2013). Defective autophagy in spastizin mutated patients with hereditary spastic paraparesis type 15. *Brain* *136*, 3119-3139.
- von Muhlinen, N., Akutsu, M., Ravenhill, B.J., Foeglein, A., Bloor, S., Rutherford, T.J., Freund, S.M., Komander, D., and Randow, F. (2012). LC3C, bound selectively by a noncanonical LIR motif in NDP52, is required for antibacterial autophagy. *Molecular cell* *48*, 329-342.
- Wada, T., Takagi, T., Yamaguchi, Y., Watanabe, D., and Handa, H. (1998). Evidence that P-TEFb alleviates the negative effect of DSIF on RNA polymerase II-dependent transcription in vitro. *The EMBO journal* *17*, 7395-7403.
- Wang, H., Bedford, F.K., Brandon, N.J., Moss, S.J., and Olsen, R.W. (1999). GABA(A)-receptor-associated protein links GABA(A) receptors and the cytoskeleton. *Nature* *397*, 69-72.
- Wang, J., Tan, D., Cai, Y., Reinisch, K.M., Walz, T., and Ferro-Novick, S. (2014). A requirement for ER-derived COPII vesicles in phagophore initiation. *Autophagy* *10*, 708-709.
- Wang, T., Ming, Z., Xiaochun, W., and Hong, W. (2011). Rab7: role of its protein interaction cascades in endo-lysosomal traffic. *Cellular signalling* *23*, 516-521.
- Ward, T.H., Polishchuk, R.S., Caplan, S., Hirschberg, K., and Lippincott-Schwartz, J. (2001). Maintenance of Golgi structure and function depends on the integrity of ER export. *The Journal of cell biology* *155*, 557-570.
- Webber, J.L., and Tooze, S.A. (2010). New insights into the function of Atg9. *FEBS letters* *584*, 1319-1326.
- Wei, A.H., and Li, W. (2013). Hermansky-Pudlak syndrome: pigmentary and non-pigmentary defects and their pathogenesis. *Pigment Cell Melanoma Res* *26*, 176-192.
- Wei, M.L. (2006). Hermansky-Pudlak syndrome: a disease of protein trafficking and organelle function. *Pigment Cell Res* *19*, 19-42.

References

- Weidberg, H., Shvets, E., Shpilka, T., Shimron, F., Shinder, V., and Elazar, Z. (2010). LC3 and GATE-16/GABARAP subfamilies are both essential yet act differently in autophagosome biogenesis. *The EMBO journal* **29**, 1792-1802.
- Wendeler, M.W., Paccaud, J.P., and Hauri, H.P. (2007). Role of Sec24 isoforms in selective export of membrane proteins from the endoplasmic reticulum. *EMBO reports* **8**, 258-264.
- Wild, P., Farhan, H., McEwan, D.G., Wagner, S., Rogov, V.V., Brady, N.R., Richter, B., Korac, J., Waidmann, O., Choudhary, C., *et al.* (2011). Phosphorylation of the autophagy receptor optineurin restricts Salmonella growth. *Science* **333**, 228-233.
- Winn, M.D., Ballard, C.C., Cowtan, K.D., Dodson, E.J., Emsley, P., Evans, P.R., Keegan, R.M., Krissinel, E.B., Leslie, A.G., McCoy, A., *et al.* (2011). Overview of the CCP4 suite and current developments. *Acta crystallographica. Section D, Biological crystallography* **67**, 235-242.
- Witte, K., Schuh, A.L., Hegermann, J., Sarkeshik, A., Mayers, J.R., Schwarze, K., Yates, J.R., 3rd, Eimer, S., and Audhya, A. (2011). TFG-1 function in protein secretion and oncogenesis. *Nature cell biology* **13**, 550-558.
- Xu, C., and Min, J. (2011). Structure and function of WD40 domain proteins. *Protein Cell* **2**, 202-214.
- Yagi, T., Ito, D., and Suzuki, N. (2014). Evidence of TRK-Fused Gene (TFG1) function in the ubiquitin-proteasome system. *Neurobiol Dis* **66**, 83-91.
- Yamamoto, H., Kakuta, S., Watanabe, T.M., Kitamura, A., Sekito, T., Kondo-Kakuta, C., Ichikawa, R., Kinjo, M., and Ohsumi, Y. (2012). Atg9 vesicles are an important membrane source during early steps of autophagosome formation. *The Journal of cell biology* **198**, 219-233.
- Yuzaki, M. (2010). Snapin snaps into the dynein complex for late endosome-lysosome trafficking and autophagy. *Neuron* **68**, 4-6.
- Zanetti, G., Pahuja, K.B., Studer, S., Shim, S., and Schekman, R. (2012). COPII and the regulation of protein sorting in mammals. *Nature cell biology* **14**, 20-28.
- Zhang, D.D., Lo, S.C., Sun, Z., Habib, G.M., Lieberman, M.W., and Hannink, M. (2005). Ubiquitination of Keap1, a BTB-Kelch substrate adaptor protein for Cul3, targets Keap1 for degradation by a proteasome-independent pathway. *The Journal of biological chemistry* **280**, 30091-30099.
- Zhao, X., Alvarado, D., Rainier, S., Lemons, R., Hedera, P., Weber, C.H., Tukul, T., Apak, M., Heiman-Patterson, T., Ming, L., *et al.* (2001). Mutations in a newly identified GTPase gene cause autosomal dominant hereditary spastic paraplegia. *Nature genetics* **29**, 326-331.
- Zick, M., and Wickner, W. (2013). The tethering complex HOPS catalyzes assembly of the soluble SNARE Vam7 into fusogenic trans-SNARE complexes. *Molecular biology of the cell* **24**, 3746-3753.
- Zoppino, F.C., Militello, R.D., Slavin, I., Alvarez, C., and Colombo, M.I. (2010). Autophagosome formation depends on the small GTPase Rab1 and functional ER exit sites. *Traffic* **11**, 1246-1261.
- Zuchner, S., Wang, G., Tran-Viet, K.N., Nance, M.A., Gaskell, P.C., Vance, J.M., Ashley-Koch, A.E., and Pericak-Vance, M.A. (2006). Mutations in the novel mitochondrial protein REEP1 cause hereditary spastic paraplegia type 31. *American journal of human genetics* **79**, 365-369.

Zusammenfassung

Bei den hereditären spastischen Paraparesen (HSP) handelt es sich um eine heterogene Gruppe neurodegenerativer Krankheiten, zu deren Entstehung über 50 Genloci und 20 Genprodukte beitragen. HSP zeichnet sich hauptsächlich durch spastische Lähmungen der unteren Extremitäten aus mit zugrunde liegendem Verlust der axonalen Integrität im Kortikospinaltrakt. Hauptsymptome sind vor allem progressive Spastizität und Paralyse der unteren Extremitäten sowie eine generelle Schwäche des Immunsystems. Weltweit leiden etwa drei bis neun von hunderttausend Menschen an HSP, wobei die Lebenszeit durch die Krankheit nicht verkürzt, aber erheblich beeinträchtigt wird.

Bei einer Genomanalyse von drei HSP-Patienten wurde eine Mutation im *TECPR2* Gen identifiziert, die zu einer Basenpaarverschiebung führt, welche ein verfrühtes Stopcodon zur Folge hat. Das Protein kann somit nicht stabil gebildet werden und wird daher im Proteasom abgebaut, wodurch den Zellen kein *TECPR2* zur Verfügung steht.

Das Protein *TECPR2* umfasst zwei Isoformen und beinhaltet drei N-terminale WD40-Domänen sowie mehrere *TECPR* Repeats im C-terminalen Bereich. Beide Strukturelemente bilden sogenannte β -Propeller aus. Dabei handelt es sich um Tertiärstrukturen, die spezielle unelastische Formen ausbilden und damit ideale Andockstellen für verschiedene Interaktionspartner bieten.

Zuerst wurde *TECPR2* mit dem Prozess der Autophagie in Zusammenhang gebracht. Autophagie ist ein Qualitätskontroll- und Recyclingprozess von zytoplasmatischen Bestandteilen wie beispielsweise fehlgefalteten Proteinen oder beschädigten Organellen mit dem Ziel die Zelle vor Schädigungen zu schützen und ihr Nährstoffe bzw. Bausteine für neue Komponenten bereitzustellen. Bei der Beseitigung von Pathogenen wie Bakterien spielt Autophagy ebenfalls eine wichtige Rolle.

In der Einleitungsphase der Autophagie werden Membranteile, sogenannte Phagophoren, ausgebildet, die zytoplasmatische Bestandteile umschließen. In der Ausdehnungsphase werden diese Membranteile verlängert und durch spezifische Rezeptoren Cargo ins Innere der sich schließenden Doppelmembran transportiert. Das geschlossene Vesikel mit dem abzubauenen Inhalt wird nun Autophagosom genannt. Im nächsten Schritt verschmilzt das Autophagosom mit einem Lysosom zu einem Autophagolysosom. Das Lysosom stellt dabei Enzyme und andere Faktoren zur Verfügung, die zum Abbau des Inhalts im angesäuerten Umfeld dienen.

Am Prozess der Autophagie und dessen Regulation sind viele verschiedene Proteine und Proteinkomplexe beteiligt, allen voran die Autophagie-verwandten Proteine (ATGs).

Eine wichtige Rolle dabei spielen die Proteine der ATG8-Familie. In Säugetieren sind sechs verschiedene ATG8-Proteine zu finden: MAP1LC3A (LC3A), MAP1LC3B (LC3B), MAP1LC3C

(LC3C), GABARAP, GABARAPL1 und GABARAPL2. Sie werden in eine LC3- und eine GABARAP-Unterfamilie eingeteilt. Während die LC3-Proteine an der Verlängerung der Phagophore mitwirken, ist die GABARAP-Untergruppe an späteren Prozessen der Autophagosomenreifung beteiligt.

Das am besten untersuchte Protein ist LC3B, welches als Mikrotubuli-assoziiertes Protein identifiziert wurde. LC3B ist hauptsächlich im Zytoplasma und Endomembransystem lokalisiert. Bei der Autophagie wird LC3B an das Lipid PE kovalent konjugiert und somit in die Membran der Autophagosomen integriert. Dort unterstützt es die Bildung der Autophagosomen und ist für die Rekrutierung von Cargo zuständig. Da LC3B von der Ausbildungsphase bis zum fertigen Autophagosom in dessen Membran eingegliedert bleibt, wird es als genereller Marker für Autophagosomen genutzt.

Alle ATG8-Proteine beinhalten eine konservierte Andockstelle für eine spezifische, nicht-kovalente Bindung an Autophagierezeptoren und Effektorproteine. Diese wiederum bilden ein sogenanntes LIR Motiv aus, welches eine spezielle Anordnung von vier Aminosäuren aufweist. Auf eine aromatische Aminosäure (W/F/Y) folgen zwei beliebige Reste und danach eine hydrophobe Aminosäure (L/I/V). Unterstützt wird die Bindung ausserdem von einer negativen Ladung ausgelöst durch dem Motiv vorangestellte, saure Aminosäuren (D/E).

In einer massenspektrometrischen Analyse der ATG8-Proteine wurde TECPR2 als Interaktionspartner von GABARAP identifiziert. Zudem wurde gezeigt, dass das Fehlen von TECPR2 in Zellen zu einem Verlust von LC3B-positiven Strukturen, also Autophagosomen führt. Diese Beobachtungen führten zu der Annahme, dass es sich bei TECPR2 um einen positiven Regulator von Autophagie handeln könnte. Obwohl ein Zusammenhang von TECPR2 zu dem Krankheitsbild der HSP und Autophagie hergestellt werden konnte, blieb die exakte Funktion des Proteins in Zellen weiterhin ungeklärt.

In dieser Arbeit sollten neue Interaktionspartner von TECPR2 gefunden werden und mit deren Hilfe eine Erklärung für den positiven Einfluss auf Autophagie gefunden werden. Zunächst aber wurde die Bindung von TECPR2 an die ATG8-Proteinen bestätigt und das LIR-Motiv in der TECPR2 Sequenz ausgemacht. Hierfür wurden die ATG8-Proteine aufgereinigt und die Bindung zu endogenem TECPR2 durch Pulldown-Assays bestätigt. Mithilfe von TECPR2-Fragmenten konnte der Bindungsbereich auf den C-terminalen Teil des Proteins eingegrenzt werden. Zur finalen Benennung des LIR-Motives wurde mithilfe eines Peptidarrays die Bindestelle am Ende des C-terminus mit passender LIR-Sequenz W-E-V-I ausfindig gemacht. In Pulldown-Versuchen mit TECPR2-Varianten, die Mutationen in dieser Sequenz enthielten, konnte das LIR-Motiv verifiziert werden. In biophysikalischen Experimentreihen wie der isothermen Titrationskalorimetrie (ITC) und der Kernspinresonanzspektroskopie (NMR) sollte die Interaktion zwischen TECPR2 und den ATG8-Proteinen genauer untersucht werden um eventuelle Bindepräferenzen zu bestimmten ATG8-Untergruppen zu detektieren. Allerdings

konnten in sämtlichen *in vitro* Untersuchungen mit überexprimierten ATG8-Proteinen keine substanziellen Unterschiede ausgemacht werden. Lediglich LC3A und GABARAPL2 scheinen eine geringere Bindeaffinität zu TECPR2 zu besitzen. In Kristallstrukturanalysen konnte bestärkt werden, dass das identifizierte LIR-Motiv von TECPR2 in die Bindetaschen von LC3B passt. Schließlich wurde bei Kollokalisationsexperimenten mit endogenem TECPR2 in Zellen eine Bindepräferenz zu LC3B und LC3C deutlich.

Zur Ermittlung neuer Interaktionspartner von TECPR2 wurde eine umfassende massenspektrometrische Analyse durchgeführt. Dabei konnten einige interessante Kandidaten ausgemacht werden, die endomembran-abhängigen Transportwegen in Zellen zuzuordnen sind.

Darunter befanden sich zwei Komplexe HOPS und BLOC-1, die beide an Prozessen der Endozytose beteiligt sind.

Die Endozytose ist ein zentraler Transportprozess in Zellen. Dabei werden Proteine, Lipide, Pathogene oder extrazelluläre Rezeptoren in Endosomen in die Zellen geschleust und dort entweder durch Recycling an ihren neuen Wiederverwendungsort gebracht oder aber mithilfe von Lysosomen abgebaut. Endosomen müssen, um ihre volle Funktion ausbilden zu können, einen Reifungsprozess durchlaufen. Frühe Endosomen fusionieren und nehmen an Größe zu bis sie zu späten Endosomen reifen. Hierbei spielt der HOPS-Komplex eine wichtige Rolle. Der Komplex, als typischer Verbindungskomplex, unterstützt die Fusion von späten Endosomen mit Lysosomen, indem er die Vesikel und regulative Komponenten zusammenbringt. HOPS besteht aus sieben Untereinheiten: VPS11, VPS16, VPS18, VPS33, VPS39 und VPS41. An den äußeren gegenüber liegenden Enden des Komplexes liegen VPS39 und VPS41, die beide an die GTPase RAB7A binden können, welche wiederum mit späten Endosomen interagiert. Die VPS33-Untereinheit von HOPS bindet an SNARE-Proteine, die den Fusionsprozess zusätzlich unterstützen.

Bei BLOC-1 handelt es sich um einen Komplex, der bei der Biogenese von lysosom-verwandten Proteinen beteiligt ist. Er umfasst acht Untereinheiten: BLOS1, BLOS2, BLOS3, CNO, DTNBP1, MUTED, PLDN und SNAPIN. BLOC-1 bindet an SNARE-Proteine, reguliert die Fusion von endosomalen Membranen und unterstützt somit die Sortierung von bestimmten Membranproteinen. Im speziellen ist BLOC-1 an der Ausbildung von Melanosomen und Thrombozyten-dichten Granula beteiligt. Ähnlich wie HOPS ist auch BLOC-1 für die korrekte Sortierung von Cargoproteinen des endo-lysosomalen Transportweges verantwortlich, allerdings arbeiten die beiden Proteinkomplexe innerhalb verschiedener Bereiche und sind an unterschiedlichen Prozessen beteiligt.

Im Rahmen dieser Arbeit konnte festgestellt werden, dass der N-terminale Teil von TECPR2 mit beiden dieser Komplexe interagiert und kollokalisiert. Darüber hinaus ist die Bindung von LC3 und dem LIR-Motiv von TECPR2 abhängig. In Abwesenheit von TECPR2 werden beide

Komplexe instabil und proteasomal abgebaut. Somit trägt TECPR2 zu deren Integrität in Zellen und damit auch zur korrekten Funktion von HOPS und BLOC-1 bei. Einen Zusammenhang zum positiven Einfluss von TECPR2 auf Autophagie konnte aber nicht hergestellt werden.

Der interessanteste Interaktionspartner von TECPR2 stellt SEC24D dar, ein Bestandteil der inneren COPII-Hülle im Sekretionsweg. Auch hier konnte eine direkte Interaktion und Kolo­kalisierung in Abhängigkeit von LC3 festgestellt werden, wobei im Fall von SEC24D LC3C den größten Einfluss zeigte. Das Fehlen von TECPR2 in Zellen führte zu einer Destabilisierung von SEC24D und dessen proteasomalem Abbau, sowie dem Abbau seines Heterodimerpartners SEC23A. Beide Proteine bilden zusammen den inneren Teil der COPII-Hülle von sekretorischen Vesikeln, während sich die äußere Hülle aus SEC13 und SEC31 zusammensetzt. COPII-Vesikel sind für den anterograden Transport von Cargo vom ER in Richtung Golgi und weiter zur Plasmamembran zuständig. Sie werden vom ER an bestimmten Stellen, den sogenannten ER-Austrittsstellen, abgeschieden und entlang des Sekretionsweges in die verschiedenen Kompartimente verteilt. An der Abspaltung der Vesikel ist unter anderem die kleine GTPase SAR1A beteiligt. Im ER gebildete Proteine werden in den COPII-Vesikeln transportiert und durchlaufen dabei das ERGIC und den Golgiapparat. Im Trans-Golgi Netzwerk werden die Bestandteile der Vesikel sortiert und entweder an ihren Zielort gebracht oder recycelt und innerhalb des Sekretionsweges zurücktransportiert. Durch die Abwesenheit von TECPR2 in Zellen kommt es zu einer Reduktion von ER-Austrittsstellen und COPII-Vesikeln und somit zu einem generellen Defekt des Sekretionsweges. Bringt man TECPR2 zurück in die Zellen, kann der Phänotyp umgekehrt werden, dies funktioniert nur mit dem Wildtyp des Proteins nicht aber mit der LIR-Mutante. In diesem Versuchsaufbau wurden mit LC3C dieselben Effekte erzielt. Die Rolle von TECPR2 und LC3C am korrekten Ablauf der ER-Sekretion wurde mithilfe verschiedener Cargoproteinen und deren Austrittsverhalten aus dem ER demonstriert. Zudem zeigte das ER eine Veränderung seiner Morphologie und eine generelle Volumenzunahme. Diese Veränderung wurde wahrscheinlich durch die Ansammlung von Cargoproteinen, die das ER nicht verlassen können, erzeugt. Diese Reihe von Experimenten zeigt, dass TECPR2 zusammen mit LC3C die Bildung von COPII-Vesikeln unterstützt und ausserdem am Aufbau und der korrekten Funktion des ERs mitwirkt. Dabei besonders erwähnenswert ist, dass Fibroblasten von HSP-Patienten, die eine TECPR2-Mutation tragen, ebenfalls reduzierte SEC24D Proteinlevel zeigen und zudem der Export von Cargo aus dem ER dieser Zellen verzögert ist. Gleichzeitig führen das Fehlen von TECPR2 oder LC3C sowie die Überexpression einer dominant-negativen Mutante von SAR1A zu einer Reduktion des frühen Autophagiemarkers WIPI2, was selbst nach Induktion von Autophagie mithilfe des Inhibitors Torin1 bestehen bleibt. WIPI2 ist an Omegasomen, frühen autophagischen Membranstrukturen am ER, lokalisiert.

Zusammenfassend demonstriert diese Studie eine Beteiligung von TECPR2 am Export von Cargo aus dem ER an den ER Austrittsstellen durch Interaktion und Stabilisation des COPII-Hüllproteins SEC24D. Dieser Prozess ist ebenfalls abhängig vom ATG8-Protein LC3C, das ebenfalls an den ER Austrittsstellen detektiert wurde. Beide Proteine zusammen erlauben die korrekte Sekretion von spezifischem Cargo der COPII-Vesikel. Darüber hinaus sind TECPR2 und LC3C, durch die Stabilisierung von WIPI2, am Aufbau von Omegasomen am ER beteiligt und unterstützen somit die Bildung von Autophagosomen.

Betrachtet man die umfassenden Ergebnisse in den verschiedenen Teilbereichen dieser Studie von einem globaleren Standpunkt, lässt sich zusammenfassend feststellen, dass das Fehlen von TECPR2 zu weitreichenden Veränderungen im ER Export und der ER Morphologie und damit auch zu generellen Defekten in den zellulären Transportwegen führt.

Es ist bekannt, dass im Zusammenhang mit HSP, Mutationen in mehreren unterschiedlichen Genen, beispielsweise SPAST, ATL1 und REEP1, zu Veränderungen der ER-Struktur und -Funktion führen. TECPR2 lässt sich in diese Auflistung einreihen was dadurch noch bestärkt wird, dass sich diese Defekte auch in Zellen von HSP Patienten beobachten lassen.

Mithilfe dieser Studie lässt sich somit ein exakteres Bild der Beteiligung von TECPR2 an HSP zeichnen. Neurodegenerative Erkrankungen lassen sich selten klar von einander abgrenzen, da es meist zu weitreichenden symptomatischen Überlappungen kommt und zudem oft mehrere dieser Erkrankungen parallel vorliegen. Vor kurzem wurde ein Zusammenhang von weiteren Mutationen von TECPR2 mit zwei anderen neurodegenerativen Erkrankungen hergestellt. Dabei handelt es sich zum einen um die hereditären sensorisch-autonomen Neuropathien (HSAN), eine Gruppe von Krankheitsbildern, die sich vor allem durch respiratorische Defekte und autonome Dysfunktionen auszeichnen und im Kontext mit der Erhaltung der Struktur und der Funktionen des ERs stehen. Das zweite Krankheitsbild umfasst die neuroaxonalen Dystrophien (NAD), die durch die Bildung spezieller Spheroide in den Basalganglien gekennzeichnet sind. Viele Gene, die an einer NAD Erkrankung beteiligt sind, spielen gleichermaßen eine Rolle im Transportweg vom ER. Darüber hinaus wurde gezeigt, dass ein Fehlen von TECPR2 zu einer Dysfunktion von Autophagie führt.

Deshalb bleibt es von enormen Interesse die Rolle von TECPR2 in einem grundlegenden Zusammenhang bei neurodegenerativen Erkrankungen einzuordnen und möglicherweise durch die Zuordnung spezifischer Krankheitsbilder zu den unterschiedlichen Funktionen von TECPR2 in zellulären Transportwegen eine neue Klassifizierung der neurodegenerativen Erkrankungen vorzunehmen.

Danksagung

Zuallererst möchte ich meinen besonderen Dank an meinem Betreuer Dr. Christian Behrends richten. Zum einen für die Möglichkeit in einem wissenschaftlich herausfordernden Gebiet meine Doktorarbeit durchgeführt haben zu dürfen, sowie beim Aufbau und der Gestaltung seiner Arbeitsgruppe wesentlich mitgewirkt haben zu können. Zum anderen für die große Hilfe beim experimentellen Aufbau der Arbeit, wo er mir mit hilfreichen Ideen und Anregungen sowie Rat und Tat bei schwierigen Fragestellungen zur Seite stand. Darüber hinaus möchte ich mich für sein stets offenes Ohr für neue Ideen und ungewöhnliche Lösungsansätze bedanken und vor allem auch für die unkomplizierte, ehrliche Arbeitsatmosphäre. Weiterhin vielen Dank für die Korrektur dieser Arbeit und die Erstellung des Zweitgutachtens.

Ein herzlicher Dank gebührt Herrn Prof. Dr. Heinz Osiewacz für die unkomplizierte Erstellung des Erstgutachtens.

Mein Dank gilt auch Herrn Dr. Hesso Farhan sowie den Doktorandinnen seiner Arbeitsgruppe, Kerstin Tillmann und Valentina Millarte, für die produktive Zusammenarbeit und große Unterstützung im Feld der Sekretion. Danke für die ideenreichen Diskussionen und die immer offenen Worte.

Bedanken möchte ich mich auch bei Herrn Prof. Dr. Volker Dötsch, Jessica Huber, Vladimir Rogov und Masato Akutsu für die Bereitstellung und Durchführung der biophysikalischen Methoden und die Fähigkeit trotz vieler Rückschläge nicht aufzugeben. Es hat sich gelohnt.

Weiterhin gilt mein Dank Herrn Prof. Zvulun Elazar und den helfenden Händen aus seiner Arbeitsgruppe für die großartige Zusammenarbeit, die Begeisterung für mein Projekt sowie die enorme Unterstützung unserer Daten mit dem Patientenmaterial.

Des Weiteren bedanke ich mich bei allen Mitgliedern des Instituts für Biochemie II für das angenehme Arbeitsklima, stete Hilfsbereitschaft durch Diskussionen und entgegenkommendes Zurverfügungstellen von Materialien und Protokollen. Vielen Dank auch an Ivan Dikic für die Chance meine Doktorarbeit in einem wissenschaftlich hochkarätigen und international anregendem Umfeld durchführen zu können.

Ein ganz besonderer Dank gilt Heide, Jenny und Anne dafür, dass ihr immer da wart bei Schwierigkeiten aber auch schönen Momenten, dafür dass ihr mir sowohl wissenschaftlich als auch freundschaftlich immer zur Seite gestanden seid. Vielen Dank Mädels! Besonderen Dank schulde ich Anne, die mir neben ihrer wunderbaren Freundschaft auch ein Zuhause geboten hat; bei dir wird immer mein Zuhause in Frankfurt sein.

Auch bedanken möchte ich mich bei der gesamten AG Behrends, auf die ich zusammen mit Steffi und Christian als „Mitstarter“ sehr stolz bin. Wo vor fünf Jahren noch leere Laborräume waren, findet man heute eine kollegiale, produktive aber auch entspannte Arbeitsatmosphäre.

Danke an euch alle: Christian, Tihana, Mira, Francois, Christian, Steffi, Heide, Jenny, Sabine und Franziska für die schöne und intensive Zeit.

Den größten Dank schulde ich meiner Familie und meinen Freunden, die mich in den letzten fünf Jahren immer unterstützt und motiviert haben. Danke, dass ihr immer an mich geglaubt habt.

Curriculum vitae

Daniela Stadel
Schottenstrasse 57
78462 Konstanz
Germany

Mobil: +49-171-2806456
Email: daniela.stadel@gmx.de



Personal information

Date of birth: 10th April 1986 in Karlsruhe
Nationality: german

Current research

Since 4/2011 PhD student at the Institute of Biochemistry II, Goethe University
Frankfurt am Main. "TECPR2 cooperates with LC3C to regulate COPII
dependent ER export" supervised by Dr. Christian Behrends

Scientific education

4/2010 - 12/2010 Diploma thesis, University Medical Center, Heidelberg, Germany
Experimental surgery, tumor cell biology
"Exosomes and their target cells: the influence of tetraspanins"
Supervised by Prof. Dr. med. Margot Zöller

10/2005 – 4/2011 Diploma in biology, Institutes of Technology Karlsruhe (KIT),
Karlsruhe, Germany
Major topics: Genetics, zoology and botanic

6/2005 Abitur, Humboldt Gymnasium, Karlsruhe, Germany

Publications

Stadel D, Millarte V, Tillmann K, Huber J, Tamin-Yecheskel BC, Akutsu M, Demishtein A, Benzeev B, Anikster Y, Perez F, Dötsch V, Elazar Z, Rogov V, Farhan H, Behrends C. TECPR2 cooperates with LC3C to regulate COPII-dependent ER export. **Mol Cell**. 2015 Oct 1, 60(1):89-104

McEwan DG, Popovic D, Gubas A, Terawaki S, Suzuki H, **Stadel D**, Coxon FP, Miranda de Stegmann D, Bhogaraju S, Maddi K, Kirchof A, Gatti E, Helfrich MH, Wakatsuki S, Behrends C, Pierre P, Dikic I. PLEKHM1 regulates autophagosome-lysosome fusion through HOPS complex and LC3/GABARAP proteins. **Mol Cell**. 2015 Jan 8, 57(1):39-54

Ulbricht A, Eppler FJ, Tapia VE, van der Ven PF, Hampe N, Hersch N, Vakeel P, **Stadel D**, Haas A, Saftig P, Behrends C, Fürst DO, Volkmer R, Hoffmann B, Kolanus W, Höhfeld J. Cellular mechanotransduction relies on tension-induced and chaperone-assisted autophagy. **Curr. Biol**. 2013 Mar, 23(5):430-5

Rana S, Yue S, **Stadel D**, Zöller M. Toward tailored exosomes: the exosomal tetraspanin web contributes to target cell selection. **Int J Biochem Cell Biol**. 2012 Sep, 44(9):1574-84

Presentations at conferences

Elucidating the role of ATG8 interacting protein TECPR2 in autophagy

Daniela Stadel¹ and Christian Behrends¹

¹Institute of Biochemistry II, School of Medicine, Goethe University, D-60590 Frankfurt, Germany

Poster at “Ubiquitin and Autophagy”, June 26-27 2013 in Amsterdam, Netherlands

TECPR2 cooperates with LC3C to regulate COPII dependent ER export

Daniela Stadel¹, Valentina Millarte^{2,3}, Kerstin Tillmann^{2,3}, Jessica Huber⁴, Bat-Chen Tamin-Yecheskel⁵, Masato Akutsu⁹, Alik Demishtein⁵, Bruria Ben-Zeev^{6,7}, Yair Anikster^{6,7}, Franck Perez⁸, Volker Dötsch⁴, Zvulun Elazar⁵, Vladimir Rogov⁴, Hesso Farhan^{2,3} and Christian Behrends¹

¹Institute of Biochemistry II, Medical School Goethe University, 60590 Frankfurt, Germany

²Department of Biology, University of Konstanz, 78464 Konstanz, Germany

³Biotechnology Institute Thurgau, 8280 Kreuzlingen, Switzerland

⁴Institute of Biophysical Chemistry and Center for Biomolecular Magnetic Resonance, Goethe University, 60438 Frankfurt, Germany

⁵Department of Biological Chemistry, Weizmann Institute of Science, Rehovot, 76100, Israel

⁶Edmond and Lilly Safra Children’s Hospital, Sheba Medical Center, Ramat Gan, 52621, Israel

⁷Sackler School of Medicine, Tel-Aviv University, Tel-Aviv 69978, Israel

⁸Institute Curie, CNRS UMR144, Paris, 75248, France.

⁹Buchmann Institute for Molecular Life Sciences, Goethe University, 60438 Frankfurt, Germany

Poster at “Autophagy signaling and progression in health and disease”, September 9-12 2015 in Chia, Italy

Eidesstattliche Erklärung

Hiermit erkläre ich, Daniela Stadel, geboren am 10. April 1986 in Karlsruhe, dass ich vorliegende Dissertation mit dem Titel:

„TECPR2 cooperates with LC3C to regulate COPII dependent ER export“

selbstständig und unter ausschließlicher Verwendung der angeführten Hilfsmittel und Quellen angefertigt habe. Die Dissertation wurde in der jetzigen oder ähnlichen Form noch bei keiner anderen Hochschule eingereicht.

Frankfurt am Main, den 14.01.16

.....

Daniela Stadel